Simultaneous sequestration of Cr(VI) and Cr(III) from aqueous solutions by activated carbon and ion-imprinted polymers

A dissertation submitted to the Faculty of Applied and Computer Sciences, Department of Chemistry, Vaal University of Technology, Vanderbijlpark, in fulfilment of the requirements for the degree of **Magister Technologiae**

By

Mahadi Lesaoana

Supervisor: Dr V.E Pakade

Co-supervisor: Prof L. Chimuka

Date: Aug 2018

DECLARATION

Prima Facie, I declare that this dissertation was composed by myself, that the work contained herein is my own except where explicitly stated otherwise in the text, and that this work has not been previously submitted for any other degree or professional qualification at another university.

.....

(Candidate's signature)

.....20th.....day of.....Aug 2018

ABSTRACT

Macadamia activated carbon (MAC) was impregnated with different concentrations of nitric acid and heated under reflux to improve the structural characteristics of the adsorbent for both considerable reduction and enhanced removal of Cr(VI). The chemical oxidation of ACs increased the surface oxygenated functional groups. Adsorption of Cr(VI) was carried out by varying parameters such as contact time, pH, concentration, and adsorbent dosage. The optimum operating conditions for the adsorption of Cr(VI) were pH 1, contact time 240 min, adsorbent dosage 10.67 g/L and Cr(VI) concentration 100 mg/L. The results showed that the *Macadamia*–based AC could be used efficiently for the treatment of chromium-containing solutions as a low-cost alternative compared to commercial AC and other adsorbent reported. The results showed that treated MAC performed better than untreated MAC, signifying the effect of secondary treatment on the enhanced removal of pollutants.

Comparable to the application of ACs is the development of imprinting technologies for selective metal ion remediation in environmental samples. The combination of ion imprinting effects and functionalized carbon adsorbents produce materials which effectively remove and selectively recognize the target analyte. *Macadamia* activated carbon (MAC) was chemically pre-treated with nitric acid to generate carboxyl groups on the surface. The carboxylated MAC was then reacted with triethylenetetramine, *N,N'*-diisopropylcarbodiimide and $CrCl_3.6H_2O$ to produce $MACN_{20}$-imprinted sorbents ($MACN_{20}$-IIP). $MACN_{20}$-non imprinted ($MACN_{20}$-NIP) counterparts were prepared, but Cr^{3+} was excluded in the synthesis. Alteration of surface structural characteristics and characterization of prepared adsorbents was confirmed by Fourier transform infrared spectroscopy,

thermogravimetric analysis, elemental analysis, *Brunauer–Emmett–Teller* and scanning electron microscopy. $MACN_{20}$-IIP and $MACN_{20}$-NIP adsorbents were evaluated for their Cr^{3+} uptake from aqueous solution in batch format. Maximum conditions were achieved at pH 5, 50 mg/L Cr(III) initial concentration and 33.33 g/L of adsorbent dosage. Presence of co-ions slightly diminished the removal of Cr(III) by MAC-IIP adsorbents. Application of the $MACN_{20}$-IIP and $MACN_{20}$-NIP on spiked acid mine drainage artificial sample led to collapse in the removal efficiency of $MACN_{20}$-NIP while $MACN_{20}$-IIP still showed good removal efficiencies. These results demonstrated that surface imprinting led to better adsorption rates and capacity. The data was better described by the Freundlich multilayer adsorption and pseudo-second order kinetic rate model. The combination of both the carbon sorbent and the surface-mediated IIPs effectively improved total chromium remediation in aqueous systems.

DEDICATION

To mama, Mataemane Christina and papa, Martin Julius Lesaoana. Be proud. I love you.

PRESENTATIONS AND PUBLICATIONS FROM DISSERTATION

Presentations

LESAOANA, M., PAKADE, V. E. & CHIMUKA, L. Chemical oxidation of *Macadamia* activated carbon through impregnation by inorganic acids for enhanced Cr(VI) adsorption. Vaal University of Technology 1st interdisciplinary conference. 2016. 04 November, Vaal University of Technology Science park, Vanderbijlpark, South Africa, *Oral presentation*.

LESAOANA, M., PAKADE, V. E. & CHIMUKA, L. HNO_3 modified *Macadamia* activated carbon for the adsorption of Cr(VI) in aqueous solutions. 2017. 25th – 29th June. The Inorganic Chemistry Conference 2017 & Carman Physical Chemistry Symposium of the South African Chemical Institute Western Cape, South Africa, *Poster presentation*.

LESAOANA, M., PAKADE, V. E. & CHIMUKA, L. Surface imprinted *Macadamia* activated carbons for selective adsorption of Cr(III) in waste water. Vaal University of Technology 1st interdisciplinary conference. 2017. 11 November, Vaal University of Technology Science park, Vanderbijlpark, South Africa, *Oral presentation*.

LESAOANA, M., PAKADE, V. E. & CHIMUKA, L. Chemical oxidation of *Macadamia* activated carbon through impregnation by inorganic acids for enhanced Cr(VI) adsorption. The 9th International Conference of the African Materials Research Society. 2017. 11-14 December, Gaborone, Botswana, *Oral Presentation*.

Publications

LESAOANA, M., PAKADE V.E., MLABA, R.P.V., MTUNZI, F.M., KLINK, M.J. & EDIJIKE, P. 2017. Influence of inorganic acid modification on Cr(VI) adsorption performance and the physicochemical properties of activated carbon. *South African Journal of Chemical Engineering,* **(submitted).**

LESAOANA, M., PAKADE V.E. & CHIMUKA, L. 2018. Crosslinkerless surface-imprinted *Macadamia* derived activated carbons for trace Cr(III) removal from aqueous solution. *Microporous & Mesoporous Materials,* **(submitted)**.

ACKNOWLEDGEMENTS

I am immensely grateful to God for the good health and well-being that were necessary to complete this research project. I wish to express my thanks to my supervisor, Dr Vusumzi Pakade. I am thankful for his aspiring guidance, invaluable criticisms and friendly advice on the project work. I also dedicate many thanks to my co-supervisor, Prof Luke Chimuka (Wits University) for his support and inputs to this work.

Many thanks to the National Research Foundation, Vaal University of Technology, New generation of Scholars bursary, and National Student Financial Aid Scheme for funding my studies.

Getting through my dissertation required more than academic support, I have plenty of people to thank for listening to and at times, having to tolerate me over the past years. I cannot begin to express my gratitude and appreciation for their friendship.

The "A Team" Semakaleng Kganyago, Daniel Makanyane, Zondi Nate, have been unwavering in their personal and professional support during the time I spent at the university. For many memorable evenings in and out, I must thank everyone above as well. I would also like to express a special thanks to you to Makosi and Liau Khoase who opened both their home and heart to me when I first started university.

Most importantly, none of this could not have happened without my family. It's hard to put in words exactly how thankful I am for you and everything you have done for me over the past years. I do not know where I would have been without you. Thank you for being my support and thank you for all the sacrifices, big and

small. It is because of you that I have the strength to grow, take chances and live, because I know that you are always behind me every step of the way.

To my sisters, Nono, Kossy, Pino, Pale, Twetsi, Neo and my only brother Thabo Lesaoana; my nephew, nieces, and malome Buti Ntholi. Every time I was ready to quit, you did not let me. I am truly blessed to call you my family. And after everything we have been through together, I cannot help but choose to love you all over again. This dissertation stands as a testament to unconditional love. Very special gratitude also goes to Eddie Jeli who have given so much of himself every moment. Thank you for everything all and above.

And finally but by no means last, also to everyone in the NCAP group: Prof M. J. Moloto, Dr E. L. Viljoen, Dr P. Edijike, Dr F. M Mtunzi, DR T. Xaba, Ntuli T.D., Mnqiwu K., Nchoe O. B, Sibokoze S.B., Masuku M., Bout W., Mofokeng T.P., More D.S., Mokubung K. E., Maremeni L. C., Nkabinde S. C., Thabethe M., Mabungela, N. and my mentee Masite, N. N. your comments and advices in the presentation group are much appreciated. My appreciation knows no bounds. To Mr M. Ngoy, Ms Pholosi A.N. and Mr Saheed O. Thank you for your assistance with all the analytical instruments. I would also like to acknowledge the Research and Higher Degrees Unit staff at the Vaal University of Technology, Ms B. Phume, Ms O. Kokoali, and Ms L. L. Hlaha.

TABLE OF CONTENTS

DECLARATION ii

ABSTRACT iii

DEDICATION v

PRESENTATIONS AND PUBLICATIONS FROM DISSERTATION vi

ACKNOWLEDGEMENTS viii

TABLE OF CONTENTS x

LIST OF ABBREVIATIONS AND ACRONYMS xiv

LIST OF FIGURES xvi

LIST OF TABLES xix

CHAPTER 1 1

Introduction 1

1.1. Background 1

1.2. Purpose of study 6

CHAPTER 2 8

Literature review 8

2.1. The occurrence of chromium 8

2.2. Toxicity of chromium 10

2.3. Fate and transport of chromium 11

2.4. Treatment methods for metal ion recovery 12

2.4.1. Reverse osmosis 12

2.4.2. Ion exchange 13

2.4.3. Chemical precipitation 14

2.4.4. Adsorption 16

2.5. Activated carbon as an adsorbent 16

2.5.1. Precursors for activated carbon 17

2.5.2. Preparation of activated carbon 20

2.6.3. Adsorption of Cr(VI) by activated carbon 25
2.7. Imprinted polymers 28
2.7.2. Polymerization reagents 30
2.7.3. Approaches in IIPs synthesis 31
2.6.3. Polymerization methods 34
CHAPTER 3 39
Research objectives 39
3.1. General research objective 39
3.2. Specific objectives 39
3.3. Research significance 40
3.4. Hypothesis 40
CHAPTER 4 41
Materials and methods 41
4.1. Chemicals, stock solutions and equipment 42
4.1.1. Chemicals 42
4.1.2. Stock solutions 42
4.1.3. Equipment 43
4.1.4. Analytical instruments and characterization 43
4.2. Preparation of activated carbons 48
4.2.1. Sample pre-treatment 48
4.2.2. Functionalization of treated *Macadamia* activated carbon (MAC) 48
4.2.3. Preparation of the Cr(III) imprinted and non-imprinted activated carbons ($MACN_{20}$-IIP/NIP) 49
4.3. Synthesis of ion-imprinted polymers for Cr(III) recovery 49
4.4. Batch adsorption experiments 51
4.4.1. Optimization of experimental parameters for chromium adsorption 51
4.4.2. Selectivity studies on the adsorption of Cr(III) by IIPs 51

4.4.3. Application of $MACN_{20}$-IIP/NIP to real samples 53

4.5. Simultaneous adsorption of Cr(VI) and Cr(III) by $MACN_{20}$ and $MACN_{20}$-IIPs 53

4.6. Kinetic models 54

4.7. Adsorption isotherms 54

4.8. Intra-particle diffusion 55

CHAPTER 5 57

Results and Discussion 57

5.1. Functionalized and unfunctionalized ACs 57

5.1.1. Characterization of adsorbents 57

5.1.1.1. Elemental analysis and BET measurements 57

5.1.2. Adsorption studies 64

5.1.2.1. Effect of solution pH on Cr(VI) adsorption 64

5.1.2.2. Effect of adsorbent mass on Cr(VI) adsorption 66

5.1.2.3. Effect of contact time on Cr(VI) adsorption 67

5.1.2.4. Kinetic models 68

5.1.2.5. Intra-particle diffusion 70

5.1.2.6. Effect of initial concentration on the adsorption of Cr(VI) 71

5.1.2.7. Adsorption isotherms 73

5.1.2.8. Adsorption capacity comparison 75

5.2. Surface imprinting of Cr(III) on $MACN_{20}$-OOH 79

5.2.1. Preparation of surface ion imprinted *Macadamia* activated carbon. 80

5.2.2. Characterization of adsorbent 81

5.2.2. Adsorption studies 89

5.2.2.1. Effect of solution pH on Cr(III) removal 89

5.2.2.2. Effect of concentration on Cr(III) removal 92

5.2.2.3. Adsorption isotherms 94

5.2.2.4. Effect of adsorbent mass on Cr(III) adsorption....97
5.2.2.5. Effect of contact time on Cr(III) adsorption....98
5.2.2.6. Kinetic modelling....100
5.2.2.7. Intra-particle diffusion....102
5.2.2.8. Effect of co-existing ions....103
5.2.2.9. Real sample analysis....106
5.3. Synthesis of Cr(III)-molecularly imprinted polymers....107
5.3.1. Characterization of adsorbent....108
5.3.2. Adsorption studies....117
5.3.2.1. Effect of solution pH on Cr(III) adsorption....117
5.3.2.2. Selectivity studies....117
5.4. Simultaneous removal of Cr(VI) and Cr(III)....119
CHAPTER 6....126
Conclusions and Recommendations....126
6.1. Conclusions....126
6.2. Recommendations....129
REFERENCES....129
APPENDIX....152

LIST OF ABBREVIATIONS AND ACRONYMS

AA	Acrylamide
AAS	Atomic absorption spectroscopy
AC	Activated carbon
ACF	Activated carbon fibre
AMD	Acid mine drainage
APDC	Ammonium pyrrolidine dithiocarbamate
BET	Brunauer, Emmett, and Teller
CHNS	Carbon, hydrogen, nitrogen and sulphur
CP	Control polymer
Cr-PDC-AA	Cr(III)-pyrrolidine dithiocarbamate-acrylamide
DDDPA	1,12-dodecanediolO,O'-diphenyl-phosphonic acid
DIC	*N,N*′-Diisopropylcarbodiimide
DPC	1, 5-diphenylcarbazide
DTA	Derivative thermogravimetric analysis
EA	Elemental analysis
EBAm	N, N´-ethylene bisacrylamide
EDTA	Ethylene diamine tetraacetic acid
EGDMA	Ethylene glycol dimethacrylate
FO	Forward osmosis
FTIR	Fourier-transform infrared
GAC	Granular activated carbon

ICP-OES	Inductively coupled plasma optical emission spectroscopy
IIP	Ion imprinted polymer
IUPAC	International union of pure and applied chemistry
MAC	*Macadamia* activated carbon
MBA	N,N'-methylenebisacrylamide
MIP	Molecularly imprinted polymer
NIP	Non-imprinted polymer
PFO	Pseudo first order
PSO	Pseudo second order
RO	Reverse osmosis
SEM	Scanning electron microscopy
SG-AAPTS	N-(2-aminoethyl)-aminopropyltrimethoxysilane
TCD	Thermoconductivity detector
SIT	Surface imprinting technology
TETA	Triethylenetetraamine
TGA	Thermo-gravimetric analysis
USEPA	United States Environmental Protection Agency
UV-vis spectroscopy	Ultraviolet visible spectroscopy
VID	1-vinylimidazole
VP	Vinyl pyridine
WHO	World health organization

LIST OF FIGURES

Figure 2.1: Pourbaix diagram of chromium.....9

Figure 2.2: Schematic diagram depicting imprinting polymerization 28

Figure 2.3: Different approaches for IIP preparation.....34

Figure 4.1: Diagram describing the process of atomization for a continuous flame atomizer.....46

Figure 5.1: FTIR spectra of MAC (a), $MACN_{20}$ (b), $MACN_{40}$ (c) and $MACN_{60}$ (d) adsorbents before adsorption 59

Figure 5.2: TGA (a) and DTG (b) of MAC, $MACN_{20}$, $MACN_{40}$ and $MACN_{60}$ .61

Figure 5.3: Scanning electron microscopy images for $MACN_{20}$ (a), $MACN_{40}$ and (c) $MACN_{60}$.....63

Figure 5.4: Effect of solution pH on Cr removal by $MACN_{20}$, $MACN_{40}$ and $MACN_{60}$.....66

Figure 5.5: Effect of adsorbent mass 67

Figure 5.6: Effect of contact time 68

Figure 5.7: Intra-particle diffusion curves for the adsorption of Cr(VI) by MACN carbons. 71

Figure 5.8: Effect of initial concentration and (a) % removal, (b) adsorption capacity on Cr(VI) adsorption.....73

Figure 5.9: Schematic representation of the preparation of $MACN_{20}$-IIP 80

Figure 5.10: N_2 adsorption and desorption isotherms of $MACN_{20}$-IIP (leached and unleached) and $MACN_{20}$-NIP 81

Figure 5.11: FTIR spectra of unleached $MACN_{20}$-IIP (a), leached $MACN_{20}$-IIP (b) and $MACN_{20}$-NIP (c).....84

Figure 5.12: TGA (a) and DTA (b) thermograms of $MACN_{20}$-IIP (leached and unleached) and $MACN_{20}$-NIP 86

Figure 5.13: SEM images of unleached $MACN_{20}$-IIP (a), leached $MACN_{20}$-IIP (b) and $MACN_{20}$-NIP (c) 89

Figure 5.14: Effect of solution pH on Cr(III) adsorption by $MACN_{20}$-IIP and $MACN_{20}$-NIP 90

Figure 5.15: Cr(III) speciation diagram at various pH 91

Figure 5.16: Effect of initial concentration on Cr(III) % removal by $MACN_{20}$-IIP and $MACN_{20}$-NIP (a), $MACN_{20}$-IIP/MeOH (b) and adsorption capacity by $MACN_{20}$-IIP and $MACN_{20}$-NIP (c) 93

Figure 5.17: Freundlich isotherms for $MACN_{20}$-IIP (a) and $MACN_{20}$-NIP (b) ..95

Figure 5.18: Effect of adsorbent mass on Cr(III) removal by $MACN_{20}$-IIP and $MACN_{20}$-NIP 98

Figure 5.19: Effect contact time on Cr(III) removal by $MACN_{20}$-IIP and $MACN_{20}$-NIP 99

Figure 5.20: PFO and PSO plots for the adsorption of chromium onto $MACN_{20}$-IIP (a) and $MACN_{20}$-NIP (b) 100

Figure 5.21: Intra-particle diffusion curves for the adsorption of Cr(III) by $MACN_{20}$-IIP and $MACN_{20}$-NIP 102

Figure 5.22: Removal efficiencies of cations adsorbed by the $MACN_{20}$-IIP and $MACN_{20}$-NIP 104

Figure 5.23: Polymerization mechanism of Cr(III)-PDC IIPs 108

Figure 5.24: N_2 adsorption (a) and desorption (b) of IIPs (leached and unleached) NIPs 109

Figure 5.25: FTIR spectra of (a) ammonium pyrrolidine dithiocarbamate and (b) Cr(III)-PDC complex 111

Figure 5.26: Resonance structures of pyrrolidine dithiocarbamate 112

Figure 5.27: FTIR spectra of IIPs and respective NIPs 113

Figure 5.28: TGA (a) and DTA (b) thermograms of polymeric materials 115

Figure 5.29: SEM micrographs of unleached Cr(III)-IIPs (a), leached IIPs (b) and the NIPs (c) 116

Figure 5.30: Effect of solution pH on the % recovery of Cr(III) by IIPs and NIPs 117

Figure 5.31: Showing % removal of Cr(VI), equilibrium total chromium Cr(III) concentration after adsorption by MACN/$MACN_{20}$-IIP adsorbent blends.....121

LIST OF TABLES

Table 2.1: Methods used in IIP synthesis.....35

Table 4.1: Operating conditions of the ICP-OES.....47

Table 5.1: Elemental analysis and BET measurements of activated carbons 58

Table 5.2: Intra-particle diffusion and kinetic models for nitric acid modified ACs 69

Table 5.3: Langmuir and Freundlich isotherms for the MACN adsorbents 75

Table 5.4: Comparing adsorption capacities of ACs derived different raw materials. 77

Table 5.5: BET surface areas, pore volumes, pore sizes and elemental analysis of $MACN_{20}$-IIP (leached and unleached) and $MACN_{20}$-NIP.....82

Table 5.6: The Langmuir and Freundlich parameters for adsorption of Cr(III) by 96

$MACN_{20}$-IIP and $MACN_{20}$-NIP.....96

Table 5.7: The Langmuir constants and the R_L values for adsorption of Cr(III) on $MACN_{20}$-imprinted sorbents.....97

Table 5.8: Kinetic parameters of pseudo-first and pseudo-second orders for Cr(III) adsorption by $MACN_{20}$-IIP and $MACN_{20}$-NIP at 100 mg/L 101

Table 5.9: Distribution coefficient (K_d), the selectivity coefficient (K) and the relative selectivity coefficient (K`) values of the cationic competitors relative to the template ion Cr^{3+}.....105

Table 5.10: The chemical composition of the AMD artificial sample.....106

Table 5.11: Application of $MACN_{20}$- IIP the corresponding NIP on unspiked and spiked real water sample 107

Table 5.12: BET surface areas, pore volumes and pore sizes of Cr(III)-IIPs (leached and unleached) and NIPs 110

Table 5.13: Imprinting factor, selectivity and separation ratios of IIPs.....119

Table 5.14: Total chromium, Cr(VI) and Cr(III) concentration by different MACN/$MACN_{20}$-IIP adsorbent blends.....123

Table 5.15: Total chromium, Cr(VI) and Cr(III) concentration by different MACN/ IIP adsorbent blends.....124

CHAPTER 1

Introduction

1.1. Background

Water pollution has recently become one of the critical global issues (Lin et al., 2014). Pollution of water sources arises as a result of random waste disposal. The discharge of inorganic waste containing toxic heavy metals poses a physiological threat to living organisms, particularly human beings and aquatic life (WHO, 2003). Therefore, the contamination of water bodies has become a key environmental priority for legislature and researchers.

Literature associates the generation of heavy metal pollutants to anthropogenic activities (Shahid et al., 2017, Saputro et al., 2014). Rapid growth in industrialization and urbanization accounts for the major generation of chemical waste including metal ions (Yue et al., 2009). Chromium is one of the reserved minerals in the world and most abundant in the earth's crust (Lansdown, 2014). Its compounds are widely utilized industrially *viz.* mining, electroplating, dye and pigment manufacturing and textile industries (Yue et al., 2009). Water streams from the mentioned industries accumulate trace amounts of metal residues and their compounds. On account of its non-degradable nature, chromium poses severe health threats to the ecosystem (Hossini et al., 2016, Ohgami et al., 2015).

Chromium exists primarily as chromite ($FeCr_2O_4$) and dichromate ($K_2Cr_2O_4$). These compounds exhibit different physiochemical, toxicological and biological properties (Lansdown, 2014, Kirti et al., 2015). Generally, Cr(III) compounds are regarded less toxic than Cr(VI) compounds, and that Cr(III) is needed to maintain mammalian biological processes such as glucose metabolism (Ramnani and

Sabharwal, 2006). Owing to its toxicity, hexavalent chromium [Cr(VI)] constitutes dreadful risks to human health and living organisms, and is listed as carcinogenic and genotoxic (WHO, 2003, Ohgami et al., 2015, Kirti et al., 2015). Exposure of living organisms to Cr(VI) may lead to dreadful health hazards to biological systems with known deleterious health effects such as lung cancer, kidney, liver and gastric damage hazards (Hossini et al., 2016, Gad, 2014). In view of this effect, the United States of Environmental Protection Agency (USEPA and OAR, 2012) has set the allowable limit of chromium into surface water and potable water as 0.1 mg/L and 0.05 mg/L, respectively.

In order to eradicate and obtain sufficient chromium removal from the environment, methods such as chemical precipitation (Mella et al., 2015), ion exchange (Korak et al., 2017, Tor et al., 2005), chemical reduction (George et al., 2015), membrane filtration and reverse osmosis (Lin et al., 2014) and adsorption (Ibrahim et al., 2016) have been used. Except for adsorption, the demerits of the mentioned processes include the high cost of equipment and chemicals, toxic sludge generation and incomplete removal of the metal ions. However, adsorption methods offer a simple, reliable technique operated on low energy, maintenance cost and it allows the usage a wide range of adsorbents for the removal of metal ions including Cr(VI) (Rao et al., 2008). Due to these, adsorption has been recognized and regarded to be the most effective for trace metal ion removal.

The adsorption methods depend on the type of adsorbents such as activated carbon, silica particles, and carbon-silica composites (Karnib et al., 2014), fibres (Razzaz et al., 2016) and polymers (Pakade et al., 2012). Among these adsorbents, activated carbons (ACs) are highly carbonaceous materials known for their large surface area, microporous structure and surface functional groups (Köseoğlu and Akmil-

Başar, 2015, Kumar and Jena, 2017). Thereby, this has led to the application of AC sorbents in the elimination of metal ion contaminants from the environment. The viability of manipulating the carbon surface features mainly encourages the production of carbon with distinct physiochemical properties (Foo and Hameed, 2012). These properties mainly depend on the nature, source, and structure of the raw material. However, commercial activated carbon remains expensive, and thus research has concentrated on finding alternative sources for producing ACs of good quality. Hence, various studies have explored the use of agro-based raw materials such as mango kernels (Rai et al., 2016), oil palm Endocarp (Silgado et al., 2014), date stones (Amor and Ismail, 2013), Terminalia arjuna (Mohanty et al., 2005), Tamarind wood (Acharya et al., 2009), peanut shell (Al-Othman et al., 2012), biomass (Gueye et al., 2014), *Macadamia* nutshell (Pakade et al., 2017) for the fabrication of AC for heavy metal remediation. Generally, the efficiency of the as-prepared ACs is relatively low and necessitating re-modification.

Usually, secondary treatment of ACs with activating agents is used to improve the adsorptive properties of the adsorbent. Moreover, activating variables such as the choice of activating agent, the method of activation and temperature need to be considerably optimized for selective removal of the pollutant of interest. It is known that chemical surface oxidation of ACs substantially facilitates the introduction of surface oxygenated functionalities (Fang et al., 2017). Several activating agents, $KMnO_4$ (Zhang et al., 2017a), HNO_3 (Yao et al., 2016), H_3PO_4 (Tan et al., 2016), peracetic acid (Fang et al., 2017), NaOH (Kopac et al., 2016), HCl (Gong et al., 2015) and cationic surfactant (Choi et al., 2009) have been used to chemically modify the properties of virgin ACs.

Strongly acidic conditions and presence of surface electron donors such as oxygen, sulphur and nitrogen promote the reduction of Cr(VI) to Cr(III) which is less toxic. However, the challenge is the incomplete removal of Cr since the so-formed Cr(III) can transform to the toxic Cr(VI) if exposed to oxidizing conditions causing recurrence of the problem (Rai et al., 1989, Saputro et al., 2014). Also, there's still a debate on the toxicity of Cr(III) compounds and their appropriateness as nutritional supplements because no Cr(III)-containing biomolecules have been isolated and fully characterized for this purpose (Hossini et al., 2016). Moreover, Cr(III) has been associated with the damage of red blood cells (Suwalsky et al., 2008) and suppressing immune system activity (Bernardo et al., 2009). It is also known that the degree of metal toxicity is considerably different for each metal. Therefore, Cr(III) compounds should be treated as other trivalent metal ions like Al(III) (Martin, 2000, Williams, 1999).

According to Zhan et al. (2011) most available, conventional adsorbents applied in trace metal remediation are non-specific and exhibit low selectivity. Therefore this necessitates the development of new adsorbents that can selectivity separate discriminately recognize target pollutant (Zhan et al., 2011). Hence, the application of synthetic polymers including the highly selective ion-imprinted polymers (IIPs) which are prepared from a template ion, functional monomer, and cross-linking agent has been explored for metal ion removal. Imprinted polymers offer a high degree of selectivity for a particular ion, stability, robustness and resistance towards a broad range of pH, solvents and temperature (Shakerian et al., 2016). To further improve the efficiency of IIPs, studies have focused on incorporating substrates or supports such as activated carbon (Li et al., 2014), silica (Li et al., 2015), carbon nanofibers (Mishra and Verma, 2017) or carbon nanotubes (Zargar

and Khazaeifar, 2017) for the selective removal of Cu(II), Cd(II), Pb(II) and Cd(II) ions, respectively . This process is referred to as surface imprinting technology (SIT).

SIT comprises a surface coated polymeric layer that specifically recognizes the imprint ion, known as a template. Since the imprinting cavities are located at or near the proximity of the surface, SIT encourages less formation of unspecific binding sites substantially increasing template selectivity. The technique also promotes uniform distribution of binding sites and accessibility of adsorption sites by template ion thus better mass transfer rates.

The properties of an adsorbent used in adsorption are vital in terms of selectivity and separation efficiency. Therefore, alternatively, an adsorbent that offers selectivity in function of separation can be used.

Studies on the removal of heavy metals including (Li et al., 2014), (Li et al., 2015) and (Mishra and Verma, 2017) using adsorbents prepared by surface imprinting technique (SIT) have been reported in the literature. SIT mediated IIPs exhibit accessible binding sites and high mass transfer rates for metal ions.

Activated carbon has a high degree of microporosity and surface area, thus can potentially be good supports for the preparation of surface imprinted polymers. The prepared carbon-polymer composite is likely to present a porous adsorbent facilitating efficient analyte removal. The sp^2 carbon network comprises of dangling sigma (σ) and pi (π) bonding resulting in the carbon surface amendable for functionalization. The advantages mentioned above allow AC to serve as adsorbents for SIT-mediated IIPs. Imprinting of metal ions on adsorbents is a well-established technique, even though less so compared to organic molecule

imprinting. However, the applicability of these adsorbents for complete total Cr removal remain very limited.

Moreover. in traditional surface imprinting, the imprinting on the support material is conducted in solution and a crosslinker monomer is added to maintain the structural rigidity as well as creating a specific cavity to fit the molecule or ion of interest. However, the same crosslinker can make the structure too rigid to the extent that complete removal of template molecules or ions become impossible. To address this setback, the current study proposes a pseudo-surface imprinting technique where the adsorbing ligand is grafted to the surface of active carbon in the presence of the template (Cr^{3+}). As opposed to traditional surface imprinting, no crosslinker monomer was used in the preparation of adsorbents. The omission of the crosslinker allows for free rotation of the ligand bonds in aqueous media due to the hydrophilicity of the grafted ligand, but the inclusion of the template ion during grafting permitted the structural rearrangement of the ligand molecules to favour Cr^{3+} uptake.

1.2. Purpose of study

The discharge of heavy metals such as chromium from industrial wastewater processes (paint, pigments, textiles, leather tanning, steel fabrication, electroplating, cement preservation and canning industries) beyond the permissible limit causes serious pollution to the environment and result in health hazard to humans due to carcinogenic and genotoxic nature of Cr(VI). Consequently, researchers have concentrated their efforts on developing various treatment technologies to regulate Cr(VI) toxins at discharge levels (Hossini et al., 2016).

Despite the variety of methods available, adsorption of pollutants on agro-based materials has attracted wide interest from researchers due to a range of advantages compared to the other methods. These advantages include low cost, abundant availability and functionalization opportunities. Agricultural by-products have been used either in their raw form or as precursors for the production of activated carbons (Yahya et al., 2015). Activated carbons exhibit high surface area, a broad range of pores (micropores, mesopores, and macropores) and surface reactivity. In this study, activated carbon derived from *Macadamia* nutshells was used. It was expected that besides acting as an adsorbent for Cr(VI) removal, the *Macadamia* activated carbon will also reduce Cr(VI) to less toxic Cr(III). Therefore, the proposed method combined processes of adsorption and reduction to remove chromium ions from aqueous solutions. In this case, the activated carbon was used to perform the adsorption and reduction of Cr(VI) and ion-imprinted polymers selective to Cr(III) ions incorporated with surface imprinted activated carbon was responsible for the removal of the so-formed Cr(III) ions.

The combination of imprinted polymers and surface imprinted activated carbon offer added advantages by incorporating high selectivity, robustness, and high surface area. The hybrid sorbents resulting from the combination of features of their constituents were found beneficial in the exploration of new avenues and applications for the analysis of trace metals.

CHAPTER 2

Literature review

This chapter discusses the chemistry of chromium, critically reviewing its speciation, toxicity, existence and its role in industrial activities. Since concerns have been made particularly on the toxicity of this element, an emphasis is made on the epidemic problems caused. Different treatment methods employed for the removal of chromium from aqueous solution are also addressed, critically highlighting the advantages and disadvantages of each. Furthermore, a detailed discussion on the chemistry of activated carbon and ion-imprinted polymers is given. Finally, the chapter is concluded with a rationale for the motivation of the study.

2.1. The occurrence of chromium

Chromium is considered a heavy transition metal under the d-block in the periodic table. It has an atomic number of 24, and it is chemically symbolized as Cr. It is derived from a Greek name "chroma" meaning colour.

Chromium is one of the earth's most abundant elements (Gad, 2014, Shahid et al., 2017). It is found in the stratosphere due to both anthropogenic activities and natural processes. Some of its attractive physical properties include high resistance to corrosion and discolouration leading to its wide application in industrial activities such as mining operations, steel manufacturing industry, dye, leather tanning (combined with alum to assist in cross-linking collagen fibres), electroplating and textile industries (Gad, 2014) and pigments production (as chrome yellow-$PbCrO_4$) (Sanches et al., 2017). Chrome red ($PbCrO_4$.PbOH) and

chrome oxide green (Cr_2O_3) are the most common dye agents used (Liang et al., 2014).

Like any other transition metal, chromium exhibits a variety of oxidation states, namely +2, +3 and +6 (Hossini et al., 2016). However, the most predominant ones are the trivalent and hexavalent form. The speciation of Cr in solutions is pH and concentration dependent. Figure 2.1 below depicts the pourbaix diagram of chromium speciation at different solution pHs. As illustrated, it is evident that Cr(III) is predominant at highly acidic pH in the form of Cr^{3+} and $Cr(OH)^{2+}$. However only small quantities of Cr(VI) which exists as $HCrO_4^-$ are prevalent at this range. Furthermore, this form tends to be converted to CrO_4^{2-} at basic pHs. This phenomenon is very important in the uptake of Cr(VI) and this is discussed in detail later in Chapter 3.

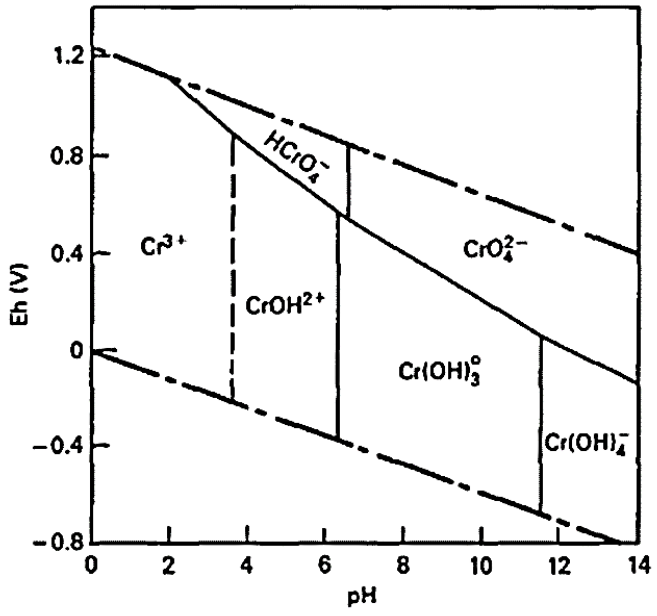

Figure 2.1: Pourbaix diagram of chromium (Cook and Olive, 2012, Rai et al., 1989).

Postulates have indicated that acidic conditions favour the reduction of Cr(VI) to Cr(III) in the presence of an adsorbent (Garg et al., 2007). According to Equation 2.1 predominant dichromate ion ($Cr_2O_7^{2-}$) gets reduced to Cr^{3+}.

$$Cr_2O_7^{2-} + 14H^+ + 6e^- \rightarrow 2Cr^{3+} + 7H_2O, \quad E^0 = 1.33\ V \qquad 2.1$$

However in basic regions less oxidation occurs and chromium species are found as:

$$Cr_2O_7^{2-} + H_2O + 3e^- \rightarrow Cr(OH)_3 + 5OH^-, \qquad E^0 = -0.130\ V \qquad 2.2$$

The plausible explanation for effective removal of Cr(VI) in acidic solutions would be based on the oxidation of $Cr_2O_7^{2-}$ to Cr^{3+}. Since the ions are relatively small sized, they are easily replaced by the positively charged species.

2.2. Toxicity of chromium

As mentioned previously, chromium is found to exist in more than one oxidation state and each form differs in terms of its characteristics and toxicities. It has been accepted and reported that Cr(III) compounds are less toxic than Cr(VI) compounds and that Cr(III) is essential to maintain mammalian biological processes (Shahid et al., 2017). It is therefore noteworthy mentioning that only trace amounts of Cr(III) can be permitted in the body cells (Ohgami et al., 2015, Lansdown, 2014). Although Cr(III) is often prescribed as a dietary supplement, excessive concentrations of the metal destroy the DNA in living cells (Hossini et al., 2016).

Also, the hexavalent form of chromium [Cr(VI)] is considered to possess a genotoxic, mutagenic and carcinogenic character (Hossini et al., 2016, Ohgami et al., 2015). In abundance, it poses a potential hazard to vegetation, marine life and living organisms due to its toxic nature. As a result, long-term exposure to the

metal results in dreadful effects to biological systems with known deleterious health effects such as lung cancer, kidney, liver and gastric damage (Hossini et al., 2016, Gad, 2014). Although the precise mechanisms of Cr(VI) carcinogenicity have not yet been understood. Its genotoxicity has been attributable to the below-listed mechanisms (Hossini et al., 2016):

2.2.1. Production of highly reactive radicals

2.2.2. Cr(VI) can directly bind DNA to form stable Cr-DNA-adducts

2.2.3. Cr(VI) can also bind DNA of the end product of Cr(III) reduction

Given these effects, toxic outcomes of Cr(VI) can be fatal and have led to legislatures setting up controls for the maximum allowable permissible levels limited to 0.05 mg/L (WHO, 2003).

2.3. Fate and transport of chromium

Generally, chromium primarily permeates the environment through improper disposal or seepages from industrial effluents (Mohan et al., 2005, Zewail and Yousef, 2014). The biochemical properties of chromium compounds, particularly Cr(VI) and Cr(III) have necessitated a need to investigate the metal's speciation. The principal concern to study chromium compounds emanates from its potential to act as an oxidant and penetrate biological membranes, in the hexavalent state (Hossini et al., 2016, Garg et al., 2007).

A generalized illustration of stable aqueous chromium species in variable redox conditions is displayed in Figure 2.1. It is evident that the variation in solution pH and concentration affects the speciation of Cr(VI) species in solution. The most predominant forms *viz.* dichromate ($Cr_2O_7^{2-}$), hydrochromate ($HCrO_4^{-1}$) or chromate (CrO_4^{2-}). According to Hossini et al. (2016), there are potentially

considerable factors that contribute to the ionic mobility of chromium compounds. At neutral and alkaline pH, Cr(III) is relatively stagnant. As a result, it gets easily retained, precipitated and subsequently adsorbed on solid surfaces. Contrarily, Cr(VI) is highly soluble thereby making it reasonably mobile prior to its reduction to Cr(III). It has been shown (Silva et al., 2008, Mohan et al., 2005), the mode of removal of Cr(VI) at low pH might be the electrostatic attraction and/ or conversion of Cr(VI) to less toxic form Cr(III) as illustrated by expression 2.3. The other challenge with adsorption of Cr(VI) at high pH is the deprotonation of adsorbent sites and formation of $Cr(OH)_3$ precipitate according to expression 2.4.

$$Cr_2O_7^{2-} + 14H^+ + 6e^- \rightarrow 2Cr^{3+} + 7H_2O \quad (2.3)$$

$$Cr_2O_7^{2-} + 4OH^- + 3e^- \rightarrow Cr(OH)_3 + 5OH \quad (2.4)$$

2.4. Treatment methods for metal ion recovery

Alternative conventional routes, specifically related to metal remediation have been proposed and used to achieve sufficient enrichment and removal of water contaminants from aqueous solutions and these include:

2.4.1. Reverse osmosis

Reverse osmosis (RO) systems involve the diffusion-controlled process of solutes in a solution through a membrane by use of an external applied pressure (Wenten and Khoiruddin, 2016). The technique works on the size and charge exclusion principle. It is mostly used in water desalination and removal of pollutants from water. Lin et al. (2014), reported metal and metalloids removal by a highly concentrated anionic reverse osmosis concentrate. The presence of sulfate ions, on the concentrate, resulted in reduced sorption Cr(VI) capacities due to the competition of sorption sites between anions and target ions. An alternative RO

process was used for the removal of metal pollutants in wastewater samples. This was presented in a study (Cui et al., 2016) where forward osmosis (FO) was coupled with RO and evaluated for the recovery of organics (phenols, aniline and nitrobenzene). Although the methods showed potential for the recovery of the afore-mentioned pollutants in wastewater. It exhibits several disadvantages such as lack of selectivity, the operations employ expensive equipment and high operating costs, membrane fouling and it allows diffusion of small-sized contaminants through the membrane (Wenten and Khoiruddin, 2016).

2.4.2. Ion exchange

Ion exchange is a process comprising of the interchange of either a cationic or an anionic ion on a solid adsorbent (Bochenek et al., 2011). The adsorbent can either be in the form of ion exchangers (either polymeric or mineralic) ion exchange resins (functionalized porous or gel polymer), natural or synthetic zeolites or clay.

Primarily, the ion exchange process comprises of a two-stage operating cycle (saturation and regeneration) (Bochenek et al., 2011). An initial mode of operation assimilates the introduction of a contaminated feed flow into the column inlet and the collection of the purified eluent at the outlet. When the pollutant concentration exceeds the permissible limit, the column becomes saturated. This necessitates column regeneration. The pollutants (in the form of ions) are removed through electrostatic interactions with the ions on the adsorbent (Kołodyńska et al., 2017). Due to relative simplicity, the technique has been widely applied in contaminants' removal from water effluents.

Tor et al. (2005) have proven ion exchange as an effective process to remove chromium ions (both hexavalent and trivalent) from water samples. In another

study, (Korak et al., 2017) an ion exchanger based on a multi-column setup was designed and periodically operated for the regeneration of pilot scale ion exchange columns for Cr(VI) removal. The lateral process required multiple regeneration steps for complete Cr(VI) adsorption. In the search for a suitable process to enhance ion exchange performance, Hua et al. (2017) proposed a promising route which consisted of anionic ion exchanger immobilized on a nano hydrous ferric oxide composite for the simultaneous removal of Cr(VI) and As(V) in wastewater. It was observable that superior recovery was attained by the nano composite than the anionic ion exchanger, especially in the co-existence of other variant anions. This signified lack of selectivity for the target ions by the ion exchange adsorbent. Therefore a need for an alternative sorption process, specifically relating to metal remediation was made clear.

2.4.3. Chemical precipitation

The removal of pollutants from water samples by usage of precipitating agents to recuperate metal ions have been studied. Chemical precipitation, requires the addition of a suitable compound, of the required amount and under proper reaction conditions to precipitate metal ions. Subsequently, the suspended precipitates settle down in solution to remove target contaminants.

According to Sanciolo et al. (2012), the application of flocculants in metal ion recovery seems promising since the process allows not only the remediation but also the agglomeration of other pollutants in large volumes at lower concentrations. Therefore, to enhance the feasibility of reverse osmosis, calcium precipitation was introduced for wastewater treatment. To avoid fouling, the water sample required pre-treatment with alum to eliminate colloidal (from phosphates and magnesium)

and surface particles which inhibit precipitation prior subsequent analyte recovery (Sanciolo et al., 2012).

Lu et al. (2016) investigated chromium removal using electrocoagulation method. Results revealed that the precipitation and co-precipitation of chromium ion resulted *in situ* electro-generated Fe ions in the excessive amounts of sludge produced. In another study, Xie et al. (2017) proposed a one-step Cr(VI) adsorption through reduction to Cr(III) with subsequent *in situ* Cr(III) precipitation. Since the toxicity of trivalent chromium is deemed to be much less than that of the hexavalent form. Therefore, a possible viable alternative approach of recovering chromium from aqueous solution is through reduction of Cr(VI) to Cr(III), followed by subsequent precipitation as $Cr(OH)_3$ (Wang et al., 2016). Generally, the precipitated residues are disposed of in the form of sludge in the landfill. This process is primarily carried out in four steps (Hossini et al., 2016), which involve:

The reduction of Cr(VI) to Cr(III) usually in the presence of electron donor surface groups

2.4.3.1. The resultant Cr(III) ions are precipitated as $Cr(OH)_3$ at highly alkaline pH

2.4.3.2. The insoluble precipitates are allowed to settle

2.4.3.3. Lastly, the generated sludge is disposed of in the landfill.

Although the method has shown effectiveness in the eradication of pollutants from the environment, it also allows the recovery of other species present in solution. In other words, the usage of precipitating agents prompt the generation of secondary waste in the form of sludge which is difficult to treat and dispose of, partial removal of chromium and high operating costs. It has also been indicated that the presence

of manganese oxides can initiate re-oxidation of less toxic Cr(III) to the most toxic Cr(VI) (Rai et al., 1989, Saputro et al., 2014). Barring adsorption, the high cost of equipment and chemicals, toxic sludge generation incomplete removal of the metal ions and poor reusability of adsorbent are some of the disadvantages associated with the methods above. This has, therefore, prompted the need for continued research in removal technologies that are capable, in addition to wastewater purification for metal ion remediation.

2.4.4. Adsorption

Considerable shortfalls of previously discussed conventional methods have instigated the use of alternative techniques for metal ion sequestration in aqueous solutions. Amongst the available techniques, adsorption methods have shown effectiveness in contaminants' recovery from water samples. The process primarily comprises an adsorbent which is commonly applied for water effluent decontamination (Fu and Wang, 2011). Owing to the easy regeneration of sorbent, low energy, and maintenance cost, simplicity and reliability adsorption methods are usually preferred in the application of metal ion sequestration (Rao et al., 2008). Moreover, the technique allows a wide range of low-cost materials as potential adsorbents to be used and incorporated with several other adsorbents. Some of the adsorbents used for trace metal ion remediation include ACs that can be functionalized to improve their selectivity toward target analyte.

2.5. Activated carbon as an adsorbent

Activated carbon is one of the typical adsorbents commonly utilized for the removal of both organic and inorganic pollutants from wastewater. Extensive efforts have been put into the usage of activated carbon for metal ion recovery from aqueous solutions. Seemingly, activated carbons exhibit different properties that

contribute to superior effectiveness such as large accessible external surface area, a microporous structure with visible fractures, high surface reactivity and effective regeneration (Yuen and Hameed, 2009). Due to its susceptibility to be produced from a variety of materials (called precursors) such as almond shell, walnut shell, almond tree pruning and olive stone (González et al., 2009), pinecone (Momčilović et al., 2011), sugar cane (Velasco-Perez and Hiscock, 2013) stalk or stem biomass (Köseoɨlu and Akmil-Başar, 2015) have rendered it a promising adsorbent in adsorption.

2.5.1. Precursors for activated carbon

Due to their significant merits, biomass derivatives raw materials for current conventional methods in water decontamination have been used. These are referred to as carbon sorbent precursors. An ideal adsorbent is characterized by several significant requirements such as abundant availability, regeneration capability, and low-cost and inconsequential release of harmful compounds.

Some other studies have used pristine sorbents such kaolin, bentonite, blast furnace slag and fly ash (Mishra and Patel, 2009) industrial waste (Ahmaruzzaman, 2011), peanut husk charcoal and natural zeolite (Abdel Salam et al., 2011) agricultural waste and by-products (Nguyen et al., 2013). Mishra and Patel (2009) investigated the removal of Pb^{2+} and Zn^{2+} ions from wastewater using activated carbon, blast furnace slag, kaolin, bentonite, and fly ash as adsorbents. Of the materials studied, activated carbon showed superior effectiveness in analyte removal. Similarly, Renu et al. (2017), evaluated the adsorption efficiency of different adsorbents for the recovery of Cr(VI) in solution. The maximum percentage removal attained was 97.80%. The magnitude of adsorption efficiency followed the order of activated

carbon > modified wheat bran > wheat bran > calcined eggshell > eggshell > alumina balls.

Moreover, some of these agro-based materials are used as alternative sources to produce activated carbons. Such materials referred to as precursors. These materials are categorized into three divisions namely: plant materials and bio-sorbents, industrial waste, lastly natural and agricultural waste adsorbents. Advantages of plant-based materials as sources for producing activated carbon over conventional adsorbents include affinity towards metal ions due to available surface binding groups, agricultural origin, easy accessibility, availability, easy processing, application and recovery of the material without unfavourable effects on the environment (Renu et al., 2017).

Some studies have compared the adsorption performance of different adsorbents based on removal efficiencies. Mishra and Patel (2009) reported that 2 g of activated adsorbent could remove 99.6% of Pb^{2+} and Zn^{2+} from 100 mL of 50 mg/L solution at pH 6 with a contact time of 6 hrs. Among the studied adsorbents activated carbon had a higher surface area (655 m^2/g) than other sorbents: bentonite (62.69 m^2/g), kaoline (19.43 m^2/g), fly ash (0.75 m^2/g) and burst furnace slag (0.70 m^2/g) (Mishra and Patel, 2009). However, relatively low adsorption capacities were observed for both Pb^{2+} (6.68 mg/g), and Zn^{2+} (11.24 mg/g) and these were comparable to the performance (94 %) of bentonite with 7.56 m^2/g and 9.52 m^2/g for Pb^{2+} and Zn^{2+}, respectively (Mishra and Patel, 2009). Practically, in search of an efficient adsorbent comparisons should not be based on % recoveries rather adsorption capacity (q_m) values.

It was found by Rai et al. (2016) that mango kernel derived activated carbon demonstrated 100% removal of Cr(VI) from wastewater than tamarind nuts activated carbon (96%) (Suganthi, 2013). Nevertheless, tamarind nuts sorbent revealed higher adsorption capacity (25 mg/g) that mango kernel activated carbon (7.96 mg/g). This suggested that even when the modifying chemical agent (H_3PO_4) is used, adsorption capacities may still vary significantly. As expected, the nature and composition of the raw precursor, experimental conditions, and pre-treatment of adsorbent affected the surface characteristics and final adsorption properties of the adsorbent.

Köseoɨlu and Akmil-Başar (2015) demonstrated the utilization of K_2CO_3 and $ZnCl_2$ to produce chemically modified orange peel activated carbons. A larger surface area was obtained by K_2CO_3 (1352 m^2/g) than with $ZnCl_2$ (804 m^2/g) modification. In contrast, Nayak et al. (2017) reported the production of saw dust based activated carbon examining the influence of activation temperature, reagent type and reaction time. Results indicated a high BET surface area with $ZnCl_2$ (2430 m^2/g), in the same conditions KOH modified activated carbon had a surface area of 1506 m^2/g (Nayak et al., 2017). Practical applications of the optimum adsorbents showed higher adsorption capacity by KOH activated carbon, 1.06 mmol/g and 1.61 mmol/g for Cd^{2+} and Ni^{2+}, respectively. Whereas $ZnCl_2$ adsorbent attained 0.23 mmol/g and 0.33 mmol/g were obtained for Cd^{2+} and Ni^{2+}, correspondingly.

Keeping this view, optimal selection of chemical activating parameters are of great significance in improving the adsorptive performance of adsorbents which can be achieved through surface modification.

2.5.2. Preparation of activated carbon

Similarly to other lignocellulosic derived materials, the basic chemical structure of activated carbon still comprises of cellulose and some lignin backbone. Modification susceptibility of activated carbon is normally used to define and characterize the extent of the material's porosity and surface characteristics (Kwiatkowski and Broniek, 2017).

Therefore, thermo-chemical processes are applied to prepare activated carbons with enhanced surface properties. To date, a variety of alternative methods have been explored to produce desired carbon adsorbents. Brief descriptions of some of the methods are given below:

2.5.2.1. Physical or "thermal" activation

In principle, the preparation of activated carbon by physical treatment involves a two-step process which entails carbonization followed by activation (Kwiatkowski and Broniek, 2017). Initially, the suitable carbon precursor is pyrolyzed under an inert environment with nitrogen or hydrogen as reducing gases. Subsequently, the resultant product is subjected to oxidative gasification at extreme temperatures (usually above 900^{o}C). Oxidizing gases such as O_2, CO_2, air, steam or a blend of the gases are used. The oxidation stage normally produces well developed and high microporous activated carbon.

In the work of Liu et al. (2014), Cu(II) ions were recovered from aqueous solution using fibreboard-based activated carbon using steam activation. The adsorption capacity of 50 mg/g was attained when the activation temperature was 800^{o}C. However, Zhang et al. (2011) reported q_m = 40.22 mg/g for Cu(II) removal by rice husk activated carbon prepared through pyrolysis and steam activation at 700^{o}C.

According to Yuen and Hameed (2009), relative surface heating during activation does not ensure uniform temperature for samples of different sizes and shapes. Thereby, generating thermal gradient from the hot sample surface to its interior. This obstructs the adsorption effectiveness of carbon sorbents (Li et al., 2008). Apart from these drawbacks, the thermal process may require longer reaction times to obtain the desired temperatures. This is often associated with overheated samples and complete combustion of the carbonaceous material.

2.5.2.2. Microwave pyrolysis

Continued development of activated carbon preparation technologies has led to the application of microwave heating as an additional route for carbon sorbents' production. The primary principle operation of microwave treatment entails the direct interaction of matter with electromagnetic radiation. The process mainly operates on internal and volumetric heating (Yuen and Hameed, 2009). Due to this reason, microwave heating allows control over heating process rapid heating from the interior of the body (Dehdashti et al., 2011, Hoseinzadeh Hesas et al., 2013b). As a sample is heated, there is induced thermal gradient arising from the interior of the char material. Thus, leading to quicker reactions and shorter processing time at lower bulk temperature.

Owing to these advantages, quite a number of studies (Dehdashti et al., 2011, Foo and Hameed, 2012, Ferrera-Lorenzo et al., 2014) have reported the application of microwave pyrolysis to produce activated carbons. However, in the case of activated carbon, microwave-induced treatment is mainly associated with the rapid elimination of surface oxygenated functionalities (Menendez et al., 1999).

Hoseinzadeh Hesas et al. (2013a) reported induced acid ($ZnCl_2$) impregnation method applied prior to the carbonization stage saving time and energy. Orange peel based AC was prepared *via* microwave-assisted K_2CO_3 activation (Foo and Hameed, 2012). Their study was based on varying the activation time, impregnation ratios, radiation time and microwave power. Based on their findings, intensifying activation parameters improves the carbon surface area and mesopore ratio.

Hoseinzadeh Hesas et al. (2013b) further elaborated that rapid heating of the material from the interior prevents effective removal of gaseous products (humic and volatile matter) with possible traces of light components remaining inside the sample and pyrolyzer. Thereby, resulting in greater energy consumption and carbon deposition. Although there is potentially considerable effectiveness in an adsorbent generation through microwave energy, relative relevant literature is limited.

2.5.2.3. Chemical activation

Chemical activation also known as wet oxidation mainly involves soaking the raw material with a chemical reagent and subsequent heating under an inert atmosphere. The impregnated sample is exposed to an invariable conventional heating system (usually a furnace) where it is carbonized and activated simultaneously. The preferable chemical reagent acts both as a dehydrator and an oxidant (Hidayat and Sutrisno, 2016). Suitable inorganic additives influence the surface structure of the carbon sorbent through the degradation and dehydration of the cellulosic materials in the carbon precursor (Shi et al., 2016). This technique has attracted great application due to its relative simplicity and wide usage of reagents to prepare adsorbent with desired properties.

Essentially, the size distribution of the adsorbent pores (micro-porosity) and surface functional groups are necessary for the application of the material's end use. Therefore a variety of reagents such as amino compounds, alkaline reagents and inorganic acids have been used to enhance the desired chemical and physical attributes of the material. Compared with conventional approaches, chemical activation offers lower processing temperatures, higher surface areas, single step process, a high degree of micro-porosity and higher carbon yield with reduced tar formation and ash content (Köseoğlu and Akmil-Başar, 2015, Nayak et al., 2017).

2.5.2.4. Activating agents

Concerning chemical activation with mineral acids, the interaction of the carbon surface with the chemical favours the formation of highly developed porous structures and variant surface functionalities (Foo and Hameed, 2012). The introduction of surface functionalities and corresponding changes in physiochemical characteristics can be achieved by carbon oxidation with suitable oxidizing agents.

Mohammadi et al. (2010) prepared Sea-buckthorn based activated carbon (AC) using different chemical reagents, $ZnCl_2$ and H_3PO_4. Both adsorbents had an irregular and porous surface. Their relative surface areas were 1071 m^2/g and 829 m^2/g for zinc chloride and phosphoric acid modified ACs, correspondingly. However, the iodine number adsorption by $ZnCl_2$ activation was slightly higher than that of H_3PO_4 AC. This signified that the chemical activation imparted some porous effect on the adsorbent.

Suganthi (2013) reported that higher values of bulk density and moisture content of H_3PO_4 treated *Tamarind* nuts AC showed the presence of surface oxygen groups.

No further techniques and procedures were used to support the observation. It was explained by Yorgun and Yıldız (2015) that the physicochemical properties of ACs derived from agro-materials strongly depend on optimal experimental conditions. H_3PO_4 activated *Paulownia* wood yielded carbon surface comprising of pores with a tunnel shape and overall honey-comb structure. The honey-comb holes of activated carbon were fully developed with increased porosity and surface groups of acidic character than those previously reported (Suganthi, 2013).

Singha et al. (2013) evaluated the adsorption capacity of granular activated carbon (GAC) treated with different mineral acids, HF, HCl and HNO_3. Nitric acid treated AC demonstrated significantly lower surface area (648.8 m^2/g) comparably to the GAC (777.7 m^2/g). Previously, Foo and Hameed (2012) reported that excess dosage of acid facilitates the formation of an insulating later that prevents further activation of the adsorbent. In their study, Köseoılu and Akmil-Başar (2015) evaluated the structural characteristics of orange peel derived ACs. A significant increase in surface area was observed from the original adsorbent (1 m^2/g) following activation with K_2CO_3 (1352 m^2/g) and $ZnCl_2$ (1215 m^2/g). Practically, both adsorbents had comparable methylene blue adsorption capacity. Therefore, the corresponding activated carbons were essentially microporous.

The activating agent and process promote either the addition or removal of some components such as oxygenated groups. Studies have evaluated the potential of HNO_3 as a chemical activator for different ACs (Qu et al., 2012, Cechinel et al., 2014). Essentially, the adsorption capacity for carbons produced using HNO_3 was higher than the corresponding values produced using KOH (Zubrik et al., 2017) and H_2O_2 (Qu et al., 2012). Given this fact, depending on the nature of the raw precursors, activating agents produce adsorbents with different properties.

2.5.3. Adsorption of Cr(VI) by activated carbon

Since Cr(VI) is relatively mobile it is easily transported in environmental compartments. Most activated carbon sorbents prepared are used to remediate chromium ions from contaminated water. Given that, it is necessary to investigate its aqueous chemistry, speciation and behaviour. In a pH range of 1-6 chromium primary, co-existing forms are $Cr_3O_{10}^{2-}$, $Cr_4O_3^{2-}$ of which $Cr_2O_7^{2-}$, CrO_4^{2-} and $HCrO_4^-$ are most predominant (Silgado et al., 2014).

Studies on the mechanisms of Cr(VI) remediation by activated carbon have been reported. Generally, chromium sequestration can be based on direct adsorption by active sites on carbon surface (Selomulya et al., 1999). Alternatively, the remaining chromium ions diffuse through the micropores on the adsorbent (Bello et al., 1999). This occurs when the active sites attain saturation. Generally, the presence of surface heteroatoms (sulphur, oxygen, and nitrogen) facilitate the interaction between the chromium ions and the electron donating moieties (Mohan et al., 2005). Thereby resulting in significantly decreased Cr(VI) concentration in solution. However, Di Natale et al. (2007) established that surface heteroatoms not only allow direct adsorption of Cr(VI) but considerably promote reduction to Cr(III).

Treatment of activated carbon with mineral acids is known to alter the surface chemistry and properties of the adsorbent. $ZnCl_2$ is one of the prominent agents used to modify ACs. The inclusion of both $ZnCl_2$ and polyvinyl alcohol (PVA) in carbon generated a high concentration of surface functional groups. In turn, this revealed the direct adsorption of Cr(VI) through interaction with surface groups (Yue et al., 2009). The two low-cost adsorbents showed more effectiveness than commercially available activated carbons tested.

Ghosh (2009) observed that waste activated carbon samples undergoing modification with acids (HNO_3 and H_2SO_4) performed better than water treated AC. They observed a remarkable drop in Cr(VI) remaining in solution while the adsorption capacity increased significantly. Furthermore, Ghosh (2009) related the better performance of acid treated adsorbents to an increase in acidic functional groups that aids in the adsorption of more Cr(VI) ions. Similar results were reported by Rai et al. (2016). Mango kernel based activated carbon was modified with H_3PO_4. They also studied the sequestration of Cr(VI) on this adsorbent, and the results indicated effective adsorption of chromium(VI). The highest Cr(VI) uptake was observed at pH 2. This was attributed to the inclusion of oxygen functionalities by H_3PO_4 thus leading to the reduction of Cr(VI) by electron donor groups on the adsorbent surface.

Though modification with mineral acids could enhance the effective removal of Cr(VI), an appropriate concentration is needed to obtain an optimal adsorbent for metal sorption. Preceding Suganthi (2013), Qu et al. (2012) revealed that after modification of activated carbon fiber (ACF) with different HNO_3 concentrations the total surface acidic groups increased. The relative order of magnitude of Cr(VI) sorption followed the order ACF-N-1 % > ACF-N-5% > ACF-N-20% > ACF-N-40%. Initially, the maximum adsorption achieved was 55.2 mg/g (unmodified ACF). The capacity considerably increased to 67.1 mg/g for (ACF-N-1%). It was deduced that the ideal adsorbent was attained with of 1% (v/v) HNO_3 modification. This corroborated that carbon modification with optimal acid concentration significantly improve selective Cr(VI) adsorption.

Literature reports (Saputro et al., 2014, Chen et al., 2015) have shown that the isoelectric point of most carbons at approximately pH2. Moreover, the most

prevalent species of Cr(VI) found near this pH are $HCrO_4^-$, CrO_4^{2-}. In addition, maximum Cr(VI) removal by various adsorbents has been obtained at a highly acidic solution of pH 1.5-3.0 (Pakade et al., 2017, Maneechakr and Karnjanakom, 2017). High mobility and concentration of H^+ at low pH promote the formation of positive hydronium ions such as $–COOH_2^+$, OH_2^+, and $=C=OH^+$. These species encourage improved adsorption through electrostatic interaction. Contrariwise, in highly basic pH there is a build-up of the negatively charged surface resulting in unfavourable Cr(VI) uptake. This was observed and substantiated when humic acids were introduced on the tested bamboo bark-derived AC (Zhang et al., 2015).

Saputro et al. (2014) also reported that the existence of organic matter, particularly humic substances attributes to Cr(VI) reduction to Cr(III). The formed Cr(III) is then eliminated by subsequent sorption and Cr(III)-organic complex formation on the surface. The resultant complexes were found to be insoluble, immobile and unreactive.

Based on the ability of surface oxygen-containing groups to readily reduce Cr(VI) to Cr(III), Pakade et al. (2017) obtained 99% removal of Cr(VI) around pH 1. Although the *Macadamia* derived carbon showed the high removal of hexavalent chromium, only 9% of the total chromium was sequestrated. The probable reason for this trend was due to the transformation of Cr(VI) to Cr(III) at the acidic region. Maneechakr and Karnjanakom (2017) observed the same behaviour on *Combretum quadrangulare Kurz* based AC. A higher degree of Cr(VI) reduction was also observed at pH 1.

To further investigate the underlying mechanisms of chromium adsorption, the present study was undertaken to provide probable routes of Cr(VI) adsorption.

Mechanisms such as particle and film diffusion, incorporating surface reduction of hexavalent chromium to Cr(III) was evaluated. Subsequent adsorption of the *in-situ* resultant Cr(III) by surface-imprinted *Macadamia* activated carbon and Cr^{3+} selective ion-imprinted polymers as potential adsorbents were also explored.

2.6. Imprinted polymers

In general, molecular imprinting can be described as the self-assemblage of functional monomers in the presence of an imprint specie (template). Subsequently, the polymer matrix is polymerized in the presence of excess cross-linker. The product polymer after removal of template creates a specific chemical "memory" complementary of shape and chemical properties of a print molecule (Rammika et al., 2011). Therefore the polymeric structure presents advantages such as selective and discriminative recognition of the target ion and thus capable of its reuptake (Mosha and Mkayula, 2005).

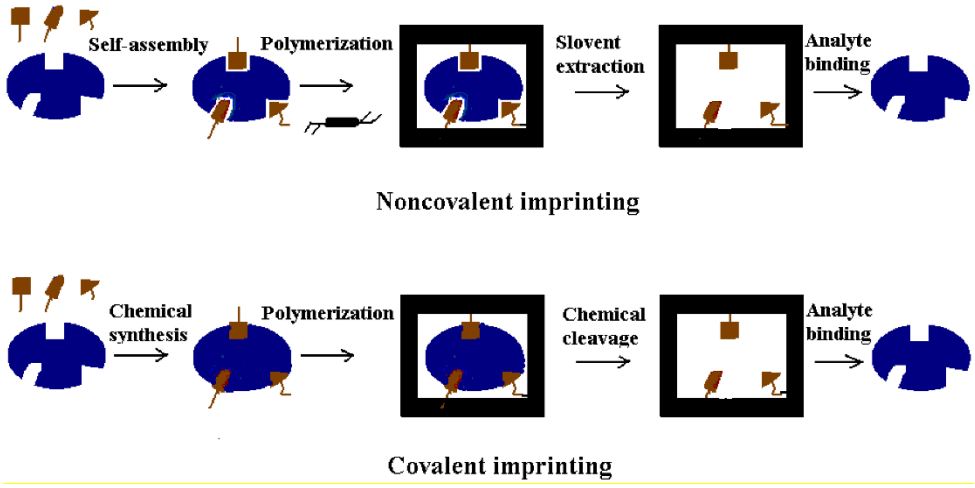

Figure 2.2: Schematic diagram depicting imprinting polymerization (Yan and Ho Row, 2008).

During both the imprinting and rebinding, molecular recognition is driven by either covalent, non-covalent or semi-covalent interactions between the functional monomers and the imprint molecule (Yan and Ho Row, 2008). In the case where the template ion and the functional monomers interact due to ionic bonding, ion-imprinted polymers (IIPs) are formed.

The general approach of molecularly imprinted polymers (MIPs) synthesis is depicted above. The concept of molecular imprinting has been widely explored and applied in various scientific fields such as biology as drug delivery systems (Cunliffe et al., 2005). Since the extraction of analytes from real samples is rather complex. MIP sorbents have been applied for the recovery of biological receptor molecules (Bergmann and Peppas, 2008). Similarly, Yang et al. (2008) synthesized MIP selective to bilirubin, a bioactive molecule found in haemoglobin. β-cyclodextrin was used as an organic functional monomer for selective recognition of the template molecule.

Pre-determined ligand selectivity of chitin-based organic polymer for the adoption of cholesterol was reported by Tong et al. (2011). Xu et al. (2011) have also demonstrated the efficient isolation of trace sulphur drugs in complex meat samples. The prepared MIP sufficiently extracted sulfonamides in pork, liver, and chicken.

Initially, MIP sorbents were targeted for the extraction of organics from matrix samples. The use of MIP for selective adsorption of quercetin forms aqueous solutions has been reported (Pakade et al., 2012). Among the selected flavonols, selectivity studies demonstrated that the MIP still retained specific recognition for quercetin.

For metal ions, the prepared polymers are referred to as ion-imprinted polymers, (IIPs). It is worth noticing that as for IIP, all virtues of MIP are entirely retained (Rao et al., 2006). Nishide et al. (1976) reported the first poly(4-vinyl pyridine) cross-linked meta ion-imprinted resins. The product resins were capable of selective target metal ion sorption in weakly acidic solutions. Since the discovery

of these ion-imprinted polymers (Nishide et al., 1976), their application has increased tremendously. Due to the environmental and biological effects of heavy metals, extensive research has been reported on the enrichment determination of metal ions using IIPs.

Branger et al. (2013) have reviewed developments on metal ion IIPs as potential sorbents for selective recognition of heavy metals at low concentrations. Metal ion IIPs have merits such as predefined selectivity and distinct analyte recognition. These advantages emanate from ligand specificity, metal-complex coordination geometry, exact ionic coordination number, charge and size of the metal ion (Zhang et al., 2010). The prominent properties of desirable polymers are governed by the composition of the reagents involved in synthesis.

2.6.1. Polymerization reagents

The functional complementarity of IIPs is dependent on various factors such as the choice of suitable functional monomers, porogenic solvent, the initiator and the nature of the polymerization method. These determinants affect the physicochemical properties and subsequent performance of the IIPs. Moreover, the selectivity of the IIPs recognition sites also depends on the type of monomer-template interactions in the pre-polymerization stage. Therefore, it is of importance to properly match the template with a desirable monomer in a complementary manner (Yan and Ho Row, 2008). Thus, the imprinting effect and complex formation are substantially enhanced. The presence of monomer units in excess result in unpolymerized monomer fragments and subsequent self-dimerization (Zhang et al., 2010). The nature and amount of cross-linker greatly influence the selectivity and stability of the imprinted polymer. To induce a permanent imprint

memory, 80-90% of the cross-linker is required (Sibrian-Vazquez and Spivak, 2004).

According to Yan and Ho Row (2008), the high degree of crosslinking substrates is important in controlling polymer morphology and serves as a stabilizer for imprinting sites. Lastly, the cross-linking agent imparts mechanical stability on the polymer matrices. In their study, Sibrian-Vazquez and Spivak (2004) developed a new cross-linkers to enhance MIP stability and performance. As for all metal-ion sorbents, the properties of IIPs are tightly linked to their morphology: their shape and porous structure. This is controlled by examining the constitution of the porogenic solvent.

The porogen determines the polymer morphology which, obviously, directly influences the polymer performance. The solvent also governs the strength of ion-template interactions and thus the porous character of the polymer (Cunliffe et al., 2005). In general, porogens of relatively low polarity are chosen as this contributes to reduced interferences during complex formation. Thereby, polymer matrices of high selectivity are obtained. In radical polymerization, polymer formation is propagated by the creation of monomer radicals with a preferable initiator. Normally, the total number of moles of monomer polymerizable double bonds controls the amount of initiator needed (Cormack and Elorza, 2004). The mode of initiator disintegration to form radicals can be activated to suit the nature and method of polymerization.

2.6.2. Approaches in IIPs synthesis

2.6.2.1. Chemical immobilization

This approach involves the immobilization of vinylated ligands in the polymer matrix. The ligand is chemically fixed to the cross-linked polymer. A first study

based on this approach was first reported by Nishide et al. (1976). A metal complex of poly(1-vinyl imidazole), 1-vinyl-2-pyrrolidone and divinylbenzene resin was synthesized.

Another new IIP sorbent was prepared using Pd(II)-iodide/thiocyanate-4-vinyl pyridinium ion with 2-hydroxyethyl methacrylate cross-linked with ethylene glycol diamine methacrylic acid though bulk polymerization (Daniel et al., 2005). Alizadeh et al. (2011) have synthesized Hg(II) IIPs based on 2-vinylpyridine cross-linked polymer. Many other IIPs based on this approach have been synthesized for metal ions such as those of Cr(VI) (Kong et al., 2014), Zn(II) (Behbahani et al., 2014), Cd(II) (Ashouri et al., 2015) and Fe(II) (Mitreva et al., 2017).

2.6.2.2. Trapping

As per the discussion above, chemical immobilization route requires the presence of a vinylated ligand. In trapping, the chelating agent ligand (vinylated or not) is entrapped inside a polymer matrix. In view of this effect, the chelator does not have any polymerizable functional groups. Otero-Romani et al. (2008) demonstrated that some imprinting properties can still be found with non-vinylated ligands. The functionalized vinylated ligands are not commercial and scarce. Therefore, this method has become a popular approach that allows the imprinting of metal complex obtained from vast ligand choices (Tsoi et al., 2012).

2.6.2.3. Cross-linking of bifunctional reagents with linear chain polymers

This procedure incorporates the formation of a linear polymer with a ligand. Metal chelation occurs with more than one ligand functional group. By this means, the ligand can act both as a functional monomer and cross-linker. A mere example of such an agent is 4-vinylpyridine. This method is one of the oldest approaches to prepare IIPs. Following a study by Nishide et al. (1976), Kabanov et al. (1979)

cross-linked a diethyl ester of vinylphosphonic and acrylic acid copolymer with various metal ions. The approach has been applied with natural linear polymers such as cellulose (Lin et al., 2011) and chitosan (Chen et al., 2011).

Cotton linter derived cellulose was dissolved and graft copolymerized with N,N'-methylenebisacrylamide (MBA) as a cross-linker for the subsequent formation of acrylic acid Pb(II) complex (Lin et al., 2011). A similar concept was taken up and applied by Chen et al. (2011) when they synthesized chitosan imprinted particles crosslinked with epichlorohydrin and a series of metal ions *viz.* Zn(II), Ni(II), Cu(II) and Pb(II) as templates.

2.6.2.4. Surface imprinting

Surface imprinting comprises of an amphiphilic functional monomer which forms a complex with a template on the interface of an emulsion. Subsequently, after polymerization and template leaching, the binding cavities are mainly confined to the surface of the material. Silica gel sorbents were modified and activated prior to grafting (Shamsipur et al., 2007). The introduction of silanol groups on the surface facilitated the surface grafting of metal ions. A "grafting from" procedure was initially developed by Shamsipur et al. (2007) where an azo-initiator was introduced on the surface of aminopropyl modified silica particles for selective recognition of uranyl ions. Many other support materials have been used for IIPs surface grafting. Li et al. (2014) prepared surface grafted activated carbon Cu(II)-based IIPs. Ni(II) IIPs were supported on glucose modified carbon spheres (Peng et al., 2015).

Silica gel was grafted by N-(2-aminoethyl)-3-aminopropyltrimethoxysilane (SG-AAPTS) and allyl thiourea as a template metal ion and a functional monomer (Li

et al., 2015). The adsorbent was used for selective adsorption of Cd(II) in aqueous media. Figure 2.3 depicts a summarized diagram of different approaches for IIPs preparation as per the approaches discussed above.

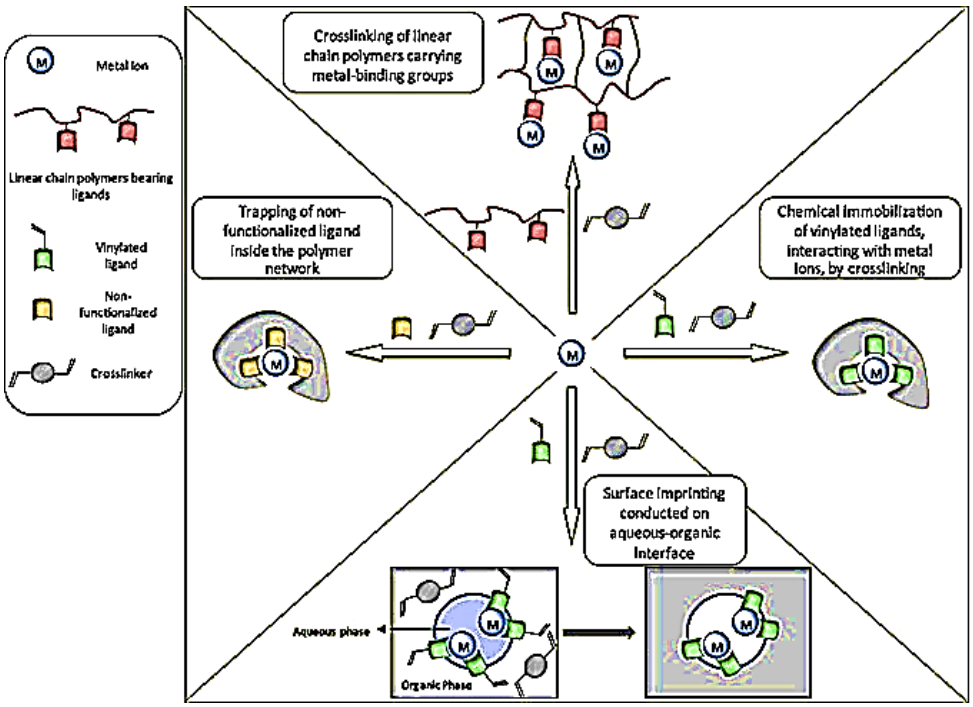

Figure 2.3: Different approaches for IIP preparation (Branger et al., 2013).

2.6.3. Polymerization methods

Normally, metal IIPs are mainly prepared by free radical polymerization. Although this is the case, different polymerization processes yield IIPs of different structures. These aspects are tabulated below as outlined by Branger et al. (2013):

Table 2.1: Methods used in IIP synthesis.

Polymerization method	Particle format
Bulk polymerization	Monolithic, irregular shaped materials
Suspension/emulsion	Well-defined particles
Dispersion/precipitation	Uniformly sized, well-defined particles

Hereafter, the following section specifically outlines the different polymerization techniques in IIP synthesis.

2.6.3.2. Bulk polymerization

By far, bulk polymerization is the most conventionally practiced method for IIP synthesis (Shakerian et al., 2016). The quantity of porogenic solvent used during synthesis is relatively small, thus leading to aggregation of bulky materials. The monolithic particles obtained usually need to be crushed, ground and sieved to attain polymer units of desired sizes (Gama and Bottoli, 2017). This process is regarded as time-consuming, and typically, less than 50% of the ground polymer is recovered (Yan and Ho Row, 2008). Moreover, irregular sized particles are unfavourable for some applications such as in chromatographic separations. Finally, the grinding process destroys binding sites and leads to considerable loss of sorption capacity (Gama and Bottoli, 2017, Yan and Ho Row, 2008). Cu(II) and Cd(II) IIPs were produced using bulk polycondensation to obtain phenol-

formaldehyde (cross-linker) and salicylic acid-formaldehyde based resins. The chosen ligands were chemically immobilized inside the polymer matrix through condensation with the cross-linker (Singh and Mishra, 2009).

Leśniewska et al. (2012) synthesized Cr(III)-pyrrolidine dithiocarbamate (PDC) IIPs using ethylene glycol dimethycralate as a cross-linker. Cr(III)-PDC polymers retain selective adsorption in the presence of other competing ions. The degree of sorption capacity was found in the order: Cr(III) > Fe(III) > Ni(II) > Cu(II). Nevertheless, the polymer particles obtained in these studies still required post-treatment procedures linked to bulk polymerization. For these reasons, efforts have been made to directly obtain beaded IIPs by heterogeneous (suspension/emulsion) and homogeneous (dispersion/precipitation) routes.

2.6.3.3. Homogeneous (precipitation/dispersion) polymerization

In practice, this procedure is closely similar to bulk polymerization. The key difference is the amount of porogen used. Bulk polymerization utilizes a small fraction of the solvent, whereas, in precipitation polymerization, the excess porogen is introduced into the polymerization mixture. This might be the reason the precipitation method is secondly practiced for IIPs synthesis following bulk polymerization method. Precipitation technique presents many attractive properties such as the generation of uniformly shaped, micro-sized particles. Because the polymer matrix formed around the metal ion is less crosslinked, this encourages easier removal of template ion. In addition, the size and particle arrangement is determined by the ratio of monomer-solvent to the stirring rate of the polymerization mixture (Shamsipur and Besharati-Seidani, 2011).

Tajodini and Moghimi (2010) synthesized Co(II) selective IIPs using diazoaminobenzene and vinyl pyridine co-polymers in the presence of ethylene glycol dimethycralate as a crosslinking agent. The polymer was applied in the separation and pre-concentration of Co^{2+} ions in water samples. The imprinted polymer surpassed the non-imprinted (NIP) counterpart in terms of capacity. The adsorption capacities were reported as 205 μmol/g and 58.6 μmol/g, for the Co-IIP and NIP, respectively. This signified that the IIPs had greater template recognition and specificity than the NIP, which is synthesized omitting the template.

Ahamed et al. (2013) used two different functional monomers, 1-vinyl imidazole (1-VID) and 4-vinyl pyridine (4-VP) to prepare N, N′-ethylene bisacrylamide (EBAm) crosslinked polymers. Both the polymers were formed using the same polymerization method. Their findings revealed that metal sorption capacity considerably increased for 1-VID-EBAm (77 mg/g) relative to 4-VP-EBAm (73 mg/g). Homogeneous polymerization has been demonstrated to be another promising route for IIP synthesis. This method was considered rapid and gave a considerable yield of usable particles. The discovery of direct formation of IIPs in microspheres by precipitation method has led to its extensive application in the recovery of metal ions in environmental samples (Shamsipur and Besharati-Seidani, 2011, Tajodini and Moghimi, 2010, Daniel et al., 2005).

2.6.3.4. Heterogeneous (suspension/emulsion) polymerization

This method is rather a simple procedure that yields aggregates of spherical particles. The reaction mixture consists of two non-miscible phases: the continuous and dispersed phase. Typically, the dispersed phase contains the template ion, functional monomer, initiator and the porogen. This liquid matrix is contacted with a continuous aqueous phase. A continuous blending of the polymerization mixture

generates monomer droplets. Subsequently, polymerization is triggered by the droplets from the dispersed phase (Branger et al., 2013). The polymer beads agglomerate as the droplets continue acting as small reactors. This procedure facilitates controlling of size and shape of the generated particles.

This was demonstrated in a study by Ashraf et al. (2011). A heterogeneous emulsion was used to prepare imprinted resins of hydrophilic nature. Methyl methacrylate and phenyl methacrylate monomers and alkyl-oligo (ethylene glycol) surfactant were polymerized to form Zn(II), Cd)II) and Hg(II)-dithiozonate IIPs. Complete removal for up to 80 ppm of Cd(II) and Hg(II) with only 200 mg of imprinted resin was obtained. Imprinting resulted in sites within the tested resin facilitated for metal-ligand bonds to the heavy metals. A water-in-oil-in-water (W/O/W) double emulsion was incorporated with a surface imprinting approach to producing Pb(II) selective IIPs. 1,12-dodecanediolO,O'-diphenyl-phosphonic acid (DDDPA) and 4-vinylpyridine were chosen to be co-functional monomers for lead ions imprinting (Zhu et al., 2011). The technique generated well-proportioned micro beads with diameters ranging from 100-500 μm. Nonetheless, emulsion polymerization sustains drawbacks such difficulties separation of particles and possible contamination by surfactants used.

Conclusively, since IIPs are of highly cross-linked nature; they are robust, stable, durable and can be reused without loss of activity. These properties facilitate their application in extreme conditions that natural systems would not tolerate *viz.* harsh acidic and basic systems, high pressures and temperatures. IIPs are of low-cost to produce, and they can be stored over prolonged times (Rao et al., 2006, Özkara et al., 2011, Branger et al., 2013).

CHAPTER 3

Research objectives

The literature survey conducted from chapter 2 indicated vast applications of different activated carbons (ACs) and ion-imprinted polymers (IIPs) in environmental remediation studies. Both these adsorbents (ACs and IIPs) have been widely used for the sequestration of inorganic and organic pollutants.

3.1. General research objective

The key aim of this study was to prepare acid modified *Macadamia*-based activated carbons and ion-imprinted polymers for simultaneous remediation of Cr(VI) and Cr(III) in aqueous solutions.

3.2. Specific objectives

3.2.1. To prepare carboxylic acid functionalized *Macadamia*-activated carbon using HNO_3 as an activating agent.

3.2.2. To prepare Cr(III) surface-imprinted activated carbons.

3.2.3. To synthesize Cr(III)-IIPs and their respective non-imprinted polymers (NIPs).

3.2.4. To characterize the carbon sorbents and imprinted polymer particles using Fourier transform infrared (FTIR) spectroscopy, Thermogravimetric analysis (TGA), Scanning electron microscopy (SEM), *Brunauer–Emmett–Teller* (BET) and Elemental analysis (EA).

3.2.5. To perform batch adsorption studies by varying solution pH, sorbent dosage, temperature, initial metal concentration and contact time.

3.2.6. To study the selective adsorption of Cr(III) onto the prepared carbon surface grafted sorbent and Cr(III) selective IIPs from aqueous solutions.

3.2.7. To investigate the influence of competing ions on Cr(VI) and Cr(III) adsorption.

3.2.8. To apply the prepared adsorbents for the removal of chromium from simulated acid mine drainage (AMD) sample.

3.3. Research significance

The usage of carbon sorbents for Cr(VI) remediation have been extensively applied. Carbon surface functionalities are known to facilitate the reduction of Cr(VI) to Cr(III) during its adsorption thus substantially leading to incomplete chromium removal. The so-formed Cr(III) can transform to the toxic Cr(VI) if exposed to oxidizing conditions causing recurrence of the problem. Therefore, adsorbents with efficient adsorption of Cr(VI) and selective recovery of Cr(III) ions are sought after. The synergistic incorporation of both adsorbents in simultaneous sequestration of chromium is relatively scarce.

3.4. Hypothesis

Acid-modified AC can be applied to efficiently sequestrate Cr(VI) and thus lead to its subsequent reduction to Cr(III). Moreover, selectively recovery Cr(III) ions can be attained by application of carbon surface-imprinted polymers and Cr(III)-IIPs. The carbon-IIP adsorbent blend can improve the efficiency of complete chromium removal.

CHAPTER 4

Materials and methods

The major intention of this chapter is to elucidate on experimental protocol of the research. A comprehensive outline of the chemical details, equipment used and procedures employed to attain the set research objectives as profiled in Chapter 3 is provided. The experimental procedures of the research were divided into a series of activities given below:

(i) Preparation of HNO_3 modified activated carbons followed by subsequent surface imprinting and the synthesis of Cr^{3+} ion-imprinted polymers and their non-imprinted counterpart.

(ii) Characterization techniques employed for the prepared nitric acid modified *Macadamia* activated carbons (MACs), and the synthesized IIPs/NIPs were: Brunauer-Emmett and Teller (BET) analysis, Fourier transform infrared (FTIR) spectroscopy, elemental analysis (EA), thermo-gravimetric analysis (TGA) and scanning electron microscopy (SEM) analysis.

(iii) Adsorption parameters including, solution pH, initial chromium concentrations, contact time and mass of adsorbent were optimized. The following techniques, flame atomic adsorption (FAAS) spectroscopy, inductively coupled plasma-optical emission spectroscopy (ICP-OES) and ultraviolet-visible (UV-vis) spectroscopy was used to measure metal ion concentration after adsorption. Synthetic wastewater was used to conduct selectivity studies on all the prepared adsorbents.

(iv) Lastly, the demonstration of selectivity through an application of the prepared adsorbents on an acid mine drainage (AMD) simulated sample.

4.1. Chemicals, stock solutions, and equipment

4.1.1. Chemicals

Macadamia activated carbon (MAC) prepared by steam activation was supplied by Innovation Carbon FILTATECH (Johannesburg, South Africa). Chromium(III)chloridehexahydrate ($CrCl_3.6H_2O$), triethylenetetraamine (TETA), *N,N′*-Diisopropylcarbodiimide (DIC) and ethylene diamine tetraacetic acid (EDTA) of analytical grade were supplied by Sigma-Aldrich (Johannesburg, South Africa). Ammonium pyrrolidine dithiocarbamate, acetate buffer (a mixture of CH_3COOH and CH_3COONH_4), acrylamide (AA), ethylene glycol dimethacrylate (EDGMA), 1,1`-azobis (cyclohexanecarbonitrile) and chloroform, were also purchased from Sigma-Aldrich. The leachants used, HNO_3 (65% v/v) and HCl (32% v/v) were from Merck Chemical Company (South Africa).

All solutions were prepared from ultrapure water obtained from Siemans LaboStar equipment (Warrendale, Pennsylvania, USA). Solutions of 0.1 mol/L HCl and sodium hydroxide NaOH, were used for pH adjustments and optimization.

4.1.2. Stock solutions

Precisely 2.8289 g of pre-dried $K_2Cr_2O_7$ (analytical reagent grade) was dissolved in a 1000 L volumetric flask to make a 1000 mg/L Cr(VI) stock solution. A Cr(III) stock solution was prepared by dissolving a pre-weighed mass of $CrCl_3.6H_2O$ (analytical grade reagent) in ultra-pure water. Stock solutions of 1000 mg/L (for selectivity studies of $MACN_{20}$-IIP/NIP and Cr(III)-IIPs/NIPs) of the following salts were used: $NiCl_2$, $CdCl_2$, $CuCl_2$, and $K_2Cr_2O_7$. Working solutions were prepared daily through serial dilutions of the stock solution. All the stock solutions were stored at 5^oC when not in use.

4.1.3. Equipment

pH measurements were monitored using a Hanna HI 220-02 ORP/pH meter equipped with a Hanna HI 1093B pH temperature probe from Hanna Instruments (Chelsea, ME, USA).

Batch adsorption experiments were performed in duplicate on a Multichannel stirrer MS-53 M model Jeio Tech (Seoul, Korea). Adsorbent-adsorbate separation was achieved using A CL10 Centrifuge ThermoScientific (Johannesburg, South Africa). Other relative experiments requiring mixing were performed on an end-over-end Labcon 3100U electrical shaker.

4.1.4. Analytical instruments and characterization

Characterization of the prepared adsorbents and subsequent determination and quantification of the metal ion concentrations were achieved by usage of the analytical techniques whose fundamental details are supplied below.

4.1.4.1. Fourier-transform infrared (FTIR) spectroscopy

The FTIR spectroscopy technique was used for the identification of functional groups in samples. The instrument employed was the Nicolet iS50 analytical FTIR spectrometer (Waltham, MA, USA). The polymer samples and all the carbon derived materials were analyzed using a diamond and germanium accessory, respectively. All spectra were recorded in solid state scanning from 4000-400 cm^{-1}.

4.1.4.2. Thermogravimetric (TGA) analysis

The thermal stability of the prepared materials was examined with PerkinElmer TGA 4000 thermogravimetric analyzer (Waltham, USA). Nitrogen was used as a purge gas at a flow rate of 20 mL/min heating from 30-900^{o}C. This particular technique was used to monitor the stability of the adsorbents over temperature

variation. The changes in sample mass fractions with temperature increase is mainly correlated with the disintegration of the sample's constituents. Resulting in notable weight loss of the analyzed sample.

4.1.4.3. Brunauer, Emmett and Teller (BET) analysis

The surface characteristics of the adsorbents were determined on Micromeritics Flow Prep 060 instrument (Aachen, Germany) and recorded at a temperature pf -196^{o}C. Prior analysis, the samples were degassed in N_2 at 60^{o}C (IIPs/NIPs) and 200^{o}C for both $MACN_{20}$-IIP/NIP MACN, respectively. N_2 adsorption/desorption was applied to assess specific surface areas and pore properties according to the BET method. Following the degassing phase, the surface area, pore volume, and pore size distributions were recorded at 196^{o}C. The BET concept extends to multi-layer gas adsorption which is graphically represented by a plot of $1/[v(p/p_0)-1]$ v/s p/p_0. The BET equation below (Equation 4.1) was used to calculate the specific surface areas of the materials. This was achieved by use of the correlating N_2 adsorption/desorption isotherms within the relative pressure (P/P_0) at a range of 0.01-0.99. The BET equation is denoted below:

$$\frac{p/p_0}{v\,(1-p/p_0)} = \frac{1}{v(p/p_0-1)} = \frac{1}{v_m c} + \frac{c-1}{v_m} * \frac{p}{p_0} \tag{4.1}$$

$$v_m = \frac{1}{(s+i)} \tag{4.2}$$

$$c = \frac{s}{i} + 1 \tag{4.3}$$

where, p is adsorbate pressure, po is adsorbate vapour pressure and v is volume adsorbed, vm is monomolecular layer volume and c is a quantity related to heats of

adsorption and liquefaction. These two constants can be attained from the slope, *s*, and the intercept, *i*, through equations 4.2 and 4.3.

4.1.4.4. Elemental analysis (EA)

The elemental composition of all materials under study was evaluated using a ThermoFlash 2000 series CHNS/O Organic Elemental Analyzer (Michigan, USA). The mass fractions of carbon, hydrogen, nitrogen, oxygen and sulphur were determined. The elemental analysis was achieved by combustion analysis. The sample was heated in excess oxygen in using a programmable controlled oxygen injection. CO_2, H_2O, N_2 and SO_X were accumulated as combustion products. Following the combustion step, the absolute gaseous products were collected and separated as per various traps. The constituents were purified and the elemental constitution was analyzed using a thermal conductivity detector (TCD) to ascertain components.

4.1.4.5. Scanning electron microscopy (SEM) analysis

Analysis by scanning electron microscopy was applied to study the pore formation and surface morphology of the prepared *Macadamia* activated carbons (acid modified and surface imprinted materials) and the ion imprinted sorbents with their corresponding non-imprinted polymers. The samples were mounted in a tightly held specimen holder. The ideal picture was captured and collected from an FEI Quanta 200 SEM microscope (FEI, Hillsboro, OR, USA). The sample was tilted in a chamber to 45° while providing continuous 360° rotation to obtain the optimum images.

4.1.4.6. Ultraviolet-visible (UV-vis) spectroscopy

Quantitative determination of Cr(VI) concentration in the aqueous medium was carried out using a UV-vis spectrometer ($T80^+$) supplied by PG Instruments.

Approximately 2 mL of the liquid samples were mixed with 0.2 mL of 10% (v/v) H_2SO_4 in 15 mL Eppendorf conical tubes where 2 mL of 1,5'-diphenylcarbazide (DPC) (chromogenic agent) was added. The solutions were then mixed. After this, an aliquot was drawn and analyzed for UV-vis analysis at the wavelength of 540 nm (Pakade et al., 2017, Pakade et al., 2016).

4.1.4.7. Atomic absorption spectroscopy (AAS)

Atomic absorption spectroscopy (AAS), AA-7000 dual atomizer model spectrometer from Shimadzu (Kyoto, Japan) was used to determine the total chromium in each sample after adsorption. The measurements were performed in a continuous flame atomizer. A chromium hollow cathode lamp operating at a wavelength of 358 nm and a spectral slit width of 0.2 m was used. Acetylene was used as a purge gas throughout the analysis. The principal concept of flame atomization assimilates the combination of a gaseous sample oxidant with the fuel. In this work, the sample was carried by acetylene and air (fuel carrier gases) followed by subsequent atomization in the flame. Once the sample has reached the flame, three more successive steps in atomization phase occurred. As depicted in Figure 4.1 the sample passes these stages as follows 1. desolvation, 2. volatilization and 3. dissociation. Upon ionization of atomic gas the process may also result in the formation of cations and electrons.

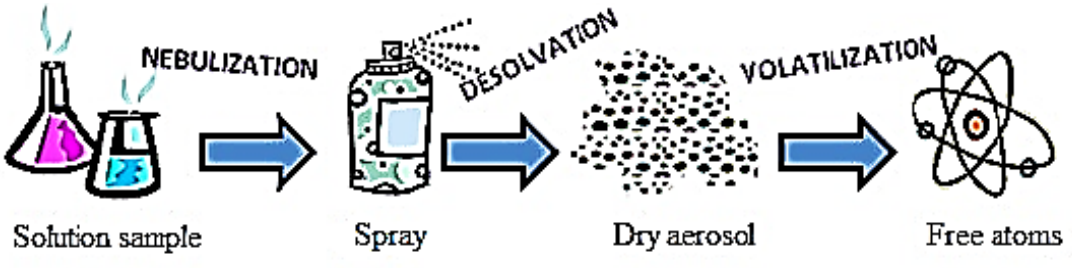

Figure 4.1: Diagram describing the process of atomization for a continuous flame atomizer.

4.1.4.8. Inductively coupled plasma-optical emission spectroscopy (ICP-OES)

An iCAP 7000 series spectrometer from ThermoScientific (Waltham, MA, USA), was used to quantify individual metal ions in multi-element solutions. The sample was drawn using an ASX-520 Cetac auto sampler and delivered to the nebulizer where it was converted into aerosol prior injection into the instrument. The instrumental operating parameters were as follows:

Table 4.1: Operating conditions of the ICP-OES.

Parameter	Instrumental setting
Replicates	3
Plasma Torch	Quartz
Processing mode	Area
Nebulizer	Cross flow
Spray chamber	Single-pass
RF power	1550 W
Coolant gas flow	12 L/min
Nebulizer gas flow	0.45 L/min
Sample pump flow	2 L/min
Auxiliary gas flow	0.50 L/min
Sample aspiration rate	2 L/min

4.2. Preparation of activated carbons

4.2.1. Sample pre-treatment

Macadamia activated carbon (MAC) was kindly supplied by Innovation Carbon FILTATECH (Johannesburg, South Africa. A portion of *Macadamia* nutshell based activated carbon was ground into powdered form and sieved between 45 and 90 μm screens for uniform size distribution. 10 g of MAC was suspended into 500 mL solution of 10 % (v/v) hydrochloric acid. The conical flask was enclosed with parafilm paper and holes were punched onto it to let the vapours escape. The mixture was shaken at 250 rpm on an electrical shaker for 24 h at room temperature to remove impurities and metal ions sorbed on the carbon material. After that, the solution was centrifuged at 2000 rpm for 15 min and the slurry was transferred to a pre-weighed Petri dish and dried in an oven at 110˚C overnight.

4.2.2. Functionalization of treated *Macadamia* activated carbon (MAC)

Pre-treated samples of MAC were contacted with different concentrations of nitric acid as a modifying agent (da Costa Lopes et al., 2015). Briefly, 10 g of the pre-treated MAC was suspended in 250 mL of 20% (v/v) nitric acid under stirring and heating reflux at 60^{o}C for 5 h. The impregnated samples were filtered, washed with distilled water to remove excess activating agent and by-products that may have formed during activation on the surface of MAC, and dried under vacuum at 110^{o}C for 24 h. The dried activated carbons (MAC-COOH derivatives) were then transferred into sealed glass bottles and kept for further characterization and application. The product was labelled $MACN_{20}$. A similar procedure was followed but 40% or 60% (v/v) nitric acid was used instead of 20% (v/v). The resultant materials were labelled $MACN_{40}$ and $MACN_{60}$ corresponding to 40% and 60% (v/v) nitric acid modification, respectively.

4.2.3. Preparation of the Cr(III) imprinted and non-imprinted activated carbons ($MACN_{20}$-IIP/NIP)

The as-prepared $MACN_{20}$ activated carbons in section 4.3 were used to prepare pseudo-Cr(III)-surface imprinted activated carbons as per the procedure described in the previous study by Li et al. (2014) with slight modifications. Approximately, 2.125g of $CrCl_3.6H_2O$ was dissolved in 80 mL of ethanol and 3 mL of triethylenetetramine (TETA) was slowly added to this solution with continuous stirring at room temperature. About 5.0 g of MAC-OOH and 1.0 g of N,N′-diisopropylcarbodiimide (DIC) were also added into the suspension then refluxed for 48 h, the product was recovered by filtration and washed with ethanol.

Lastly, the recovered particles were stirred at a speed of 250 revolutions per minute (rpm) in 100 mL of 0.1 mol/L ethylene diamine tetraacetic acid (EDTA) to remove Cr(III) ions for 10 h. The final product ($MACN_{20}$-IIP) was cleaned with ultrapure water and dried under vacuum at 70°C for 12 h. The non-imprinted ($MACN_{20}$-NIP) sorbent was prepared using an identical procedure without adding $CrCl_3.6H_2O$. The above method involved no addition of crosslinker monomers that would have allowed for formation of cavities in solution, hence, it was termed pseudo-imprinting because the added template ions created unique ligand rearrangements to favour Cr(III) uptake.

4.3. Synthesis of ion-imprinted polymers for Cr(III) recovery

A method adapted from Leśniewska et al. (2012) was used for the preparation of Cr(III)-IIP. To this effect, the ion-imprinted polymer of chromium-pyrrolidinedithiocarbamate-acrylamide (Cr-PDC-AA) was prepared in two steps:

(i) formation of a binary complex of Cr(III)–PDC

(ii) copolymerization of the formed binary complex with acrylamide and ethylene glycol dimethacrylate (EGDMA).

Cr(III)-ammonium pyrrolidinedithiocarbamate (APDC) complex was prepared by slowly adding a chromium solution (10 mL of 2 mg/L) to a buffered (acetate buffer, pH 4.6) APDC solution (20 mL, 0.1 mol/L) and stirred at 60°C for 1 h. The formed complex was filtered, washed with ultrapure water to remove excess ligand, and dried in the oven. The imprinted polymer was prepared by dissolving the Cr(III)–PDC (0.05 g) complex in 2 mL of chloroform, followed by addition of acrylamide (AA) (1.4 g, 20 mmol) functional monomer, ethylene glycol dimethacrylate (EGDMA) (2.8 mL, 15 mmol) cross-linking agent and 1,1`-azobis(cyclohexanecarbonitrile) (50 mg) initiator. The polymerization mixture was transferred into a glass polymerization flask (250 mL), purged with nitrogen for 10 min, sealed and heated at 80°C for 12 h. The non-imprinted polymer (NIPs) were synthesized in a similar manner, but no Cr(III) was added.

After polymerization has stopped, the solid IIPs and NIPs formed were crushed, washed with dichloromethane and ethyl acetate to remove excess of reagents, dried at room temperature and ground to a desirable particle size using mortar and pestle. The imprinted Cr^{3+} ions were leached from the Cr-PDC-AA polymer grains by stirring with and 3 mol/L and 6 mol/L solutions of HCl and HNO_3 several times, respectively. The resultant ion-imprinted polymers (IIP) and its control polymers (CP) were filtered, rinsed with ultrapure water, dried at room temperature and sieved. The resultant filtrate was retained for metal ion analysis. The particles were subjected to a fresh leachant solution (same volume and concentration) in repeated cycles until the chromium content was almost undetectable.

4.4. Batch adsorption experiments

4.4.1.Optimization of experimental parameters for chromium adsorption

Adsorption studies investigating the effect of pH were performed varying the pH (1, 2, 3, 5, 7 and 9) while other parameters such as stirring rate (150 rpm), solution volume (30 mL), initial chromium concentration (100 mg/L), adsorbent dosage (1.67 g/L) and contact time (120 min) were kept constant. The range investigated for adsorbent mass was (0.05, 0.1, 0.2, 0.4, 0.8, and 1.2 g) contact time was (10, 30, 60, 120, 360, and 480 min) and for initial concentration was (50, 100, 150, 200 and 300 mg/L). In all the optimization experiments a similar procedure was followed where all other parameters kept constant barring the parameter that is being optimized. All experiments were conducted in duplicate and the reported results are averages. The adsorption capacity, q_e and percentage removal (% R) were calculated using Eq. 4.4 and 4.5, respectively.

$$qe = \frac{(C_0 - C_e) \times V}{M} \tag{4.4}$$

$$\% R = \frac{(C_o - C_e)}{C_o} \times 100 \tag{4.5}$$

where, q_e is adsorption capacity (mg/g), C_o and C_e are initial and equilibrium concentration (mg/L) respectively, M is the adsorbent dosage (g) and V is the volume of solution (L).

4.4.2. Selectivity studies on the adsorption of Cr(III) by IIPs

Binary mixtures of other cationic species namely Ni^{2+}, Cd^{2+}, Cu^{2+} and Cr^{6+} were used to investigate the selectivity of Cr^{3+} by IIPs. Stock solution (1000 mg/L) was prepared by dissolving appropriate mass fractions of the salts: $NiCl_2$, $CdCl_2$, $CuCl_2$ and $K_2Cr_2O_7$ in ultra-pure water. Working and standard solutions were prepared by serial dilution of the stock solution. The remaining metals' concentration were

determined using ICP-OES. The obtained results were used to determine the distribution ratios, the selectivity coefficients and the relative selectivity coefficients of Cr^{3+}, Cr^{6+}, Ni^{2+}, $Cd^{2+}$and Cu^{2+} through the application of equations listed below:

The distribution coefficient, K_d is given as

$$K_d = \frac{(C_o - C_e)V}{C_e\ M} \tag{4.6}$$

where, K_d is the distribution coefficient (L/g) and the other parameters are as described by equation 4.4. Equation 4.7 below was used to calculate the selectivity coefficient of Cr^{3+} ions in the presence of the aforementioned competing cations.

$$K = \frac{K_d\ (Cr^{3+})}{K_d\ (B)} \tag{4.7}$$

where, K is the selectivity coefficient and B represents the competing cation mentioned above. The value of K is an important factor in selectivity studies. It indicates how selective the polymer is towards its template ion (Cr^{3+}). K values higher than 1 suggest that the template ions were selectively adsorbed by the IIPs. Whereas if K=1, suggests that both the Cr^{3+} and the competing ions are equally bound to the polymers.

The enhanced imprinting selectivity effect and affinity of the template ion by the polymers is indicated by K'. This is calculated as follows:

$$K' = \frac{K_{IIP}}{K_{NIP}} \tag{4.8}$$

where, K_{IIP} and K_{NIP} represent the selectivity coefficients of IIPs and NIPs, respectively.

4.4.3.Application of pseudo-$MACN_{20}$-IIP/NIP to real samples

The synthetic acid mine drainage (AMD) sample was obtained from wetland crust. The sample was dissolved in ultra-pure water, treated and stored in accordance to published methods (Rajesh et al., 2008). The sample pH and conductivity were measured befortoe the application of pseudo-$MACN_{20}$-IIP to the mine decant. The metal composition of the sample was determined using ICP-OES in duplicate. The recovery of Cr(III) from the AMD sample was then performed in batch mode.

The mine drainage pH was adjusted to 5 for optimal removal of Cr(III) and subdivided into three portions of 100 mg/L. The samples were spiked with 10, 15 and 30 mg/mL of Cr(III) solution. Batch adsorption experiments were done in duplicates. In this effect, 30 mL of each sample was added to 0.1 g of $MACN_{20}$-IIP and stirred for 4 h at room temperature. All solutions were analyzed for metal ion content using ICP-OES. The same procedure was adopted for the corresponding $MACN_{20}$-IIP. The solutions were also subjected to the same treatment (described above) with the AMD water sample.

4.5. Simultaneous adsorption of Cr(VI) and Cr(III) by $MACN_{20}$ and pseudo-$MACN_{20}$-IIPs

To investigate the recovery of chromium in both oxidation states (as Cr^{6+} and Cr^{3+}), different compositions of adsorbent phases were chosen.

Stock solution (1000 mg/L) of Cr(VI) was prepared by dissolving an appropriate mass of the Cr salt in 1 L of ultra-pure water. Working standard solution of Cr(VI) (100 mg/L) was prepared through serial dilution of the stock solution. To investigate the concurrent uptake of chromium species 0.2 g of $MACN_{20}$ and pseudo-$MACN_{20}$-IIP was stirred with 30 mL of the Cr(VI). The same procedure was done with $MACN_{40}$ and $MACN_{60}$. The initial pH of the solution was adjusted to that optimized above. After 240 min. The solution was centrifuged and the

filtrate was analyzed for Cr(VI) and Cr(III) content with UV-vis spectroscopy and FAAS, respectively.

In parallel to the above method, 30 mL of Cr(VI) solution (100 mg/L) was stirred with 0.2 g $MACN_{20}$, $MACN_{40}$ and $MACN_{60}$, respectively. After 120 min. The mixture was filtered and the supernatant was analyzed for both Cr(VI) and Cr(III) content. The pH after adsorption was measured and adjusted to the optimum to favour the uptake of Cr(III). Pseudo-$MACN_{20}$-IIP was added to the solution and adsorption was continued for a further 120 min. Afterward, the solution was filtered and the concentration of Cr(VI) and Cr(III) was examined. The same method was carried out using IIPs instead of pseudo-$MACN_{20}$-IIP.

4.6. Kinetic models

Pseudo-first-order (PFO) and pseudo-second-order (PSO) rate models were used to analyze the kinetic data of the adsorption process in order to infer on rate controlling step and adsorption mechanism. The PFO rate equation (also, known as Lagergren equation) and the PSO kinetic model (Ho and McKay, 1999) are represented in Equations 4.9 and 4.10.

$$q_t = q_e(1 - exp^{k_1 t}) \tag{4.9}$$

$$q_t = \frac{tk_2.q_e^2}{(1 + k_2 t q_e)} \tag{4.10}$$

where, q_t (mg/g) is the adsorbate sorption capacity at time t, k_1 (1/min) is the PFO rate constant of adsorption and k_2 1/[g (mg/min)] is the PSO rate constant of adsorption.

4.7. Adsorption isotherms

Two well-known adsorption isotherms, Langmuir and Freundlich, describing adsorbent-adsorbate interaction phenomena were used to fit in the adsorption data

to deduce the removal mechanism. The Langmuir model assumes a monolayer coverage of a homogenous adsorbent surface by the adsorbate (Langmuir, 1918) and nonlinear Langmuir isotherm equation is given below.

$$q_e = \frac{q_m b C_e}{(1+bC_e)} \quad (4.11)$$

where, b the Langmuir isotherm constant (L/mg) related to energy of adsorption, q_m is the maximum metal uptake (mg/g), q_e and C_e as previously described. The dimensionless parameter, R_L, also known as the equilibrium parameter or separation factor is given by Equation 4.12 (Weber and Chakravorti, 1974) was calculated and used to interpret adsorption conditions from the Langmuir isotherm.

$$R_L = \frac{1}{(1 + bC_o)} \quad (4.12)$$

The R_L parameter gives information on the nature of adsorption, where $0<R_L<1$ is regarded as favourable adsorption, $R_L>1$ is unfavourable, $R_L = 0$ is irreversible and $R_L = 1$ implies linear adsorption (Weber and Chakravorti, 1974). The Freundlich model relates the sorption of adsorbate to heterogeneous surfaces and it assumes multilayer adsorption (Freundlich and Heller, 1939). The equation is given below.

$$q_e = K_F C_e^{1/n} \quad (4.13)$$

where, K_F is the Freundlich constant (L/g) and n_F the Freundlich exponent describing biosorption capacity and biosorption intensity, respectively.

4.8. Intra-particle diffusion

Equation 4.14 proposed by Weber and Chakravorti (1974) was used in this study in order to gain insights into the mechanism and the rate controlling steps for the adsorption of Cr(VI) by the different ACs.

$$q_t = k_d t^{0.5} + C \quad (4.14)$$

where, k_d (mg/(g $min^{0.5}$) is the intra-particle diffusion rate constant and C (mg/g) is the intercept representing the boundary layer thickness. Plots of q_t vs $t^{0.5}$, intra-particle diffusion is the only rate-limiting step if a plot of q_t vs $t^{0.5}$ yields a straight line that passes through the origin (Poots et al., 1976). Tseng and Tseng (2005) stated that the adsorption of an adsorbate on a porous adsorbent surface could take place through film diffusion (external mass transfer) and/ or the intra-particle diffusion.

CHAPTER 5

Results and Discussion

In this Chapter, the ability of ACs to remediate Cr(VI) and Cr(III) at ppm levels is examined as per the experimental procedures discussed in Chapter 4. The adsorption efficiencies of functionalized and unfunctionalized ACs, surface imprinted carbons and Cr(III)-IIPs and their respective NIPs are compared and discussed. Subsequently, the prepared adsorbents are variably combined and evaluated in the simultaneous adsorption of Cr(VI) and Cr(III) in aqueous solutions. The influence of critical adsorption parameters such as solution pH, initial adsorbate concentration, contact time and mass of adsorbent were studied. Finally, kinetic modelling and adsorption isotherms were used to describe the adsorption processes and predict mechanisms of adsorbate-adsorbent interactions.

5.1. Functionalized and unfunctionalized ACs

5.1.1. Characterization of adsorbents

5.1.1.1. Elemental analysis and BET measurements

Table 5.1 shows the percent C, H, N and O content for MAC, $MACN_{20}$, $MACN_{40}$ and $MACN_{60}$. The ultimate analysis revealed that *Macadamia* based activated carbon derivatives are very carbonaceous as depicted by high carbon content of about 80%. HNO_3 modification attenuated the % C from 78.09 to 73.43% as nitric acid concentration was increased from 20 to 60% (v/v). Relatively low nitrogen compounds were detected on MAC (0.77%), subsequent treatment with different concentrations of HNO_3 yielded materials with nitrogen contents of 1.46% ($MACN_{20}$), 1.70% ($MACN_{40}$) and 1.69% ($MACS_{60}$). HNO_3 treatments seemed to strip away the H atoms from MAC as H_2 gas due to their hydrating nature. The

increase in oxygen content avowed that treatment of MAC with inorganic acid oxidized its surface to produce oxygenated functional groups like COOH, C=O, C-O-C. Virgin MAC had a BET surface area of 549.72 m^2/g which increased slightly to 583 m^2/g upon treatment with 60% (v/v) HNO_3. BET surface area values of 600-1500 m^2/g for *Macadamia* nut endocarp based (ACs) have been reported in the literature (Pezoti Junior et al., 2014, Dejang et al., 2015). Modification with nitric acid resulted in an increase of %N as the concentration of HNO_3 increased. Less nitrogen content was detected on MAC but treatment with different concentrations of HNO_3 yielded materials with nitrogen contents of 1.46% ($MACN_{20}$), 1.70% ($MACN_{40}$) and 1.70% ($MACN_{60}$). The presence of nitrogen proved incorporation of amino compounds on MAC. All the studied ACs exhibited mesopores according to IUPAC definition because pore size diameter was greater than 2 nm.

Table 5.1: Elemental analysis and BET measurements of activated carbons.

	Ultimate analysis				Surface characterization		
Adsorbent	%C	%H	%N	%O*	Pore volume (cm^3/g)	BET Surface area m^2/g	Pore size (nm)
MAC	84.51	5.45	0.77	9.27	0.354	549.72	2.590
$MACN_{20}$	78.09	1.35	1.46	19.10	0.369	565.23	2.640
$MACN_{40}$	74.86	1.47	1.70	21.97	0.373	581.61	2.670
$MACN_{60}$	73.43	1.48	1.69	23.40	0.388	582.94	2.533

*Computed by a difference

5.1.1.2. Fourier transform infrared (FTIR) spectra

The FTIR spectra of MAC, $MACN_{20}$, $MACN_{40}$, and $MACN_{60}$ are shown in Figure 5.1. The spectra show similar characteristics, but signal attenuation and appearance

of new peaks as a result of modification were observed. The notable differences (deformation, shifts and intensities) in MAC, $MACN_{20}$, $MACN_{40}$ were observed at the following wavenumbers, 2851, 2380, 1829, 1625, and 1107 cm^{-1}. This could be attributed to the presence of OH group and the overlapping of the sp^2 hybridization, carboxyl group (COOH), methoxyl group (C-O-CH_3), hydroxyl (C-OH) bending of phenolic structure in the lignin (Pakade et al., 2016) and –C-O functional groups, respectively.

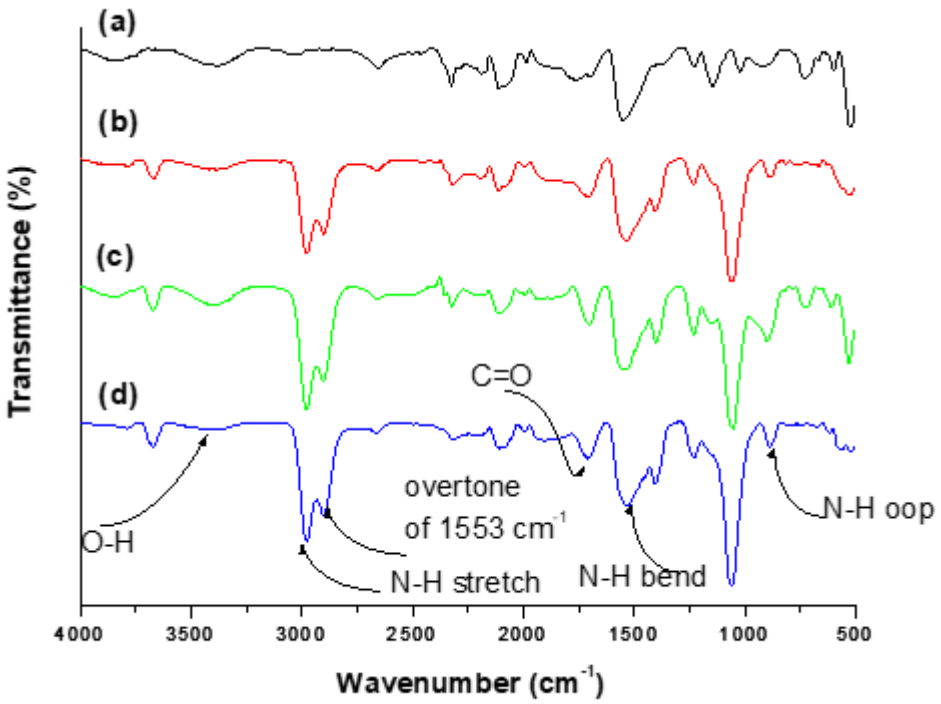

Figure 5.1: FTIR spectra of MAC (a), $MACN_{20}$ (b), $MACN_{40}$ (c) and $MACN_{60}$ (d) adsorbents before adsorption.

The spectra showed similar backbone typical of activated carbons based on *Macadamia* nutshells. On closer inspection, it could be observed that all the adsorbents spectra displayed a broad band at 3400 cm^{-1} attributable to bonded OH^- functional group (Pezoti Junior et al., 2014). Also, a peak at 1366 cm^{-1} attributable to C-O of the carboxylic group was observed in MAC and $MACN_{20}$ spectra even

though it was diminished in $MACN_{20}$. However, this band together with a shoulder band at 2456 cm^{-1} were absent in $MACN_{60}$. This may suggest different surface characteristics of the material as the HNO_3 concentration was increased. The in-plane vibration of N-H at 1000 cm^{-1} was enhanced by acid treatment which could imply the introduction of amine groups by acid treatment. This correlates to an increase in nitrogen content as illustrated in Table 5.1. Furthermore, there was a peak at 1690 cm^{-1} in MAC but this peak diminished in $MACN_{20,}$ $MACN_{40}$ and $MACN_{60}$. After the modification process, the formation and disappearance of several peaks were observed. This could avow the breaking of chemical bonds (such as C=C) in the raw material subsequently leading to oxidized MAC surface (Pezoti Junior et al., 2013).

Additionally, the peak at 1379 cm^{-1} in MAC became more pronounced and shifted to higher intensities *viz.* 1496, 1404 and 1412cm^{-1} in $MACN_{20,}$ $MACN_{40}$ and $MACP_{60}$, respectively. These observations led to a deduction that during heating of MAC in the presence of nitric acid, carboxylic acid groups reacted with adjacent hydroxyl groups to form ester linkages.

5.1.1.3. Thermogravimetric analysis

Thermogravimetric analysis (TGA) and derivative thermogravimetric analysis (DTA) of MAC, $MACN_{20}$, $MACN_{40}$, and $MACN_{60}$ were conducted to evaluate the stability and decomposition patterns as a function of temperature. The thermograms are displayed in Figure 5.2(a-b). It can be observed that the pristine carbon exhibited a different decomposition pattern compared to oxidized carbons in both Figure 5.2a and b. All carbons in Figure 5.2a shared a distinct degradation peak around 120ºC associated with loss of moisture content estimated to about 10, 4.5, 5 and 3% for MAC, $MACN_{20}$, $MACN_{40}$ and $MACN_{60}$, respectively. The

higher moisture content in MAC could be due to the presence of hydroxyl groups on the surface of carbon which in turn attract water via the hydrogen bonding (Azwa and Yousif, 2013).

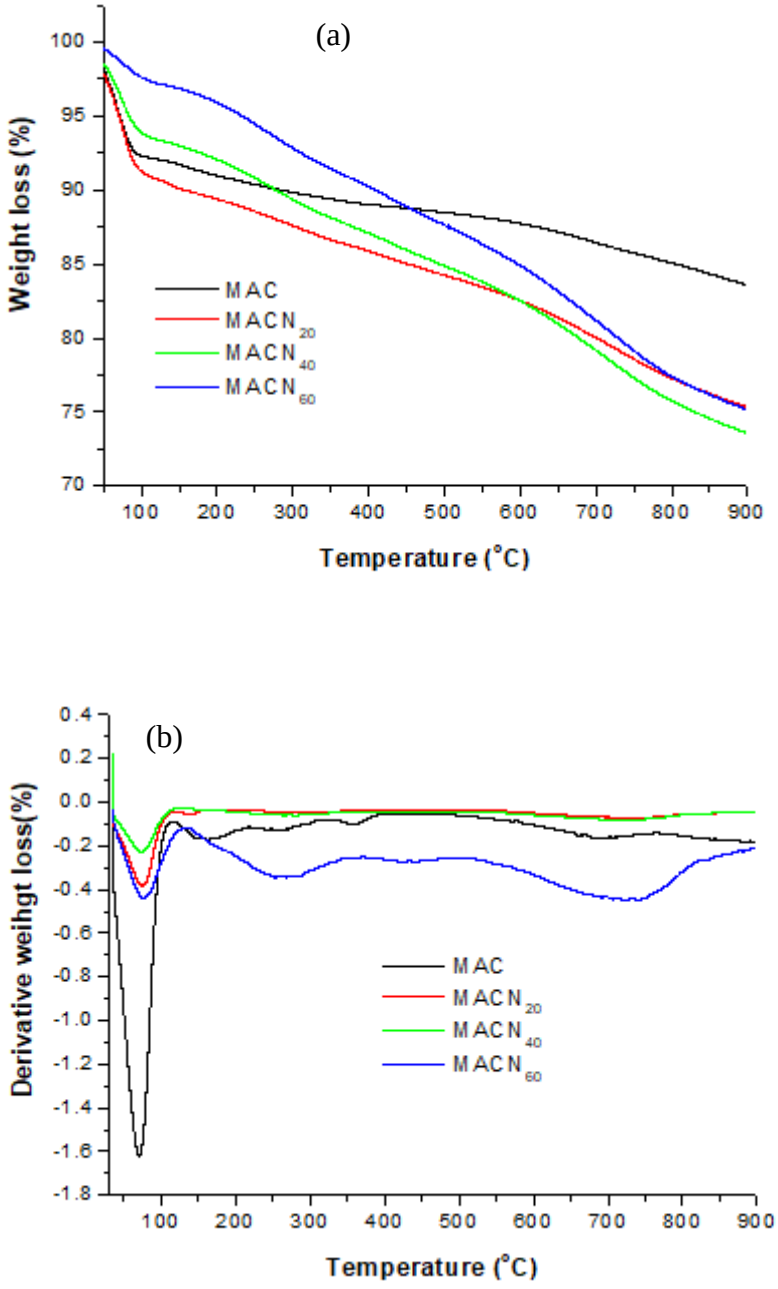

Figure 5.2: TGA (a) and DTG (b) of MAC, $MACN_{20}$, $MACN_{40}$, and $MACN_{60}$.

Treatment of the native MAC with acid solutions led to the extraction of water-associating functional groups resulting in less moisture content and greater thermal stability. The residue content was above 75% in all carbon materials.

5.1.1.4. Scanning electron microscopy (SEM) analysis

Scanning electron microscopic images for $MACN_{20}$, $MACN_{40}$, and $MACN_{60}$ are shown in Figure 5.3a-c. The SEM images of $MACN_{20}$ were similar to those of pristine *Macadamia* activated carbon (MAC) reported by Dejang et al (2015) implying that 20% (v/v) nitric acid did not alter the pristine carbon properties greatly.

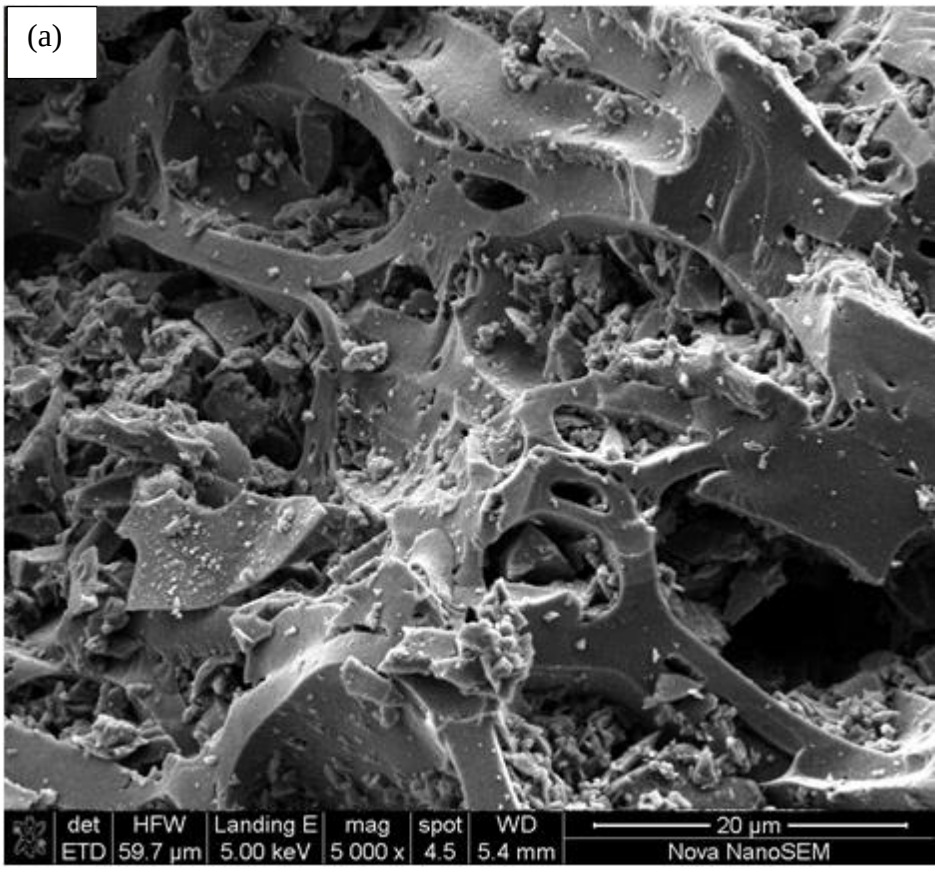

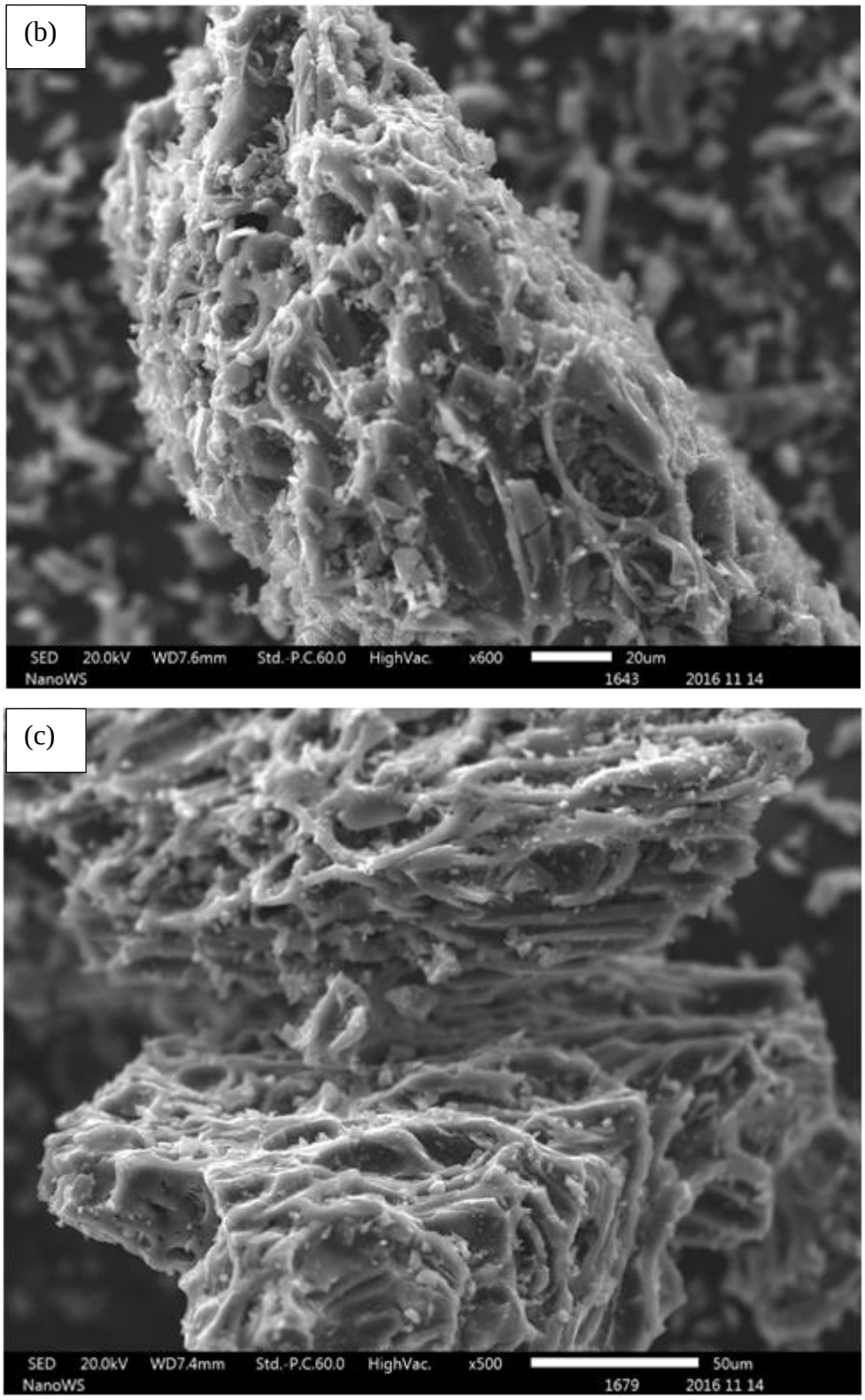

Figure 5.3: Scanning electron microscopy images for $MACN_{20}$ (a), $MACN_{40}$ and (c) $MACN_{60}$.

However, observations revealed that the nitric acid treatment of ACs resulted in materials with visible porosity (Figure. 5.3a-c). On closer inspection, it can be seen that the pore structure and size were different. $MACN_{40}$ possessed somewhat elongated pores, $MACN_{60}$ exhibited uniform elongated pores with a nest-like morphology. These observations showed that the different concentrations of HNO_3 produced materials with different physical attributes.

Figure 5.3a for $MACN_{20}$ depicts a rougher texture with small pores, and Figure 5.3b displays a nest-like type of pores and Figure. 5.3c shows disruption and widening of pores. The changes in pore structure and pore volume could be attributed to the increased strength of the activating agent. The higher concentration of HNO_3 led to a rupture of the cell walls and eventually breaking of surface groups. Therefore, the optimum concentration of activating agent needs to be used to prevent damaging the surface characteristics of the adsorbent. Too high concentrations may result in the extraction of the binding functional groups rendering the adsorbent poor for adsorption.

5.1.2. Adsorption studies

5.1.2.1. Effect of solution pH on Cr(VI) adsorption

The effect of solution pH on the adsorption of Cr(VI) by $MACN_{20}$, $MACN_{40}$ and $MACN_{60}$ are shown in Figure 5.4. It was observed that the % removal of Cr(VI) decreased as the pH was increased from pH 1 to 9 and the highest percent removal was at pH 1. Below pH 2 MACN adsorbents had the highest % removal. Modification of MAC with HNO_3 imparted some amide groups on the surface of activated carbon as demonstrated in Table 5.1. This was credited by a considerable increase observed in the % N content comparably for virgin MAC (0.77 %) and MACN (1.70 %) upon acid modification. The higher % removal of Cr(VI) by

HNO_3-modified carbons implied that chromium had a greater affinity for nitrogen-based ligands. This can be explained on the basis of hard-base and hard-acid relationship. Chromium is a hard acid while nitrogen is a hard-base. Therefore, the interaction between the two species is favourable. Besides, the protonation of amino groups at lower pH allowed for electrostatic interactions with the anionic Cr(VI) species is expected.

Cr(VI) may exist in different ionic forms such as chromate (CrO_4^{2-}), hydrogen chromate ($HCrO_4^-$) or dichromate ($Cr_2O_7^{2-}$) at different pH values and concentrations. The hydrolysis reaction of dichromate ion ($Cr_2O_7^{2-}$) at low pH often yield $HCrO_4^-$ which then becomes the most predominant Cr(VI) species in acidic conditions. However, an increase in pH causes $HCrO_4^-$ equilibrium to shift towards producing CrO_4^{2-} and $Cr_2O_7^{2-}$ species. At low pH, the negatively charged species (dichromate/chromate) electrostatically bind to the positively charged functional groups on the surface of the AC. At low pH the surface of the AC possesses more positively charged functional group due to protonation (e.g., $-COOH_2^+$ or $-RNH^+$). It has been suggested that treatment of ACs with mineral acids impart positive hydronium ions like $-COOH_2^+$, $-OH_2^+$, and $=C=OH^+$ on the surface of modified carbons which then act as adsorption sites for electrostatic attraction of Cr(VI) anions leading to higher removal (Park et al 1999; Valdes et al 2002). Also, elemental analysis (Table 5.1) showed an increase in %N in HNO_3 modified ACs indicating a presence of amino groups on the surface of MACN which could be protonated at low pH resulting in the electrostatic attraction of anionic Cr(VI) species. Hence, the mode of removal of Cr(VI) at low pH might be the electrostatic attraction and/or conversion of Cr(VI) to less toxic form Cr(III) as illustrated by expression (i) (Silva et al., 2009).

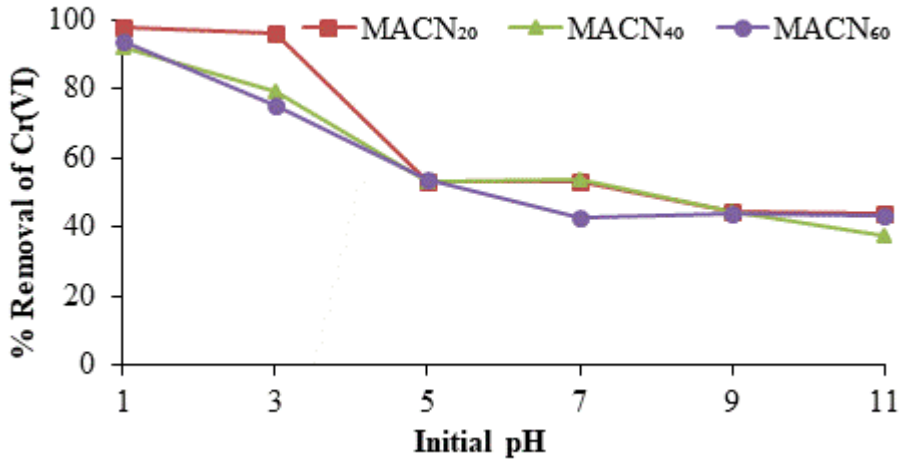

Figure 5.4: Effect of solution pH on Cr removal by $MACN_{20}$, $MACN_{40}$ and $MACN_{60}$ (conditions: solution concentration 100 mg/L amount of adsorbent 0.1 g; solution volume 30 mL; contact time 2 h).

At higher pH Cr(VI) anions tend to compete for adsorption sites with OH- ions used to modify the pH (Yavuz et al., 2007). The other challenge with adsorption of Cr(VI) at high pH is the deprotonation of adsorbent sites and formation of $Cr(OH)_3$ precipitate according to expression (ii) (Silva et al., 2009).

$$Cr_2O_7^{2-} + 14H^+ + 6e^- \rightarrow 2Cr^{3+} + 7H_2O \quad \text{(i)}$$

$$Cr_2O_7^{2-} + 4OH^- + 3e^- \rightarrow 2Cr(OH)_3 + 5OH \quad \text{(ii)}$$

5.1.2.2. Effect of adsorbent mass on Cr(VI) adsorption

The effect of adsorbent mass for $MACN_{20}$, $MACN_{40}$ and $MACN_{60}$ is shown in Figure 5.5. The percent removal for Cr(VI) increased as the adsorbent mass was increased from 0.01–0.32 g for all adsorbents. The percentage removal for Cr(VI) increased from 3.40 to 99.41% for $MACN_{20}$, 3.43 to 99.49% for $MACN_{40}$ and 6.85 to 98.76% for $MACN_{60}$ as the masses were increased from 0.01–0.32 g.

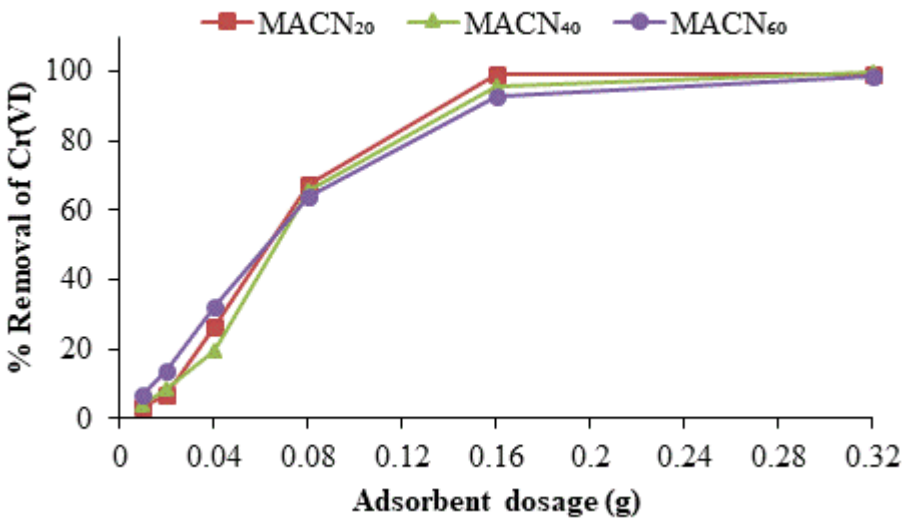

Figure 5.5: Effect of adsorbent mass on Cr (VI) removal (conditions: pH 1; solution concentration 100 mg/L; solution volume 30 mL; contact time 2 h).

The maximum percent removal was observed at 0.32 g corresponding to 99.41%, 99.49 and 98.76% Cr(VI) removal by $MACN_{20}$, $MACN_{40}$, and $MACN_{60}$, respectively. At 0.32 g dosage MACN adsorbents achieved close to 100% adsorption. Increasing the adsorbent mass also increases the surface area of the adsorbent and the number of available binding sites leading to increased %removal of adsorbate (Liu et al 2010). Based on the experimental results adsorbent dosage of 10.67 g/L gave a higher % removal of Cr(VI) thus was selected as the optimum adsorbent for MACN adsorbents.

5.1.2.3. Effect of contact time on Cr(VI) adsorption

Figure 5.6 illustrates the influence of contact time on Cr(VI) adsorption by MACN adsorbents. The removal of Cr(VI) increased sharply from 0 to 10 min then slowed down from 60 to 120 min and eventually attained equilibrium from 240 to 480 min. In addition to faster removal kinetics, $MACN_{20}$ displayed higher percent removal than $MACN_{40}$ and $MACN_{60}$ counterparts from 0 to 120 min. It was predicted that

mineral acids penetrated MAC pores during impregnation and once heated to elevated temperatures, they escaped through the pores together with extractants leaving complementary porosity behind.

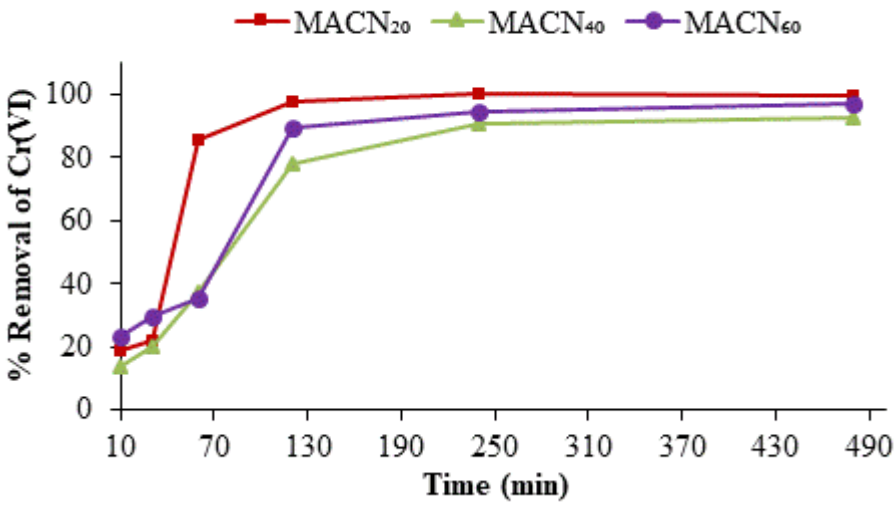

Figure 5.6: Effect of contact time on Cr(VI) removal (conditions: pH 1; solution concentration 100 mg/L; solution volume 30 mL; adsorbent dosage 10.67 g/L).

As shown in Figure 5.3(a) $MACN_{20}$ displayed a high degree of porosity than the other adsorbents ($MACN_{40}$ and $MACN_{60}$). The channels left behind aid in the uptake of adsorbates through physical and chemical interactions with the resultant functional groups. For uniformity reasons, 8 h was chosen and used as an optimum time for the succeeding experiments.

5.1.2.4. Kinetic models

Pseudo-first order (PFO) and pseudo-second order (PSO) rate models were used to analyze the kinetic data of the adsorption process to infer on rate controlling step and adsorption mechanism.

Table 5.2: Intra-particle diffusion and kinetic models for nitric acid modified ACs.

Models	Parameters	$MACN_{20}$	$MACN_{40}$	$MACN_{60}$
PFO	qe (mg/g)	29.13	27.83	30.01
$q_t = q_e (1-exp^{-k_1 t})$	k_1 (1/min)	0.012	0.010	0.020
	q_m (mg/g)	30.10	29.05	31.09
	R^2	0.908	0.967	0.896
	Var*	13.11	4.84	18.11
PSO	k_2 1/[(g(mg/min)]	0.000	0.000	0.001
$qt = t.k_2.q_e^2/(1+k_2 q_e)$	q_m (mg/g)	36.20	36.06	36.05
	R^2	0.885	0.943	0.847
	Var*	16.37	8.33	26.47
Intra-particle diffusion#	k_d (mg/(g $min^{0.5}$))	0.199	0.376	0.057
	C (mg/g)	24.50	20.11	28.86
	R^2	0.937	0.788	0.673

*Var - sum of square error/DF #Values for the second part of intra-particle diffusion.

The PFO rate equation (Equation. 4.9) and the PSO kinetic model (Equation 4.10) were used for the kinetic modelling. The two terms associated with error [(correlation coefficient (R^2) and variance (Var)] were used to choose the best fit model. $MACN_{20}$ (R^2 = 0.908), $MACN_{40}$ (R^2 = 0.943) and $MACN_{60}$ (R^2 = 0.896) obeyed the PFO (Table 5.2). Also, the closeness of the q_m and q_e values was used to reach at the conclusion of the best fit model and it can be said that from the

inferences made above, the q_m and q_e values were in agreement with the error terms. However, the q_m and q_e values were close to the PFO for $MACN_{40}$. Therefore, a physisorption mechanism was predicted for all adsorbents since they best fitted PFO. Both physisorption and chemisorption (Doke and Khan, 2017, Maneechakr and Karnjanakom, 2017) have been reported in the literature for the adsorption of Cr(VI), but thermodynamics studies give more conclusive mechanistic inferences (Gerçel et al., 2007).

5.1.2.5. Intra-particle diffusion

Equation 4.14 was used to gain insights into the mechanism and the rate controlling steps for the adsorption of Cr(VI) by the different ACs. Plots of q_t vs $t^{0.5}$ in Figure 5.7 showed a multi-linearity indicating that adsorption of Cr(VI) by the ACs was not controlled by intra-particle rate diffusion solely but it involved two or more steps controlling the adsorption process (Saha, 2010, Doke and Khan, 2017). Intra-particle diffusion is the only rate-limiting step if a plot of q_t vs $t^{0.5}$ yields a straight line that passes through the origin (Poots et al., 1976). Tseng and Tseng (2005) stated that the adsorption of an adsorbate on a porous adsorbent surface could take place through film diffusion (external mass transfer) and/ or the intra-particle diffusion.

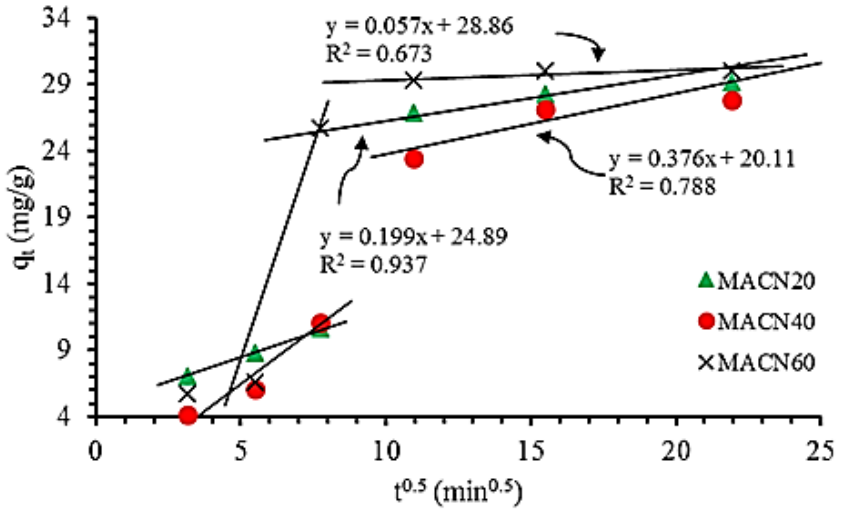

Figure 5.7: Intra-particle diffusion curves for the adsorption of Cr(VI) by MACN carbons.

Therefore, it was suggested in this study that the initial linear plots were due to external mass transfer (film diffusion) and the second upper plots was due to intra-particle pore diffusion, meaning that both mechanisms participated in the adsorption of Cr(VI) by the ACs. In the graph above (Figure 5.7), film diffusion rates were greater than the intra-particle diffusion rates, indicating that higher uptake of Cr(VI) occurred in the former. The values of k_d and C given in Table 5.2 taken from the second linear plots (intra-particle diffusion) and good linearity was achieved judging by the R^2 values.

5.1.2.6. Effect of initial concentration on the adsorption of Cr(VI)

The effect of initial Cr(VI) concentration was investigated by shaking known amounts of $MACN_{20}$, $MACN_{40}$ and $MACN_{60}$ adsorbents in different concentrations of Cr(VI) ranging from 10-300 mg/L while all other parameters remained unchanged. The results are depicted in Figure 5.8(a-b). The percent removal of Cr(VI) by $MACN_{20}$, $MACN_{40}$ and $MACN_{60}$ was almost 100% from 10-100 mg/L and decreased to about 73, 68 and 69%, respectively. At 30 mg/L, all adsorbents achieved 99% removal, but when the concentration was increased to

100 mg/L a significant decrease was observed particularly for MAC_{40} and MAC_{60} to about 67 and 66%, respectively.

It is known that at low concentrations there are more adsorption sites to adsorbate ratio, hence 99% removal. At higher adsorbate concentrations the adsorbents tend to get saturated at the surface thus leading to blockage of pores and restriction of adsorbate uptake. At this range (30 to 150 mg/L) the removal efficiency of Cr(VI) by MACNs followed this order $MACN_{20}$>$MACN_{40}$>$MACN_{60}$ but from 150 to 300 mg/L the order was $MACN_{20}$>$MACN_{60}$>$MACN_{40}$. This shows that $MACN_{60}$ had deeper lying pores than $MACN_{40}$ which was able to accommodate higher concentrations. The observed decreased removal efficiency as the function of increased initial concentration was credited to the exhaustion of adsorption sites in relation to the number of Cr(VI) molecules in solution (Pakade et al., 2016, Anirudhan and Suchithra, 2010).

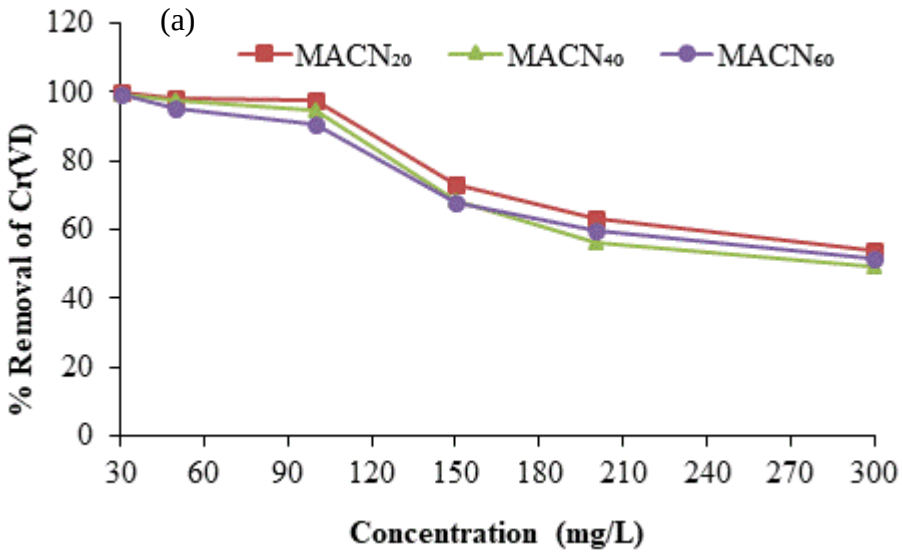

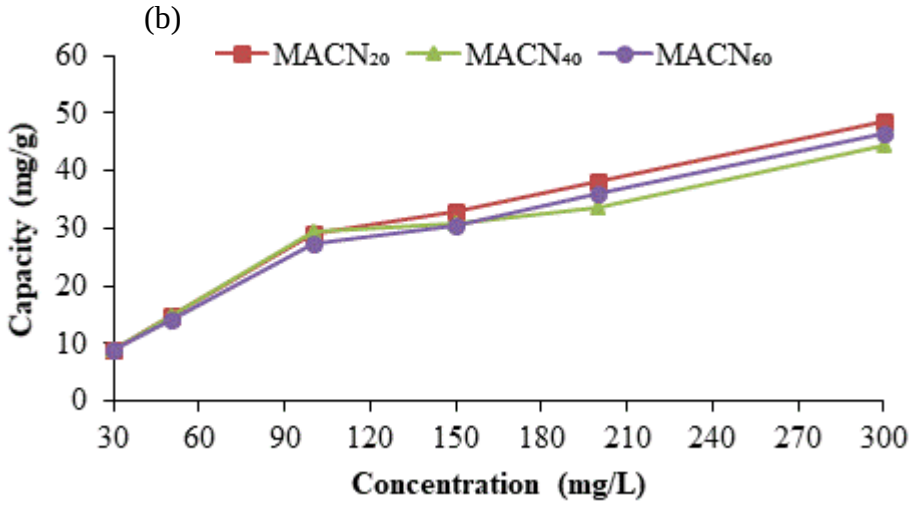

Figure 5.8: Effect of initial concentration and (a) % removal, (b) adsorption capacity on Cr(VI) adsorption (conditions: pH 1; amount of adsorbent 0.32 g; solution volume 30 mL; contact time 8 h).

On the other hand, the adsorption capacity increased with an increase in concentration. Jung et al. (2013) postulated that higher adsorption capacities at high initial concentrations are a result of greater collision chances between adsorbate and adsorbent which is then the driving force overcoming all mass transfer resistances. Several other researchers came to the same conclusion (Pakade et al., 2016, Islam et al., 2015, Anirudhan and Suchithra, 2010). The enhanced adsorption can be related to the profound changes in the physicochemical properties of the carbon composites after acid treatment.

5.1.2.7. Adsorption isotherms

Two well-known adsorption isotherms, Langmuir and Freundlich, describing adsorbent-adsorbate interaction phenomena were used to fit in the adsorption data in order to deduce the removal mechanism. The Langmuir model assumes a monolayer coverage of a homogenous adsorbent surface by the adsorbate

(Langmuir 1918). The Freundlich model relates the sorption of adsorbate to heterogeneous surfaces and it assumes multilayer adsorption (Freundlich and Helle, 1939). The data for the two isotherms were calculated using Equation 4.11 and 4.13, respectively.

Comparing the models based on the R^2 and Var (Table 5.3), it can be said that the acid modification of MAC altered the removal mechanism. $MACN_{20}$ (R^2=0.848), $MACN_{40}$ (R^2=0.763) and $MACN_{60}$ (R^2=0.811) were better described by Freundlich model. In all cases, the variance error in the best fit model was lesser than in the non-fitting model. In addition, for Langmuir fits, the q_m and q_e values were closer to each other. The Langmuir b term for $MACN_{20}$ (0.78 L/mg) and $MACN_{60}$ (0.90 L/mg) were between $0<R_L<1$, which implied favourable adsorption but on closer inspection these values were close to one another. Therefore, the adsorption of Cr(VI) was favourable and irreversible probably due to the transformation of Cr(VI) to Cr(III) upon contact with an adsorbent. All the n_F values in Table 5.3 were greater than 1 which then implied favourable sorption.

Table 5.3: Langmuir and Freundlich isotherms for the MACN adsorbents.

Models	Parameters	$MACN_{20}$	$MACN_{40}$	$MACN_{60}$
	q_e (mg/g)	48.56	44.49	46.61
Langmuir	q_m (mg/g)	40.99	37.16	38.53
$q_e = q_m \cdot b \cdot C_e / (1+bC_e)$	b (L/mg)	0.78	1.13	0.90
	R^2	0.819	0.761	0.776
	Var*	49.15	50.53	53.93
Freundlich	K_F ($mg^{1-1n}L^{1/n}/g$)	19.26	20.18	18.59
$q_e = K_F \cdot C_e^{1/nf}$	n_F	5.77	7.34	6.08
	R^2	0.848	0.763	0.811
	Var*	40.97	50.16	45.51

*Var - sum of square error/DF

5.1.2.8. Adsorption capacity comparison

Table 5.4 shows a detailed comparison of adsorption capacities, dosages and initial concentrations for the removal of Cr(VI) by ACs produced from variant precursors. The adsorption capacities values reported in Table 5.4 are rather low compelling researchers to explore other precursors and alternative activating agents to obtain ACs with superior qualities than their commercial counterparts. The adsorption capacities of the ACs prepared in this study were promising and higher than some in literature but the dosage was also higher even when compared to the pristine AC (Pakade et al., 2017).

As indicated in Table 5.4, the highest comparable q_m value from literature was 34.98 mg/g obtained from commercial AC following HNO_3 modification. Though the usage of different carbon sources limits direct comparison of capacities, herein the MACN showed improved adsorption of Cr(VI), with maximum q_m (40.99 mg/g) achieved at 20% modification. The adsorption capacity increased with 18.69

mg/g for $MACN_{20}$ from 22.3 mg/g for pristine MAC as reported by Pakade et al. (2017).

The higher dosages needed to achieve efficient adsorption could imply that chemical oxidation of MAC with HNO_3, removed adsorption sites. Specifically, $MACN_{40}$ (37.16 mg/g) and $MACN_{60}$ (38.53 mg/g) modifications produced ACs with inferior performances compared to $MACN_{20}$ (40.99 mg/g) when taking into account the dosage and initial concentration used. Hence, the effect of the acid modification on the performance of ACs cannot be generalized based on the studies employing with different acid precursors and varying acids.

Table 5.4: Comparing adsorption capacities of ACs derived different raw materials.

Precursor	Modification agent	Method of modification	q_e (mg/g)	q_m (mg/g)	Initial concentration (mg/L)	Dosage (g/L)	Optimum pH	References
Combretum quadrangulare Kurz	Fe^{2+}	Soaked for 24 h	1.32	1.68	40	4	2-3	Maneechakr and Karnjanakom (2017)
Mango kernel	40% H_3PO_4	Chemical activation	-	7.8	80	2	2	Rai et al. (2016)
Commercial AC	Conc. HNO_3	Boiled for 2 h	-	34.98	800	30	7	Singh et al. (2016)
Peanut shell	Breathing grade air	Air at 450°C for 1 h	-	16.26	100	2.5	2-4	Al-Othman et al. (2012)
Trapa natans husk	Ferric chloride	AC stirred in Fe^{3+} solution for 12 h	-	11.83	20	1.5	2-3	Liu et al. (2010)
Wood	Conc. HNO_3	Heat at 110°C for 3 h	-	16.1	25	2	4	Huang et al. (2009)
Waste material	Conc. H_2SO_4	Heated at 160°C for 2 h	-	7.485	10	2	2	Ghosh (2009)
Waste material	7 mol/L HNO_3	Stirred at 90°C for 12 h	-	10.929	10	2	2	Ghosh (2009)
Coconut shell	2% (v/v) H_2SO_4	Incubated at 110°C for 24 h	4.05	8.94	25	4.5	6	Babel and Kurniawan (2004)
Coconut shell	65% (w/v) HNO_3	Incubated at 110°C for 3 h	10.88	15.47	25	2.5	4	Babel and Kurniawan (2004)

Macadamia nutshell	Pristine	-	26.22	22.3	100	4	2	Pakade et al. (2017)
Macadamia nutshell	20% HNO_3	Reflux	48.56	40.99	200	10	1	This work
Macadamia nutshell	40% HNO_3	Reflux	44.49	37.16	200	10	1	This work
Macadamia nutshell	60% HNO_3	Reflux	46.61	38.53	200	10	1	This work

In the context of the results presented above, and suggested in the literature by Pakade et al. (2016) the redox mechanisms that result in the reduction of Cr(VI) to Cr(III) must be carefully considered. Such a reduction is coupled with oxidation of carbon surface as a result of mineral acid modification leading to the presence of carboxyl moieties. Thus, it can be argued that there are carboxyl functionalities on the oxidized activated carbon surface as displayed in Figure 5.1 [*v*: 3373 cm^{-1} (O-H) and 1077 cm^{-1} (C-O)] which are adsorbing and reducing Cr(VI) to Cr(III) that remain in solution at low pH. The following section incorporates amidation of acid functionalized activated carbon for the subsequent removal of Cr(III) following Cr(VI) reduction. This was done through the surface ion imprinting technique.

5.2. Surface imprinting of Cr(III) on $MACN_{20}$-OOH

Surface ion imprinting technique is an alternative method used for the preparation of IIPs. The process entails coating of a polymeric layer that selectively binds the metal ion on a substrate or support such as nano materials (Polyakova et al., 2016), silica particles (Li et al., 2015), activated carbon (Li et al., 2014) or carbon nanofibres (Mishra and Verma, 2017). This is done in the quest to increase selectivity, the rate of mass transfers, uniform distribution of binding sites and accessibility of adsorbent adsorption sites by template ion because the imprinting is done at the surface (Shakerian et al., 2016). In this study, the surface imprinting was conducted on the activated carbons pre-treated with nitric acid using Cr(III) template ion. However, no crosslinker was used in this present study. Meaning that the imprinting sites were not formed in solution due lack of rigidity provided by the crosslinker. Hence, our method was referred to as pseudo-imprinting and the

inclusion of template Cr(III) ions during grafting helped to maintain the arrangement favouring the readsorption of Cr(III).

5.2.1. Preparation of surface ion imprinted *Macadamia* activated carbon.

The Cr(III) amino functionalized adsorbent was prepared using triethylenetetramine as a complexing agent. The activated carbon ($MACN_{20}$) was *in situ* mixed with Cr(III) and the ligand. Amines tend to transform carboxylic acids to their unreactive carboxylates, therefore, to account for this, N,N′-diisopropylcarbodiimide (DIC) was added as a stimulating molecule to form a good leaving group. This results in displacement of the leaving group by amine during nucleophilic substitution. The ion imprinted *Macadamia* activated carbons (pseudo-$MACN_{20}$-IIP) and the non-imprinted *Macadamia* activated carbon (pseudo-$MACN_{20}$-NIP) were prepared following the mechanism of carboxylic acid conversion to an amide as represented below.

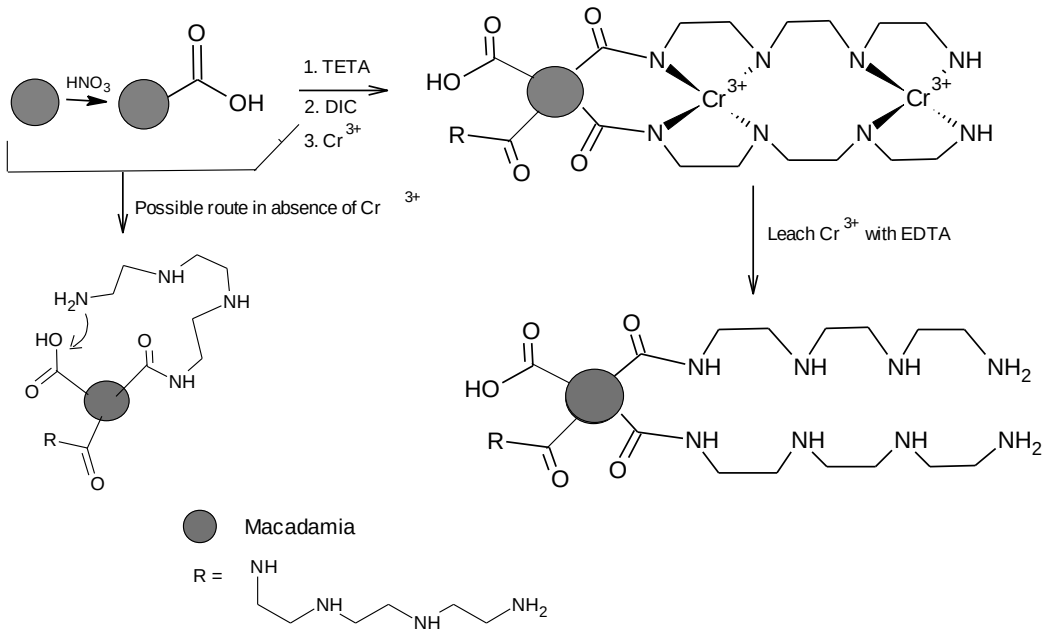

Figure 5.9: Schematic representation of the preparation of pseudo-$MACN_{20}$-IIP.

5.2.2. Characterization of adsorbent

5.2.1.1. Brunauer-Emmett-Teller (BET) and elemental analysis

Figure 5.10 represents the N_2 adsorption/desorption curves of the MAC_{20} grafted polymers. The isotherms displayed a similar shape indicative of a Type II isotherm (characterized by a nearly vertical plane to P/P_0). The occurrence of a narrow knee at relatively low pressure, suggesting the formation of well-developed micropores (Figure 5.10). An increase in relative pressure (P/P_0 = 0.78) the adsorbents exhibited a hysteresis loop signifying the distribution of mesoporous structure of the adsorbents (Groen et al., 2003). According to Van Der Voort et al. (2002) and Groen et al. (2003) the development of plugged materials containing both open and encapsulated pores was observed.

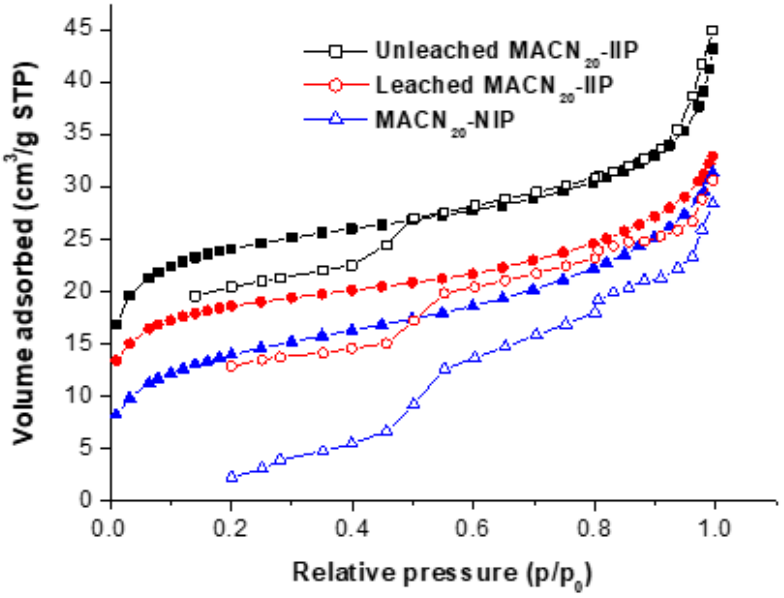

Figure 5.10: N_2 adsorption and desorption isotherms of pseudo-$MACN_{20}$-IIP (leached and unleached) and pseudo-$MACN_{20}$-NIP.

N_2 desorption isotherms resulted in a stepwise branch associated with bimodal porosity. A similar trend was observed in the desorption curves of all the $MACN_{20}$

imprinted materials. The gradual desorption branch was indicative of enclosed emptying of pores at a lower pressure than the open pores of similar size.

The BET surface area, corresponding pore volumes and widths and the elemental analysis of pseudo-$MACN_{20}$-IIP (leached and unleached) and NIP are presented in Table 5.5.

Table 5.5: BET surface areas, pore volumes, pore sizes and elemental analysis of $MACN_{20}$-IIP (leached and unleached) and pseudo-$MACN_{20}$-NIP.

Adsorbent	Surface area (m^2/g)	Pore volume (cm^3/g)	Pore size (nm)	Ultimate analysis			
				%C	%N	%H	%O*
$MACN_{20}$-IIP (unleached)	83.15	0.064	3.070	50.60	13.30	6.50	29.60
$MACN_{20}$-IIP (leached)	64.20	0.049	3.102	45.10	12.40	5.70	36.80
$MACN_{20}$-NIP	49.92	0.047	3.789	46.00	12.50	6.00	35.50

*computed by difference

The change in surface area and pore volume was in the order of $MACN_{20}$-IIP (unleached) > $MACN_{20}$-IIP (leached) > $MACN_{20}$-NIP. The obtained results suggested that the absence of template ion (leached in $MACN_{20}$-IIP and omitted in $MACN_{20}$-NIP) led to the development of lower pore volumes.

A considerable decrease in surface area for leached pseudo-$MACN_{20}$-IIP (64.20 m^2/g) than the unleached $MACN_{20}$-IIP (83.15 m^2/g) was related to the linking effect of the metal ion and the adsorbent surface (Li et al., 2015). According to Mishra

and Verma (2017), an observable greater surface area for leached $MACN_{20}$-IIP (64.20 m^2/g) than $MACN_{20}$-NIP (49.92 m^2/g) was attributable to the exposure of internal surface area resulting from formed cavities in leached $MACN_{20}$-IIP, hence a rougher surface (refer to Figure 13b). The pore sizes of all the materials were distributed at a range between 2~50 nm, unleached $MACN_{20}$-IIP (3.070 nm), leached $MACN_{20}$-IIP (3.102 nm) and MAC_{20}-NIP (3.789 nm). Therefore, the pore structure characteristics of the MAC_{20} polymers were primarily constituted of mesopores. Moreover, the elemental analysis results in Table 5.5 indicated that surface imprinting of $MACN_{20}$-IIP attenuated the %N content of the materials. The %N decreased from 13.3% to 12.4% in the unleached and leached pseudo-$MACN_{20}$-IIP, respectively. These may be indicative of the removal of excess ligand during the leaching step (Li et al., 2014). However, a significant increase in the nitrogen content was observed before and after imprinting. These values sharply increased from 1.46% (20% acid modified MAC, Table 5.1) to 13.3% upon imprinting. Generally, amidation involves the conversion of a carboxylic moiety in the presence of an amine group. Therefore, a considerable increase in nitrogen avowed that the ligand was anchored on the surface of the MAC-OOH during Cr^{3+} imprinting.

5.2.1.2. FTIR spectroscopic analysis

In order to ascertain the amide grafting on $MACN_{20}$-COOH, the FTIR spectra of the unleached, leached and non-imprinted $MACN_{20}$ sorbents were compared in Figure 5.11. The three spectra displayed a similar structural backbone with similar location and appearance of major peaks, but signal attenuation and shifts were observed. The absorption peaks at around 1232 cm^{-1} in all the adsorbents were assigned to the stretching vibrations of C-N bonds and stretching and bending

vibrations of N-H at 3014-3005 cm^{-1} and 685 cm^{-1}, respectively, indicating the presence of tetraethylenetriamine.

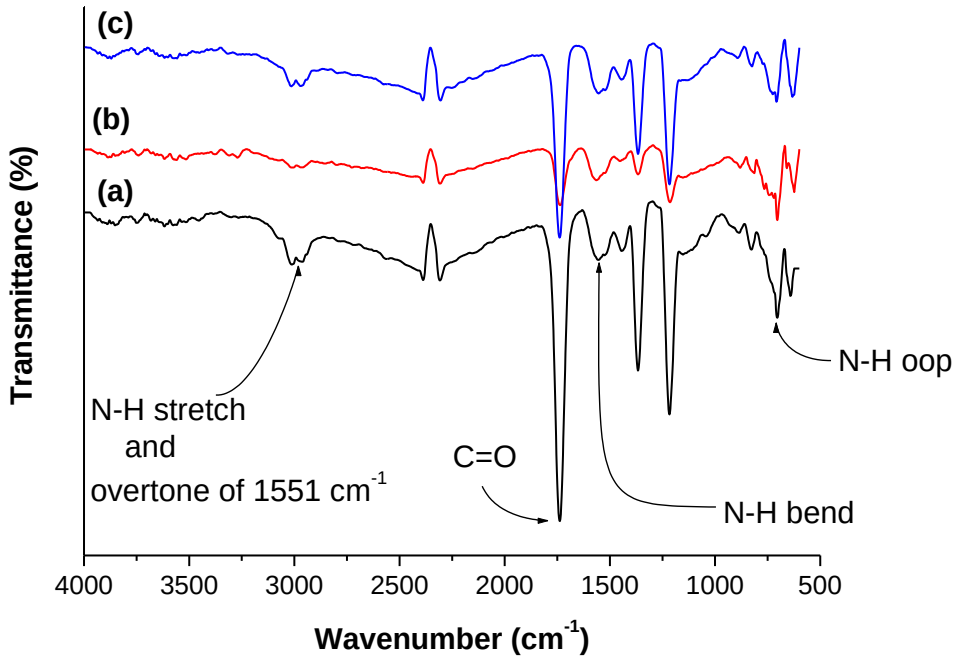

Figure 5.11: FTIR spectra of unleached pseudo-$MACN_{20}$-IIP (a), leached $MACN_{20}$-IIP (b) and $MACN_{20}$-NIP (c).

An observable shift in the C-N band at 1216 cm^{-1} in the unleached pseudo-$MACN_{20}$-IIP to a lower frequency (1208 cm^{-1}) in the leached pseudo-$MACN_{20}$-IIP which could suggest successful removal of Cr(III) ions in the leached material as well as its involvement in the Cr(III) complexation. Li et al. (2014) prepared a similar adsorbent for selective Cu(II) adsorption, but diethylenetriamine was used as a ligand. The study reported the existence of N-H vibrations at 3424 cm^{-1} and C-N stretch at 1594 cm^{-1} in the leached, unleached IIP and NIP confirming the grafting on amino groups on the surface of ACs (Li et al., 2014). Since the adsorbents were prepared from a carboxylic derivative, responsible for the formation of an amide from an amine, it was therefore of necessity to establish

whether there was a complete conversion of the carboxylic acid surface functionalities to the desired amide derivatives. The amide C=O vibrations at 1690 cm^{-1}, 1684 cm^{-1} and 1686 cm^{-1} for the unleached pseudo-$MACN_{20}$-IIP, leached $MACN_{20}$-IIP and the $MACN_{20}$-NIP, respectively confirmed successful grafting of amide on the surface of MAC_{20}.

5.2.1.3. Thermogravimetric analysis

The thermal behaviour of the pseudo-$MACN_{20}$-IIP before and after Cr^{3+} removal and their respective non-imprinted counterpart ($MACN_{20}$-NIP) is illustrated in Figure 5.12. The pseudo-$MACN_{20}$-NIP followed a different decomposition pattern as compared to the $MACN_{20}$-IIP (leached and unleached) as it possessed higher thermal stability than the $MACN_{20}$-IIPs. In the case of $MACN_{20}$-IIP (leached and unleached) the different disintegration steps were afforded by a disrupted physical interaction between the template ion and the polymer (Rusen et al., 2017).

A slight deep at around 75^{o}C corresponding to the loss of moisture content and adsorbed water was observed in all materials, and this was estimated to 4.6%, 5.7% and 2.8% for the leached pseudo-$MACN_{20}$-IIP, unleached $MACN_{20}$-IIP, and the $MACN_{20}$-NIP, respectively. The decomposition peak at 270^{o}C was credited to the loss of volatile compounds such as CH_4, CO_2, CO, NO_2, aldehydes, and distillation of tar (Cagnon et al., 2009; Kumar and Jena 2015).

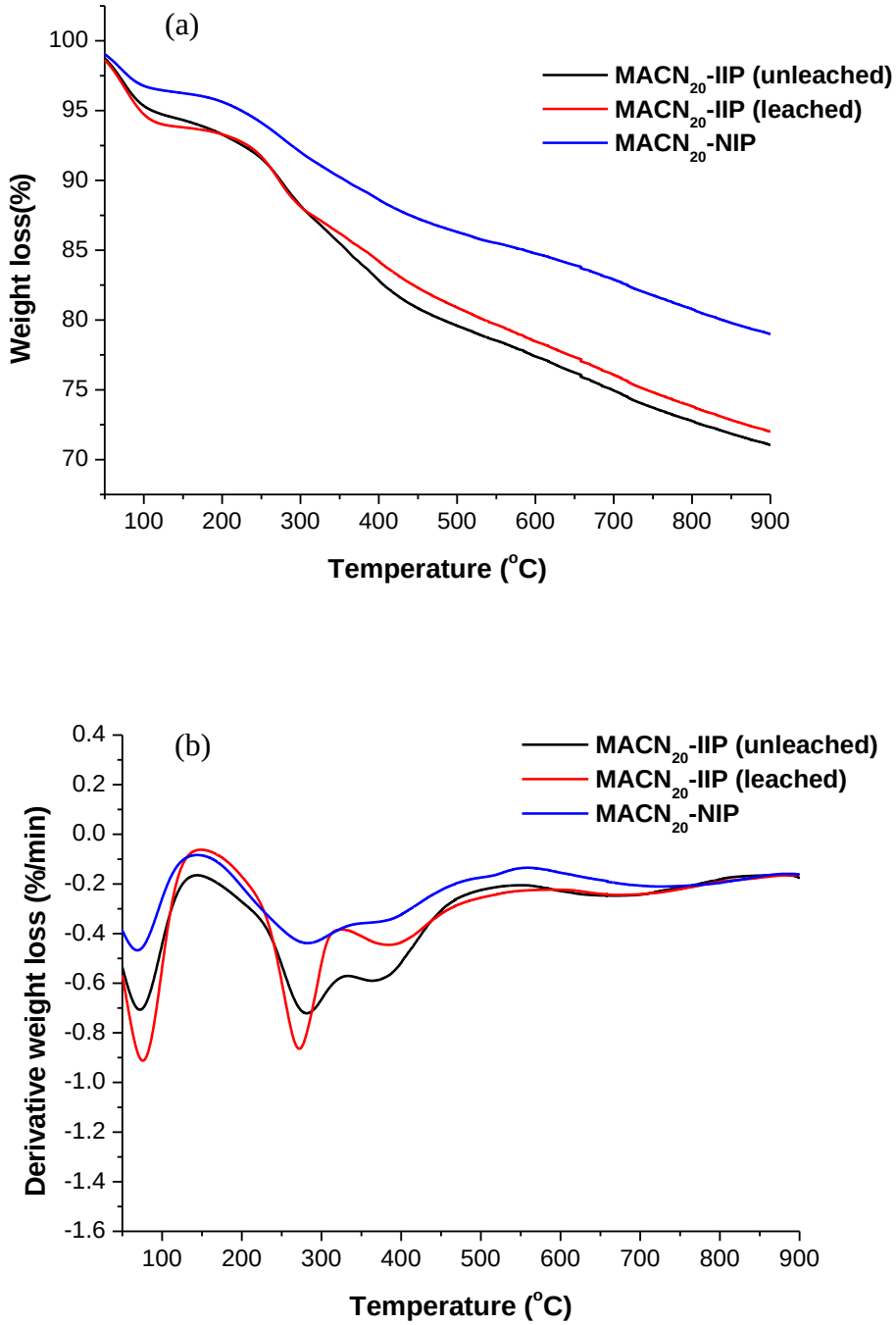

Figure 5.12: TGA (a) and DTA (b) thermograms of pseudo-$MACN_{20}$-IIP (leached and unleached) and $MACN_{20}$-NIP.

A third weight loss observed from 348°C to 444°C approximated to 8.1 and 7.0% weight loss for unleached pseudo-$MACN_{20}$-IIP and leached $MACN\text{-}IIP_{20}$, respectively, was attributed to the decomposition of ligand in the polymer (Li et

al., 2015). The total weight loss was found to be 27.94 %, 26.35 % and 19.98 % for $MACN_{20}$-IIP (unleached), $MACN_{20}$-IIP (leached) and $MACN_{20}$-NIP, respectively.

5.2.1.4. Scanning electron microscopy

The surface morphology of pseudo-$MACN_{20}$-IIP (unleached and leached) and pseudo-$MACN_{20}$-NIP was examined using SEM and the micrographs are depicted in Figure 5.13 (a-c), respectively. The unleached pseudo-$MACN_{20}$-IIP (Fig 5.13a) showed an unsmooth, dense surface with small particles stacking on top of each other and a lower degree of porosity. On the other hand, after leaching with a dilute solution of ethylenediaminetetraacetic acid (EDTA), the leached IIP material (Figure 5.13b) possessed a relatively rough surface in comparison to unleached pseudo-$MACN_{20}$-IIP. This could be a result of cavities formed by the template metal ion during the leaching step thus implying successful removal of the template. This morphology was essential particularly for the specific adsorption of the imprint ion. During the synthesis of NIP, the template ion was omitted; therefore, no cavities are formed hence a smooth surface observed in Figure 5.13c. Li et al. (2015) related the rougher surface of Cd(II)-imprinted silica adsorbent to the imprint cavities created from Cd(II) leaching step. This was rather less distinct in Cd(II) loaded IIP sorbent due to the combining effect between the metal ion and the active sites on the silica surface.

(a)

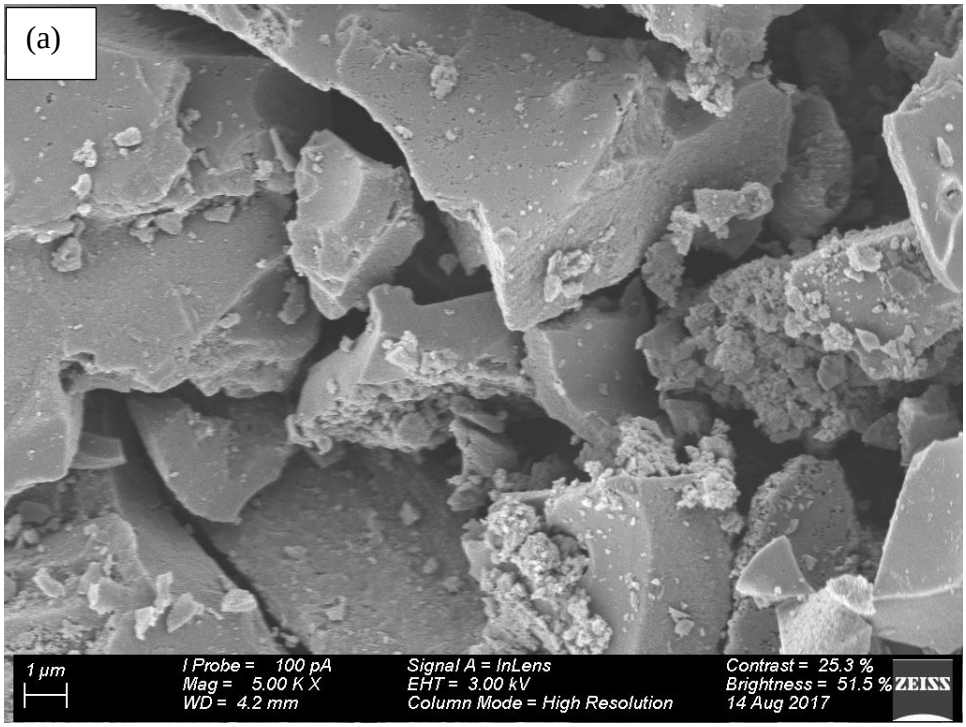
1 µm
I Probe = 100 pA
Mag = 5.00 K X
WD = 4.2 mm
Signal A = InLens
EHT = 3.00 kV
Column Mode = High Resolution
Contrast = 25.3 %
Brightness = 51.5 %
14 Aug 2017
ZEISS

(b)

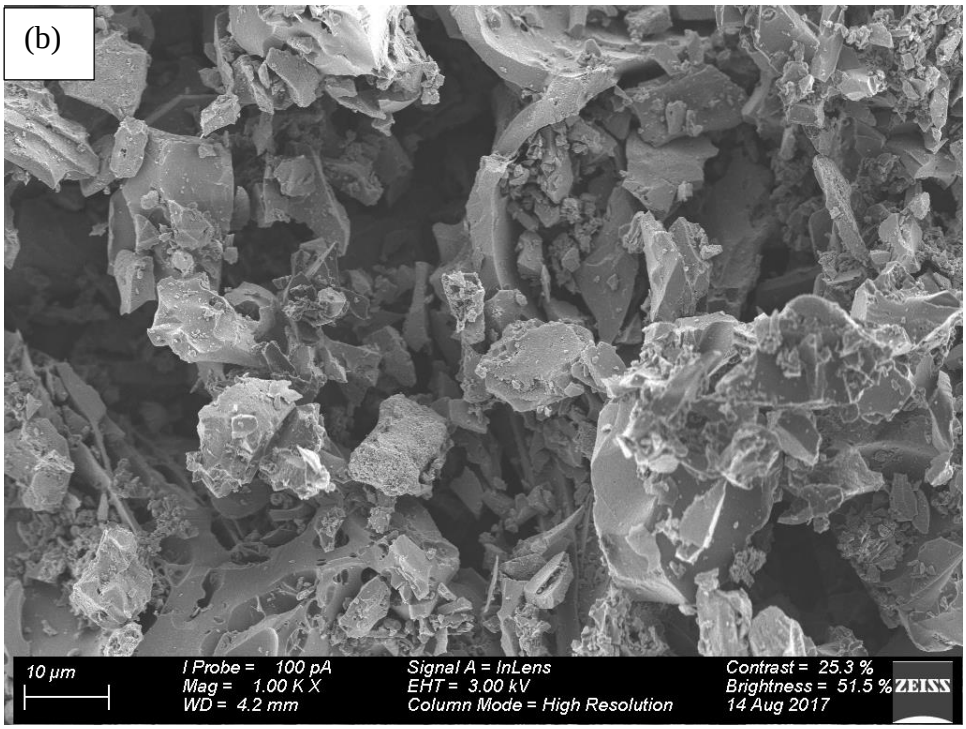
10 µm
I Probe = 100 pA
Mag = 1.00 K X
WD = 4.2 mm
Signal A = InLens
EHT = 3.00 kV
Column Mode = High Resolution
Contrast = 25.3 %
Brightness = 51.5 %
14 Aug 2017
ZEISS

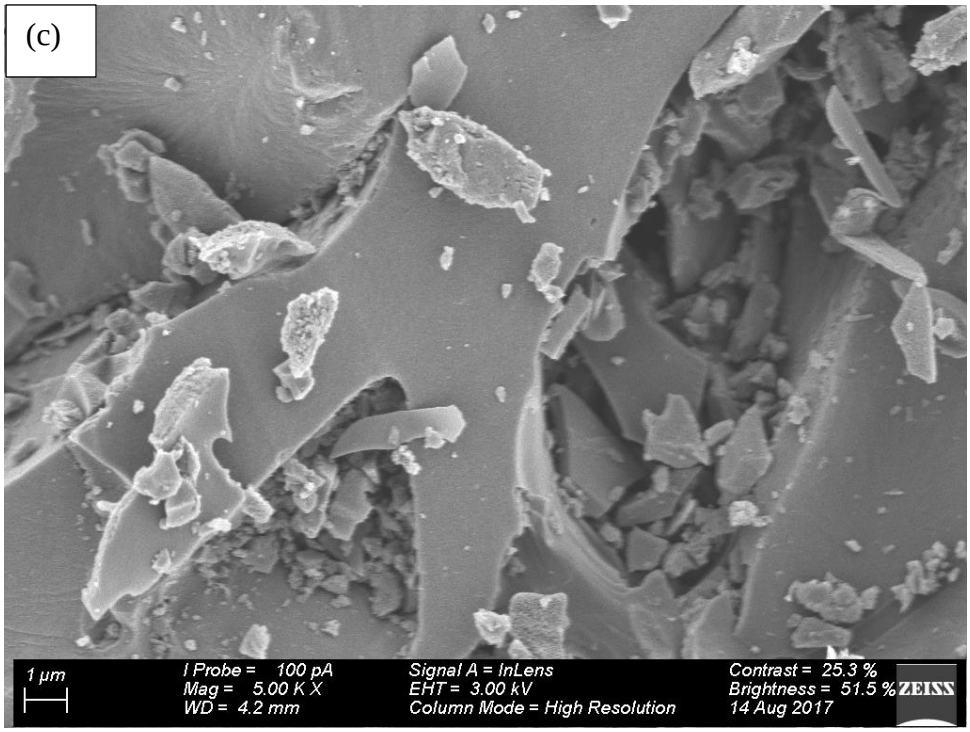

Figure 5.13: SEM images of unleached $MACN_{20}$-IIP (a), leached $MACN_{20}$-IIP (b) and $MACN_{20}$-NIP (c).

5.2.2. Adsorption studies

5.2.2.1. Effect of solution pH on Cr(III) removal

Figure 5.14 depicts the effect of initial solution pH on the adsorption of Cr(III) by pseudo-$MACN_{20}$-IIP and $MACN_{20}$-NIP. The adsorption was studied by varying the pH from pH 1 to pH 9. It was observed that an increase in pH from 1 to 3 resulted in a slight increase in metal uptake from 38.1% to 56.8% for pseudo-$MACN_{20}$-IIP and from 32.7% to 52.1% for pseudo-$MACN_{20}$-NIP. The low % removal of Cr(III) at acidic conditions was probably because the adsorbents (amino groups) tend to get protonated. In addition, at acidic pH (pH < 3), Cr(III) exists as Cr^{3+} and $Cr(OH)_2^+$ (Figure 5.15). These two conditions will result in the repulsion of Cr^{3+} ions by the adsorbent. Both the leached pseudo-$MACN_{20}$-IIP and $MACN_{20}$-NIP attained the highest % removal of Cr(III) at *ca.* pH 5. As the pH of the solution was increased to pH 5, the surface becomes less protonated and more neutral

allowing the removal of Cr(III) species in the form of $Cr(OH)^{2+}$. The diagram of concentration distribution of Cr(III) shows that at pH 5 and above, Cr(III) exists as the $Cr(OH)_2^{+}$ (monovalent) and $Cr(OH)^{2+}$ (divalent) forms (Figure 5.15).

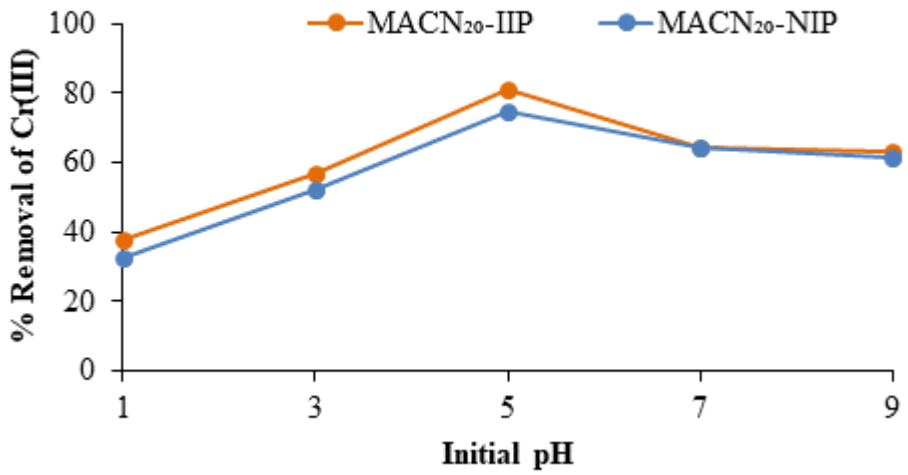

Figure 5.14: Effect of solution pH on Cr(III) adsorption by pseudo-$MACN_{20}$-IIP and $MACN_{20}$-NIP (conditions: solution concentration 100 mg/L; adsorbent dosage of 3.33 g/L; solution volume 30 mL; contact time 2 h).

Since Cr(III) prefers an octahedral geometry, its existence in both the monovalent and divalent state favours the binding of these chromium species to the polymer through the amino groups which were found to be present on the FTIR spectra (Figure 5.11) of the adsorbents. Presumably, due to the imprinting effect, specificity and multidentate nature of the polymer, the binding of Cr(III) occurred as compared to the monodentate Cl^- (starting material was $CrCl_3.6H_2O$) and OH^- ions. As expected, $MACN_{20}$-IIP outperformed $MACN_{20}$-NIP, and this was attributed by the inclusion of Cr(III) as an imprint metal ion which encouraged an orderly ligand arrangement. These fabricated sites favour the remediation of Cr(III).

Li et al (2014) experimented the removal of Cu(II) by activated carbons imprinted using diethylenetriamine as a ligand and reported that more than 95% removal of Cu(II) was achieved at low pH but decreased from pH 6 to pH 7. No sorption studies were carried out beyond pH 7 particularly to avoid metal hydrolysis. Similarly, in this study, a sharp decrease of Cr(III) adsorption was observed at pH 7 with no apparent difference until pH 9. Another factor contributing to the diminished remediation at neutral pH could be the formation multinuclear species of chromium (i.e. $[(H_2O)_4\ Cr(OH)_2Cr(H_2O)_4]^{4+}$) referred to as bridging ligands as suggested in Kumar et al. (2009). This was observed in the adsorption of Cr^{3+} by an amine-based polymer aniline formaldehyde condensate. pH 5 gave maximum adsorption and was therefore used in subsequent experiments.

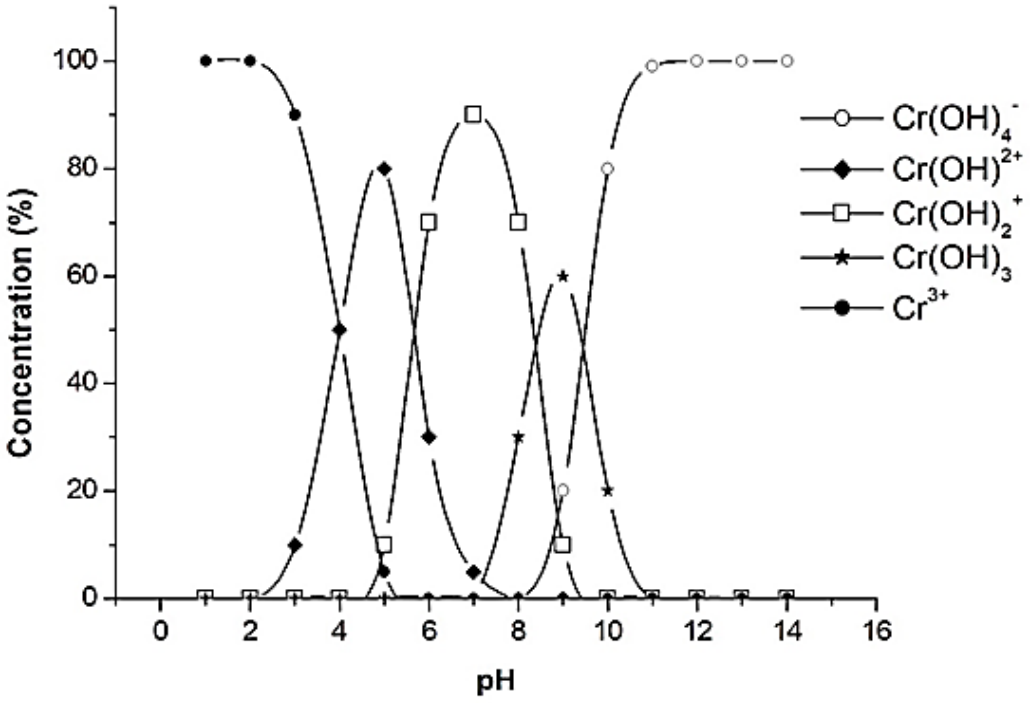

Figure 5.15: Cr(III) speciation diagram at various pH (Cook and Olive, 2012, Puigdomenech and Beverskog, 1997).

5.2.2.2. Effect of concentration on Cr(III) removal

Figure 5.16 illustrates the effect of initial concentration on the percentage removal of Cr(III). The percentage of Cr(III) adsorbed decreases as the initial concentration increases. The % Cr(III) adsorbed decreased significantly from 90.70% to 67.94% ($MACN_{20}$-IIP) and from 88.03 % to 64.92 % ($MACN_{20}$-NIP) from 50 mg/L to 300 mg/L, respectively. Although a favourable % R was achieved at 50 mg/L [$MACN_{20}$-IIP (90.70%) and $MACN_{20}$-NIP (88.0%)], 100 mg/L was chosen as the optimum concentration due to high adsorbent to adsorbate ratio at extremely low concentrations. During the preparation of the $MACN_{20}$-Cr(III)-imprinted sorbent, as per procedure in Chapter 4, a certain amount of Cr(III) was reacted with a ligand (tetraethylenetriamine) solution and a purple-violet coloured precipitate was formed. The same coloured precipitate was observed in the resultant the supernatant liquid after the adsorption of Cr(III) by $MACN_{20}$-IIPs. It was suspected that some of the ligands leached into the solution to complex with unabsorbed Cr(III) ions.

In the quest to address this matter, the adsorbent was washed several times with methanol to remove unreacted tetraethylenetriamine (TETA), and the resultant material was labelled as $MACN_{20}$-IIP/MeOH. Figure 5.16b compares the $MACN_{20}$-IIP and $MACN_{20}$-IIP/MeOH adsorbents. It was evident from Figure 5.16b that post-treatment of the $MACN_{20}$-IIP with methanol enhanced Cr(III) adsorption probably because the excess TETA on the surface was blocking some of the pore channels.

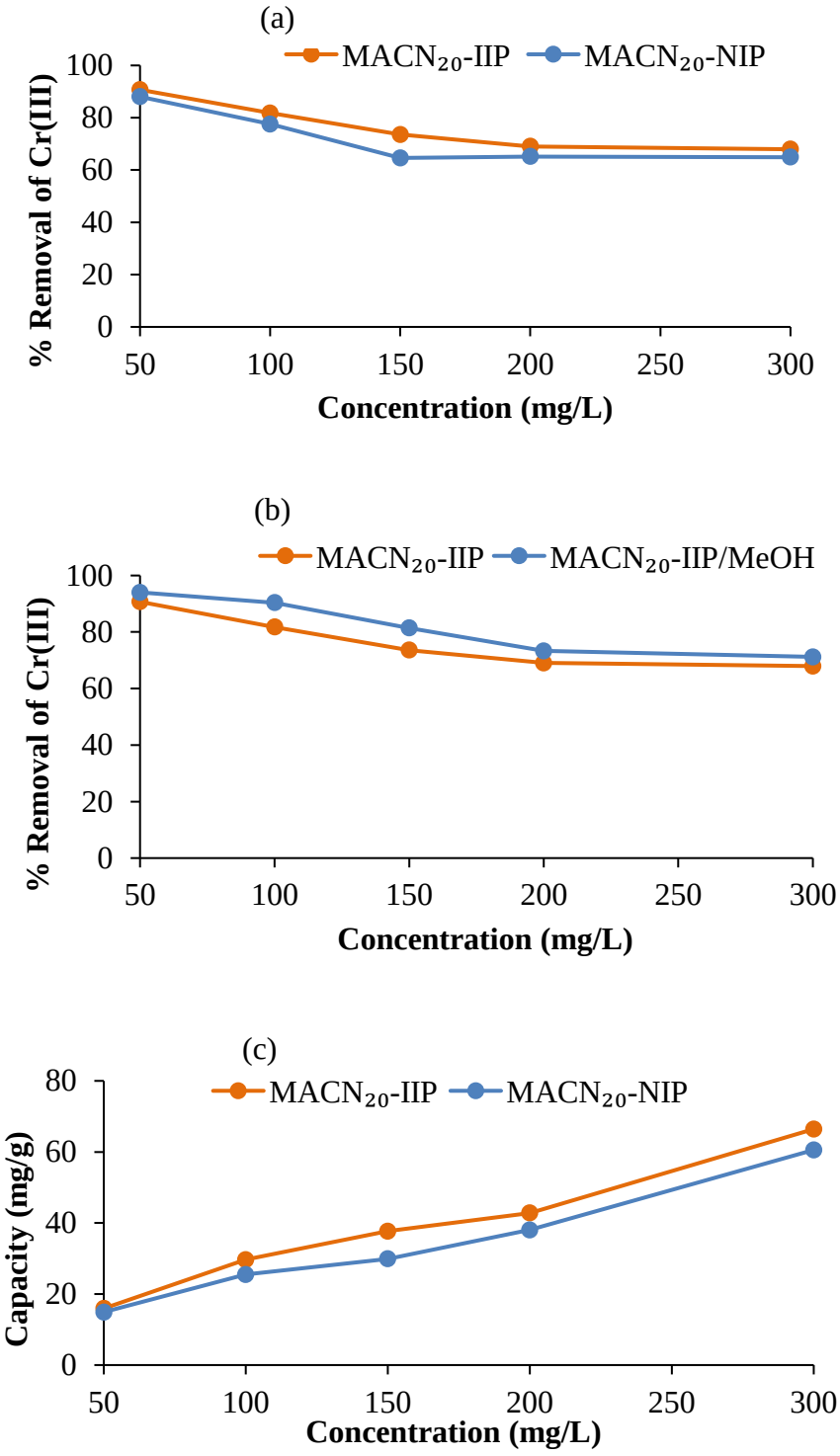

Figure 5.16: Effect of initial concentration on Cr(III) % removal by $MACN_{20}$-IIP and $MACN_{20}$-NIP (a), $MACN_{20}$-IIP/MeOH (b) and adsorption capacity by $MACN_{20}$-IIP and $MACN_{20}$-NIP (c) (conditions: solution pH 5; adsorbent dosage of 3.33 g/L; solution volume 30 mL; contact time 2 h).

The percent removal decreased from 90.7% to 67.9% for $MACN_{20}$-IIP and from 94.0% to 71.2% for $MACN_{20}$-IIP/MeOH. Henceforth, the methanol-washed adsorbent was used in subsequent batch experiments and was re-labelled as $MACN_{20}$-IIP to avoid confusion. The maximum adsorption capacities were 66.42 mg/g and 60.55 mg/g for the $MACN_{20}$-IIP and the corresponding NIP, respectively (Figure 5.16 (c)).

During this experiment, the dose of adsorbents was fixed at 0.1 g; hence the number of active surface adsorption sites available remained unchanged. The active adsorption sites eventually became saturated as the concentration of Cr(III) was increased thus inhibiting the uptake of an analyte. Lin et al. (2010) reported higher surface grafted Th(IV)-IIPs compared to their non-imprinted particles. The adsorption capacities were found to be 64.8 mg/g [Th(IV)-IIP) and 37.4 mg/g (Th(IV)-NIP). The higher capacity of IIP was related to the imprinting factor on the adsorbent behaviour. Implying predetermined orientation of specific binding sites and functional groups in the IIPs, no such specificity is found in the NIP.

5.2.2.3. Adsorption isotherms

Figure 5.17 shows the Langmuir and Freundlich adsorption isotherms. The adsorption capacity (mg/g) of Cr(III) increased as the initial concentration was increased. In both cases, IIP and NIP, the Freundlich isotherm curve was much closer to the experimental points compared to the Langmuir method implying a good fit. Table 5.6 shows the data obtained by fitting the results of concentration in the Langmuir and Freundlich non-linear isotherms. Three error terms, the coefficient of determination (R^2), chi-squared (X^2) and residual standard error (RSE), were used to infer which model fitted the data best.

The values of the dimensionless term R_L all lied between zero and one, implying a favourable adsorption. The Freundlich constant [(mg/g)/(mg/L)$^{1/n}$] and the Freundlich exponent denoted as K_f and n_f were evaluated to describe the adsorption capacity and adsorption intensity, respectively. The K_f values for MAC-IIP and MAC-NIP were estimated at 9.60 and 3.17, correspondingly. According to Pakade et al. (2016), $1/n_f$ values between 0-1 signify favourable adsorption. Conclusively, MAC-IIP and MAC-NIP were effective adsorbents for Cr(III) recovery.

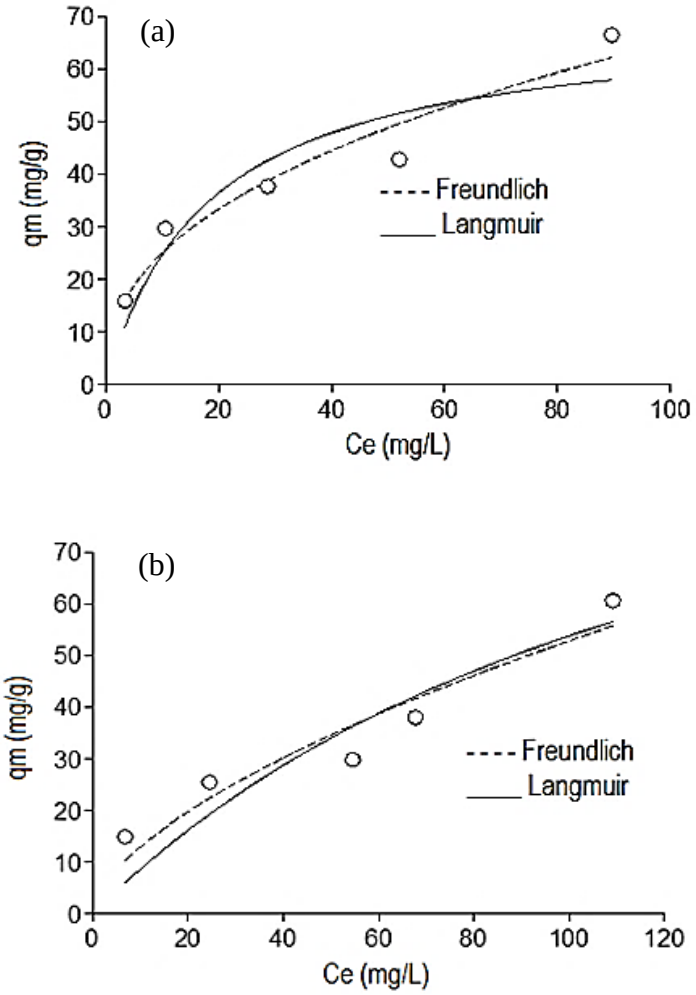

Figure 5.17: Freundlich isotherms for pseudo-MACN$_{20}$-IIP (a) and MACN$_{20}$-NIP (b) (conditions: solution pH 5; adsorbent dosage of 3.33 g/L; solution volume 30 mL; contact time 2 h).

The R^2 value of Freundlich (R^2, 0.921 for IIP; 0.873 for NIP) was higher than those from the Langmuir model (R^2, 0.791 for IIP; 0.783 for NIP). The RSE values from the Freundlich model (RSE, 5.24 IIP, 6.10 NIP) were lesser than those in the Langmuir model (RSE, 8.50 IIP, 7.99 NIP). No X^2 values were reported for Freundlich method due to lack of q_m value in Freundlich. It can, therefore, be concluded that the Freundlich isotherm explained the data best suggesting a multi-layer adsorption model for both IIP and NIP.

Table 5.6: The Langmuir and Freundlich parameters for adsorption of Cr(III) by Pseudo-$MACN_{20}$-IIP and $MACN_{20}$-NIP.

Models	Parameters	$MACN_{20}$-IIP	$MACN_{20}$--NIP
	q_e (mg/g)	66.43	60.56
Langmuir	q_m (mg/g)	69.61	68.37
$q_e = q_m \cdot b \cdot C_e / (1+bC_e)$	b (L/mg)	0.055	0.0072
	R^2	0.791	0.783
	χ^2	89.45	57.70
	RSE	8.50	7.99
Freundlich	K_F ($mg^{1-1n}L^{1/n}/g$)	9.60	3.17
$q_e = K_F \cdot C_e^{1/nf}$	n_F	2.41	1.64
	R^2	0.921	0.873
	χ^2	-	-
	RSE	5.24	6.10

*RSE - residual standard error

Table 5.7: The Langmuir constants and the R_L values for adsorption of Cr(III) on pseudo-$MACN_{20}$-imprinted sorbents.

C_o (mg/L)	$MACN_{20}$-IIP	$MACN_{20}$-NIP
50	0.267	0.581
100	0.154	0.481
150	0.108	0.409
200	0.083	0.357
300	0.057	0.316

According to (Rangabhashiyam and Selvaraju, 2015) R_L values indicate favourable and unfavourable adsorption when $0>R_L<1$ and $R_L > 1$, respectively. However, $R_L=0$ and $R_L=1$ signifies an irreversible and unfavourable adsorption, respectively. Table 5.7 summarizes the R_L constant values relative to adsorption by $MACN_{20}$-IIP and $MACN_{20}$-NIP. As outlined above, the calculated separation factor, R_L for $MACN_{20}$-IIP and $MACN_{20}$-NIP were all found to be less than 1 respectively. Based on these values ($0<R_L<1$) the adsorption of Cr^{3+} was considered favourable.

5.2.2.4. Effect of adsorbent mass on Cr(III) adsorption

The removal of Cr(III) by $MACN_{20}$-IIP/NIP polymers was studied by varying adsorbent mass from 0.05 g to 1.0 g. The results are presented in Figure 5.18. In both cases, it was found that the %removal increased with increased adsorbent mass. This was associated with increased exposure and abundant availability of the active adsorption sites which facilitated increased metal ion uptake.

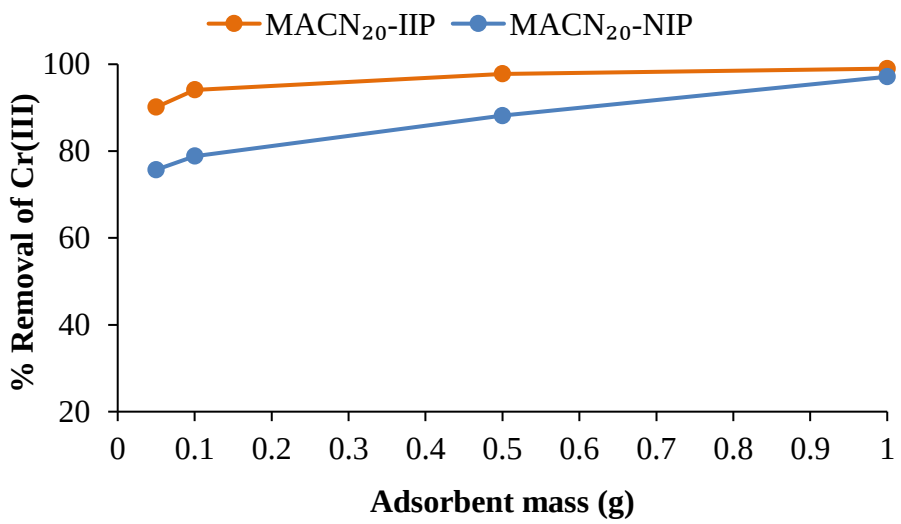

Figure 5.18: Effect of adsorbent mass on Cr(III) removal by $MACN_{20}$-IIP and $MACN_{20}$-NIP (conditions: solution pH 5; solution concentration 100 mg/L; solution volume 30 mL; contact time 2 h).

For the $MACN_{20}$-IIP an increase in the studied adsorbent dose range (0.05-0.1 g) resulted in a significant increase in % Cr removal from 90.1% to 98.9% while for the respective NIP the efficiency increased sharply from 75.7% to 97.1%. At the lower dosage levels, i.e., 0.05 g, 0.1 g and 0.5 g, $MACN_{20}$-IIP out-performed $MACN_{20}$-NIP with *ca*. 14.4%, 15.3%, and 9.64%, respectively. However, at 1.0 g the sorption percentage for both $MACN_{20}$-IIP and $MACN_{20}$-NIP were almost the same with a slight difference of 2%. Since the maximum Cr(III) removal was achieved at a dosage of 33.33 g/L, it was considered an optimum dose.

5.2.2.5. Effect of contact time on Cr(III) adsorption

The effect of contact time on the adsorption efficiency of Cr(III) by $MACN_{20}$-IIP and $MACN_{20}$-NIP was studied at varying times (30 to 480 min). From the results depicted in Figure 5.19, an increase in contact time led to increased adsorption efficiency of Cr(III). Initially, rapid uptake of the metal ion was observed from 30

min to 120 min due to boundary layer adsorption. The % removal increased from 71.6% to 91.7% for $MACN_{20}$-IIP while for $MACN_{20}$-NIP the increase ranged from 69.4% to 80.1%. From 120 min to 240 min, the % removal increased gradually from 91.6 to 92.5% and 80.7 to 88.7% for $MACN_{20}$-IIP and $MACN_{20}$-NIP, respectively. The gradual increase was attributed to the slow diffusion into internal pores. No notable change in analyte uptake was observed from 240 to 480 min which implied an equilibrium condition due to saturation of active adsorption sites for both adsorbents. Further adsorption would be based on the intra-particle diffusion of analyte solutes (Li et al., 2015). After grafting Cd(II) ion imprinted polymer on N-propylmaleamic functionalized silica support, Li et al. (2015) reported a similar observation when allylthiorea was used as a ligand. Results found showed fast uptake of Cd(II) ions in the first 8 min followed by a subsequent gradual decrease leading to equilibrium being attained between 15 and 20 min.

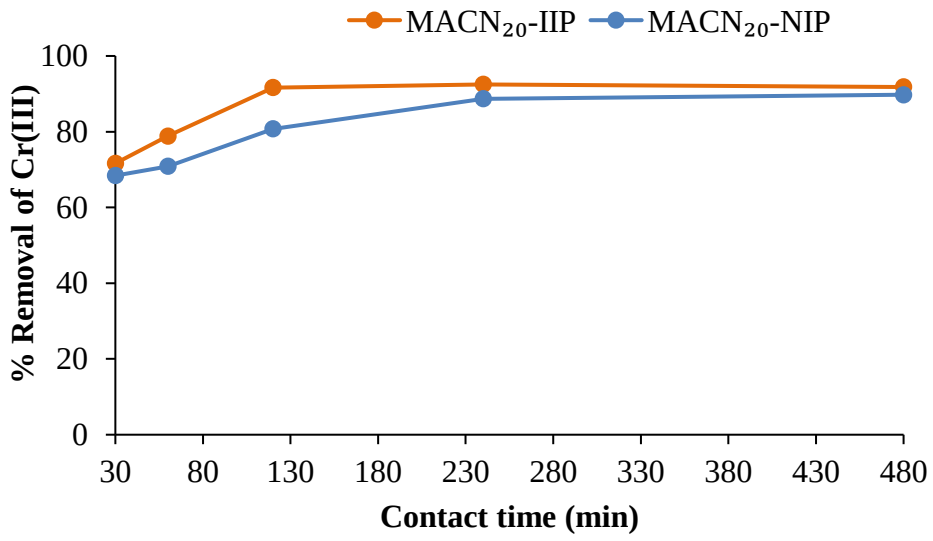

Figure 5.19: Effect contact time on Cr(III) removal by $MACN_{20}$-IIP and $MACN_{20}$-NIP (conditions: solution pH 5; solution concentration 100 mg/L; solution volume 30 mL; adsorbent dose 33.33 g/L).

5.2.2.6. Kinetic modelling

The key adsorption controlling process of Cr^{3+} (adsorbate) on pseudo-$MACN_{20}$-IIP/NIP were evaluated by kinetic models. The non-linearized forms of the Pseudo-first order (PFO) and pseudo-second order (PSO) models were used as given in Equation 4.11 and 4.13, respectively. Figure 5.20a and b show the adsorption capacity (mg/g) data for $MACN_{20}$-IIP (a) and $MACN_{20}$-NIP as a function of time as well as the PFO and PSO kinetic data modelling, respectively.

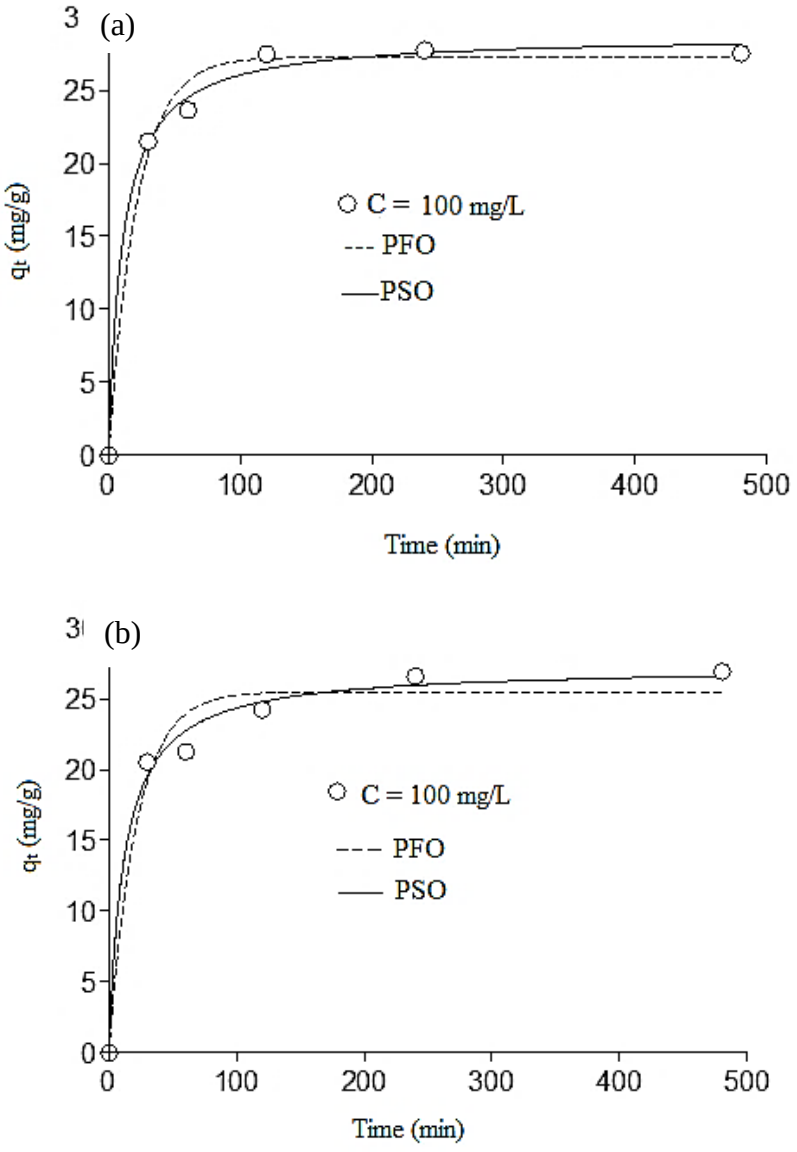

Figure 5.20: PFO and PSO plots for the adsorption of chromium onto $MACN_{20}$-IIP (a) and $MACN_{20}$-NIP (b).

It can be observed that both the PFO and PSO rate models were closer to the experimental data. However, more conclusive evidence as to which model fitted the data best was achieved by evaluating the kinetic parameters in Table 5.8. The adsorption capacity of $MACN_{20}$-IIP (Figure 20(a)) were slightly higher than those of $MACN_{20}$-NIP (Figure 20(b)) probably because of the imprinting effect.

The constants deduced from the two kinetic plots are presented in Table 5.8 below. Higher R^2 values were found for both $MACN_{20}$-IIP (0.995) and $MACN_{20}$-NIP 0.99 for the PSO model. A PSO model suggests that chemisorption predominated the adsorption of Cr(III) onto activated carbon surface imprinted polymers. This arises due to the presence of the nitrogen-containing group in the polymer matrix which encourages the formation of bonds between the metal template ion and the nitrogen atoms (Mishra and Verma, 2017).

Table 5.8: Kinetic parameters of pseudo-first and pseudo-second orders for Cr(III) adsorption by $MACN_{20}$-IIP and $MACN_{20}$-NIP at 100 mg/L.

Models	Parameters	$MACN_{20}$-IIP	$MACN_{20}$-NIP
PFO	q_t (mg/g)	27.54	26.93
$q_t = q_e (1-\exp^{-k_1 t})$	q_e (mg/g)	27.25	25.47
	k_1 (1/min)	0.047	0.046
	R^2	0.988	0.967
	X^2	1.71	1.86
	RSE	1.13	1.85
PSO	q_e (mg/g)	28.74	24.22
$q_t = t.k_2.q_e^2 / (1+k_2.t.q_e)$	k_2 1/[g(mg/min)]	0.0033	0.0031
	R^2	0.995	0.990
	X^2	2,87	1,47
	RSE	0,74	1,01

*RSE - residual standard error

5.2.2.7. Intra-particle diffusion

The Weber-Morris (1963) equation (Equation 4.14) was used to deduce the rate controlling steps and the intra-particle diffusion mechanism influencing the adsorption of Cr(III) by $MACN_{20}$-IIP and $MACN_{20}$-NIP.

Figure 5.21 illustrates multi-linearity graphs indicating that intra-particle diffusion was not the only rate determining step involved in the adsorption of Cr(III) by $MACN_{20}$-IIP and $MACN_{20}$-NIP (Saha, 2010, Doke and Khan, 2017). The slope in the first curves was steeper while it was much slower in the second linear graphs. The steeper slope part of the graph was credited to the boundary layer diffusion (Cheung et al., 2007). That is, the movements of Cr(III) ions from the bulk solution to the boundary layer of adsorbents was a fast process more so for the $MACN_{20}$-IIP probably due to the created sites at the proximity of the surface.

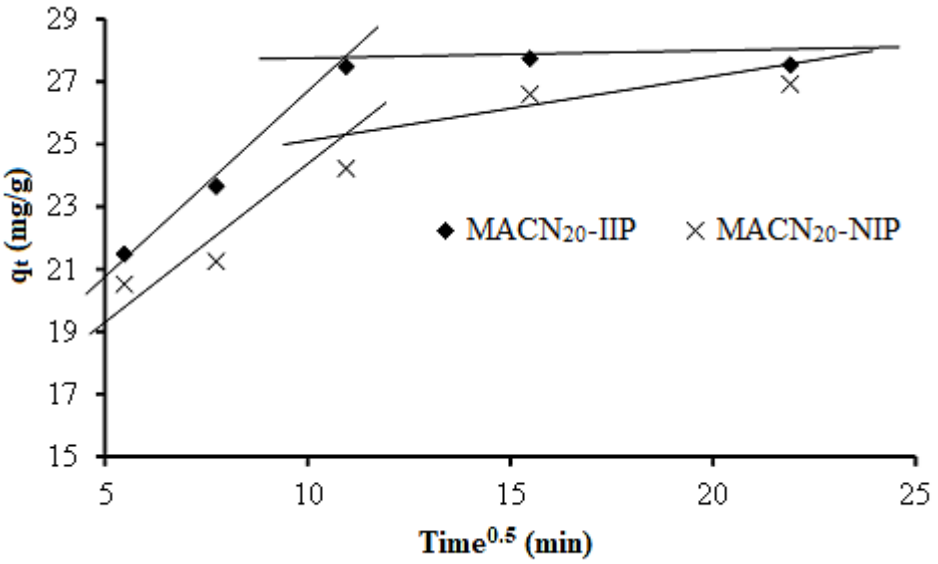

Figure 5.21: Intra-particle diffusion curves for the adsorption of Cr(III) by $MACN_{20}$-IIP and $MACN_{20}$-NIP.

The second portion of the graph was attributed to the intra-particle diffusion rate limiting step. None of the straight line graphs passed through the origin indicating

that intra-particle diffusion was not the only rate limiting step. Consistent with other studies in literature Tseng and Tseng (2005), it was then concluded that the adsorption of Cr(III) by $MACN_{20}$-IIP and $MACN_{20}$-NIP followed two mechanisms, i.e., external mass transfer (film diffusion) and/ or the intra-particle diffusion. In addition, the film diffusion rates were much faster than the intra-particle diffusion rates as determined by the slopes of the curves indicating that greater sorption took place at the initial period.

5.2.2.8. Effect of co-existing ions

The effect of competitive ions on the removal of Cr(III) was conducted using synthetic water containing 100 mg/L of each of Cr^{3+}, Cr^{6+}, Ni^{2+}, Cu^{2+} and Cd^{2+}. As illustrated in Figure 5.22, both adsorbents selectively bound Cr^{3+} even in the presence of other competing ions. According to Li et al. (2015), metal-ligand binding preference is governed by the concept of hard-soft acid and bases. Generally, species are classified as hard due to a smaller ionic radii and high charge state whereas soft species have a bigger size and a low charge state. The basic theory stipulates that soft acids preferentially bind to soft bases and hard acids to hard bases. The categories are as follows: Ni^{2+} and Cu^{2+}, "borderline" acids both Cr^{3+} and Cr^{6+}, hard acids and Cd^{2+}, soft acid. Hence, hard base amine ($-NH_2$) on the surface of the adsorbents (from tetraethylenetriamine ligand) formed strong metal-ligand complexes with both the hard (Cr^{3+}, Cr^{6+}) and "borderline" (Ni^{2+}, Cu^{2+}) acids. From Figure 5.22, the removal efficiency of the metal ions by $MACN_{20}$-IIP followed the trend Cr^{3+}(92.15%) >Ni^{2+} (80.1%)> Cr^{6+} (70.1%) >Cu^{2+} (65.2%) >Cd^{2+} (42.1%).

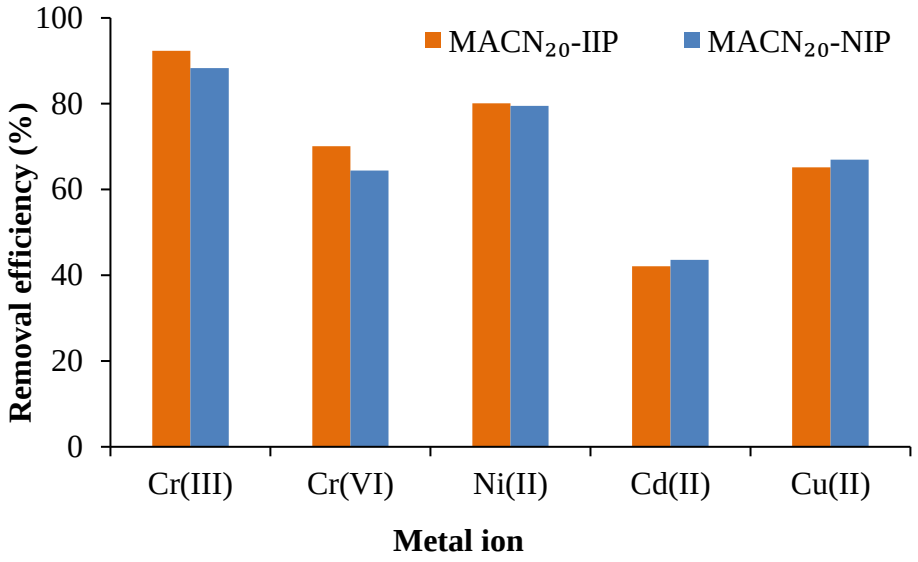

Figure 5.22: Removal efficiencies of cations adsorbed by the $MACN_{20}$-IIP and $MACN_{20}$-NIP (conditions: solution pH 5; solution concentration 100 mg/L; solution volume 30 mL; adsorbent dosage 10.67 g/L; contact time 240 min).

According to Kumar et al. (2009), divalent metal ions possess faster ligand exchange rates than trivalent metals. These rates were reported to be: 1.09×10^{9} s^{-1}, 4×10^{4} s^{-1} and 2×10^{-6} s^{-1} for Cu(II), Ni(II) and Cr(III), respectively. As per this explanation, Cu^{2+} was expected to have higher sorption efficiency compared to Ni^{2+} and Cr^{3+} as a result of a greater ligand exchange rate value. However, Cr^{3+} uptake was favoured. The different degrees in extraction efficiencies have been accounted to the imprinted memory (imprinting effect) created on the polymer matrices which encourage an orderly ligand arrangement leading to the superior selectivity of Cr(III) ion over other species.

Table 5.9 outlines the distribution coefficient, selectivity coefficient and the relative selectivity coefficient of the cationic ions in a competitive environment with regards to the target analyte (Cr^{3+}). K_d is referred to as the ratio of how the concentration of a particular ion equilibrates between the imprinted polymer and

the aqueous solution. This value represents the ability of imprinted polymer per unit mass to extract a particular ion per unit volume. As presented in Table 5.9, $MACN_{20}$-IIP exhibited slightly higher K_d values than its corresponding NIP. This suggested specific coordination geometry within the polymer matrix host of the IIP for target ion. Cd^{2+} had the highest K_d value implying that it could infiltrate the polymer imprinting sites. The metal sorption followed the trend $Cd^{2+} > Cr^{6+} > Ni^{2+} > Cu^{2+}$.

Table 5.9: Distribution coefficient (K_d), the selectivity coefficient (K) and the relative selectivity coefficient (K`) values of the cationic competitors relative to the template ion Cr^{3+}.

Metal ion	Radius/pm	K_d (L/g)		K		K'
		$MACN_{20}$ -IIP	$MACN_{20}$ -NIP	$MACN_{20}$ -IIP	$MACN_{20}$ -NIP	
Cr(III)	62	18.01	11.34	-	-	-
Cr(VI)	52	3.52	2.72	5.12	4.17	1.23
Cd(II)	95	6.05	5.81	2.98	1.95	1.53
Cu(II)	73	1.09	1.16	16.49	9.77	1.69
Ni(II)	70	2.81	3.03	6.41	3.74	1.72

Moreover, the closeness in pseudo-$MACN_{20}$-IIP competitor ions' K_d values inferred that considerable fractions of the imprinted sites occupied by the competing cations. Huang et al. (2017) also reported similar NIP K_d values for a competitive study of Cr^{6+}-IIP based on graphene oxide silica nano-sheet. The authors related this behaviour to non-specific adsorption process by the NIP. Elsewhere, Mishra and Verma (2017) described the distribution ratios in the order

Cd^{2+} > Ni^{2+} > Zn^{2+} when they applied Pb(II)-IIP allylthiourea based imprinted carbon nano fibres for the removal of the Pb^{2+} ion.

5.2.2.9. Real sample analysis

This study was conducted using an artificial acid mine drainage (AMD) sample obtained from a wetland crust. The removal efficiency was monitored at previously reported optimum conditions. The AMD sample was spiked with Cr(III) at different concentrations and adsorption was carried out as per the procedure described in published methods (Rajesh et al., 2008).

Table 5.10: The chemical composition of the AMD artificial sample.

Metal ion	Cr	Fe	Ni	Cu	Zn	Al	Cd	Sc	Co	U	Au
AMD conc (mg/L)	32.0	26.9	165.	74.1	391.	15.9	8.46	5.20	19.5	4.84	0.22

The solution pH and conductivity of the AMD sample were also measured before adsorption and were found to be 2.97 and 8.86 S/m, respectively. The acidic pH was associated with the effect of AMD whereas the solution conductivity suggested that the contaminants which constitute the sample to be in their ionic form. As illustrated in Table 5.11, $MACN_{20}$-IIP and $MACN_{20}$-NIP extraction efficiencies were above 72% and 56%, respectively. These results demonstrated the potential, application, and suitability of $MACN_{20}$-IIP adsorbents for the selective adsorption of Cr(III) from complex wastewater matrix.

Table 5.11: Application of $MACN_{20}$- IIP the corresponding NIP on unspiked and spiked real water sample (conditions: pH 5; solution volume 30 mL; adsorbent dosage 33.33 g/L).

Sample	Concentration of Cr (mg/L)			Extraction efficiency (%)	
	Spiked	Found		$MACN_{20}$-IIP	$MACN_{20}$-NIP
		$MACN_{20}$-IIP	$MACN_{20}$-NIP		
AMD	-	32.02	32.02	-	-
	5	39.02	41.87	< DL	< DL
	10	43.15	43.00	72.20	56.0
	30	67.20	58.60	65.80	57.3

DL: below detection limits

The full chemical composition of the sample was determined by Inductively coupled plasma optical emission spectroscopy (ICP-OES), and the results are presented in Table 5.10.

5.3. Synthesis of Cr(III)-molecularly imprinted polymers

In this section, a Cr(III) imprinted polymer was synthesized following a protocol from Leśniewska et al. (2012) through bulk polymerization method. The possible mechanism of IIP formation is shown in Figure 5.23. This mechanism entails direct interaction of both the functional monomer (acrylamide (AA)) and the ligand ([ammoniumpyrrolidinedithiocarbamate (APDC)) with the template ion (Cr^{3+}). The coordination of chromium ion and AA occurred through the lone pairs on both the oxygen and nitrogen atoms. As for the complexation with APDC, the bond formation arose from the coordination with the sulphur atoms. Cr(III) ions were

removed from the polymer matrix using 0.1 mol/L HNO_3 solution to create adsorption sites complementary to Cr(III) ions for size, shape, and functionality.

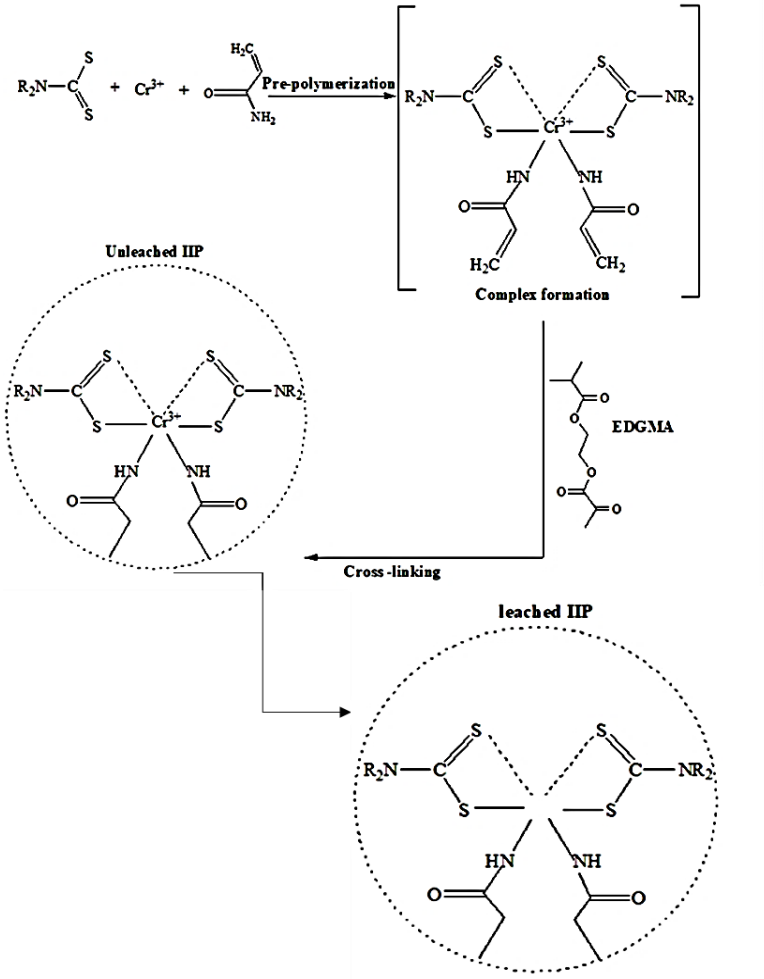

Figure 5.23: Polymerization mechanism of Cr(III)-PDC IIPs.

5.3.1. Characterization of adsorbent

5.3.1.1. Brunauer Emmett Teller (BET) analysis

Pore size distribution and surface porosity of the imprinted polymers were evaluated using their relative N_2 adsorption/desorption isotherms. As depicted in Figure 24 a and b the N_2 adsorption/desorption curves exhibited a similar profile indicative of a Type III isotherm (characterized by a convex to the x-axis over its entire range). At increased relative pressures the IIPs latter demonstrated a prominent hysteresis assigned to the formation of microporosity, which was absent

in corresponding NIPs. Both isotherms (adsorption and desorption) displayed only a single step demonstrating a fraction of both open and blocked pores.

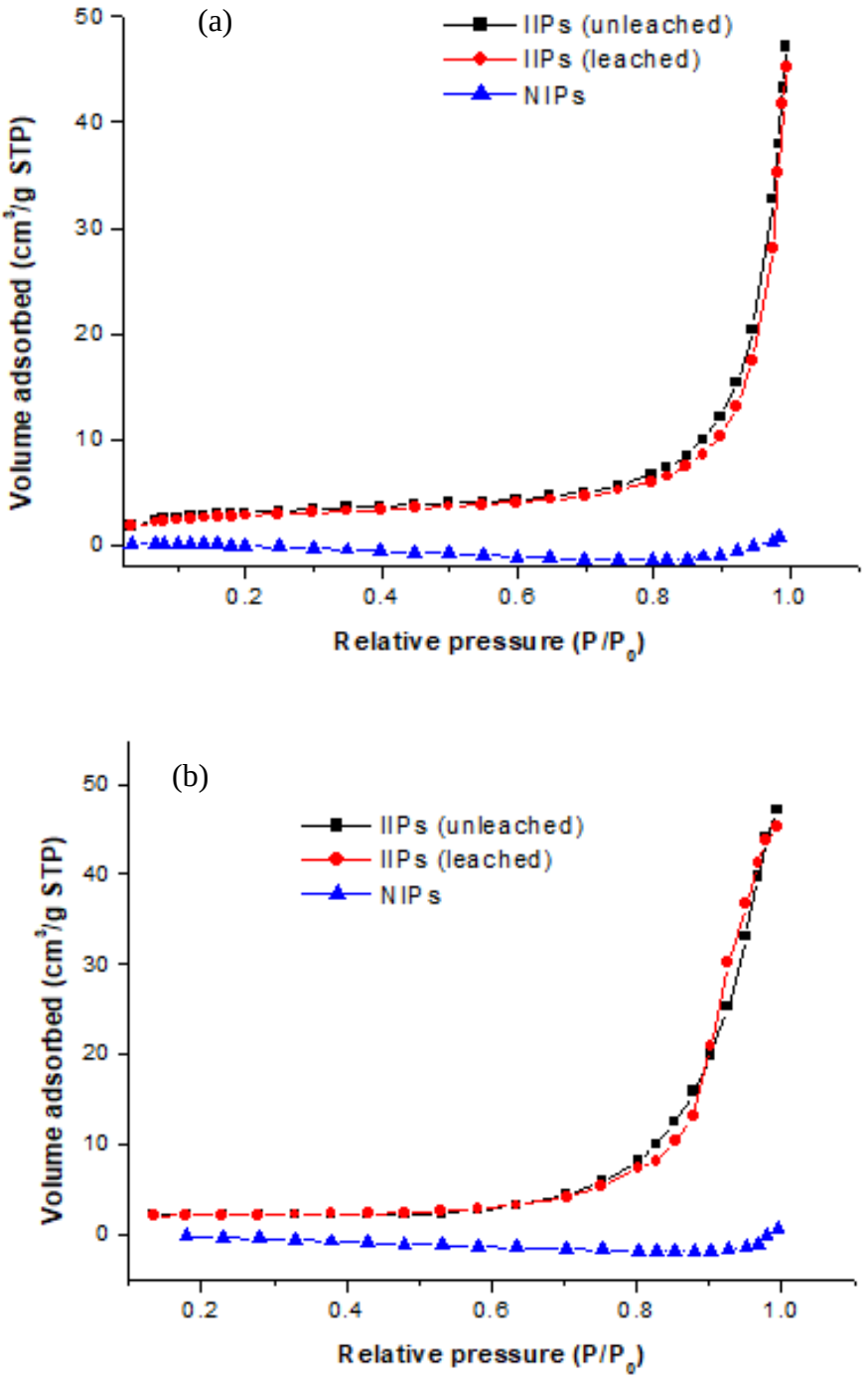

Figure 5.24: N_2 adsorption (a) and desorption (b) of IIPs (leached and unleached) NIPs.

BET analysis was employed to elucidate the surface area and pore characteristics of the Cr(III)-IIPs/NIPs. The results are presented in Table 5.12 below.

Table 5.12: BET surface areas, pore volumes and pore sizes of Cr(III)-IIPs (leached and unleached) and NIPs.

Adsorbent	Surface area (m^2/g)	Pore volume (cm^3/g)	Pore size (nm)
IIPs (unleached)	11.41	0.067	23.46
IIPs (leached)	10.15	0.070	25.45
NIPs	3.12	0.00055	13.36

Observed surface area values were as follows, for unleached IIPs (11.41 m^2/g), leached IIPs (10.15 m^2/g) and NIPs (3.12 m^2/g). Unleached IIPs had higher surface area than leached IIPs probably because the extra Cr^{3+} bonded to the polymer created additional surface exposure. On the other hand, the pore volume and pore size in the leached IIPs were higher than that of the unleached IIPs because the extracted Cr^{3+} ions created such pores upon leaving the imprinted sites. NIPs had the lowest surface area (3.12 m^2/g) and pore size (13.36 nm) because Cr^{3+} ion was not included in the synthesis of NIPs. IIPs and NIPs are characterized by low surface area values as indicated in the work by Yang et al. (2013) where IIP and NIP exhibited 9.28 m^2/g and 7.50 m^2/g surface area values, respectively.

5.3.1.2. FTIR spectroscopy

A binary complex of Cr(III) and PDC was formed and used to prepare the Cr(III)-PDC IIPs. To confirm the complexation, the FTIR spectra of commercial APDC and the complex were compared (Figure 5.25). A strong vibration at 1412 cm^{-1}

suggested the presence of the double bond character attributable to C=S functional group of the APDC while the absorption band at 938 cm^{-1} was associated with *v*(–CSS) vibrations (Figure 5.25a) (Sarwar et al., 2006). Noticeably, from Figure 5.25b these characteristic peaks shifted to 1436 cm^{-1} and 946 cm^{-1}, respectively, in the complex suggesting the involvement of the functional groups in Cr(III) complexation.

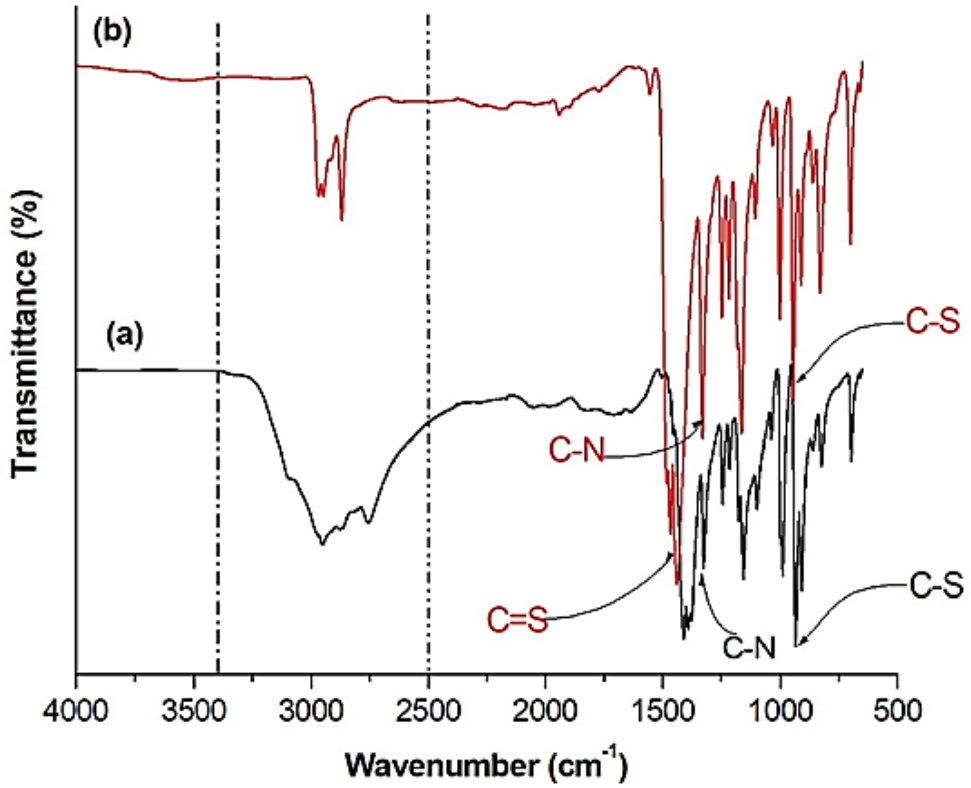

Figure 5.25: FTIR spectra of (a) ammonium pyrrolidine dithiocarbamate and (b) Cr(III)-PDC complex.

Mishra and Verma (2017) also observed vibrations around similar regions, C-N (1261cm^{-1}) and C=S (1586 cm^{-1}) from their Pb(II)-allylthiorea IIP. Another observable change was in the shape of a broad distinct peak between 3087 and 2744 cm^{-1} observed in Figure 5.25a to a suppressed, double spiked band at 2948 cm^{-1} in

Figure 5.25b. The alteration suggested successful coordination between the metal ion and the PDC ligand.

In accordance to Musthak Ahamad et al. (2012), vibration bands in the range of 940–1000 cm^{-1} were used to distinguish between monodentate and bidentate dithiocarbamate ligand chelation. The authors inferred that bidentate coordination of the dithio ligand was supported by the presence of only one strong band, but the monodentate coordination was signified by a doublet. It was then concluded in the present study that the metal-ligand coordination was through bidentate chelation as depicted by a single band observed in the complex at 946 cm^{-1}. Sarwar et al. (2006) inferred that v(N–CSS) band defines a carbon-nitrogen bond order intermediate between a single bond (v = 1350–1250 cm^{-1}) and a double bond (v = 1690–1640 cm^{-1}). The scheme below depicts the four possible resonance structures of pyrrolidine dithiocarbamate ligand. The carbon-nitrogen character of (C-N) from v(N-CSS) mode was shifted to higher frequencies (Figure 5.25 a and b) suggesting a greater contribution of the structure (iv) below.

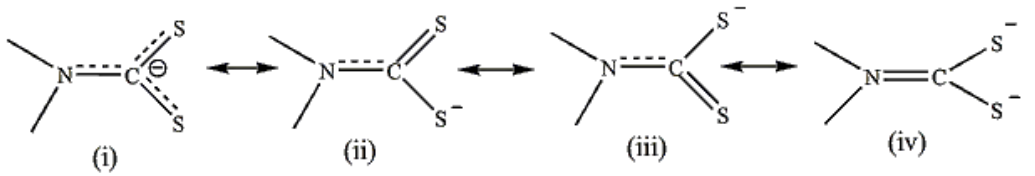

Figure 5.26: Resonance structures of pyrrolidine dithiocarbamate.

The FTIR spectra of Cr(III)-PDC IIPs (leached and unleached) and NIP are shown in Figure 5.27. All the polymer adsorbents exhibited similar structural profiles associated with excessive EGDMA used in polymer synthesis to achieve structural rigidity. Strong vibrational stretches at 1714 cm^{-1} and 1130 cm^{-1} corroborated the existence of C=O of carboxyl groups and C-O of linkages of the AA and EGDMA.

There was an observable change in acrylamide N-C=O (1654 cm^{-1} in unleached IIPs) stretching frequency to the higher region in the leached (1668 cm^{-1}) polymer. This ascertained the successful inclusion of chromium ion from the imprinted polymer during the polymerization step. The presence of a distinguished peak at 1636 cm^{-1} confirmed that there was almost complete conversion of the C=C groups of the acrylamide allyl moieties.

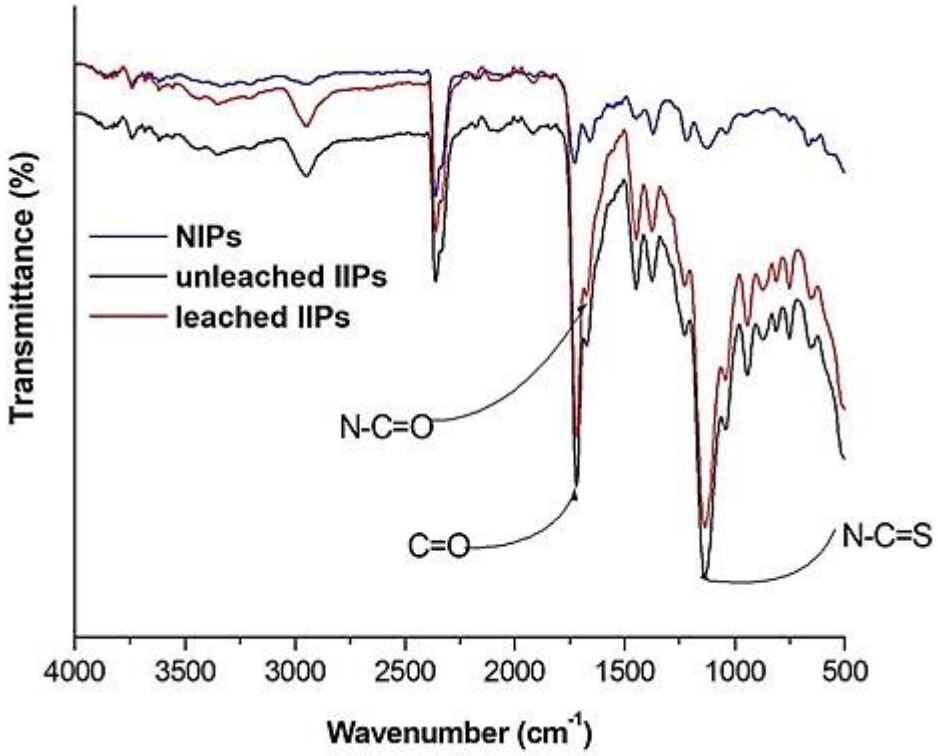

Figure 5.27: FTIR spectra of IIPs and respective NIPs.

5.3.1.3. Thermogravimetric analysis

Figure 5.28 illustrates the thermal stability of the polymers and their decomposition patterns. An initial weight loss of about 11%, 12% and 2% around 102°C, and 134°C for the unleached IIPs leached IIPs and NIPs was associated with the loss of moisture. The second decomposition occurred between 162°C, and 243°C was assigned to the disintegration of organic groups attached to the adsorbent surface (particularly the volatile components like CH_4, CO, and CO_2). A significant

weight loss at 289ºC, 281ºC, and 321ºC estimated to 86% (unleached IIP), 88% (leached IIP) and 90% (NIP) was ascribed to the decomposition of polymer structure (Figure 5.27b). NIP displayed higher thermal stability than the IIP probably due to less exposed surface. Zhang et al. (2017b) synthesized Cu(II) selective IIPs from salicylaldoximes, used as chelating ligands, were anchored onto the polymer networks through quaternary ammonium cation spacers. Thermal studies also revealed a pronounced mass loss in the polymer materials at the temperature of 300ºC-500ºC attributed to the disintegration of polymer back bone.

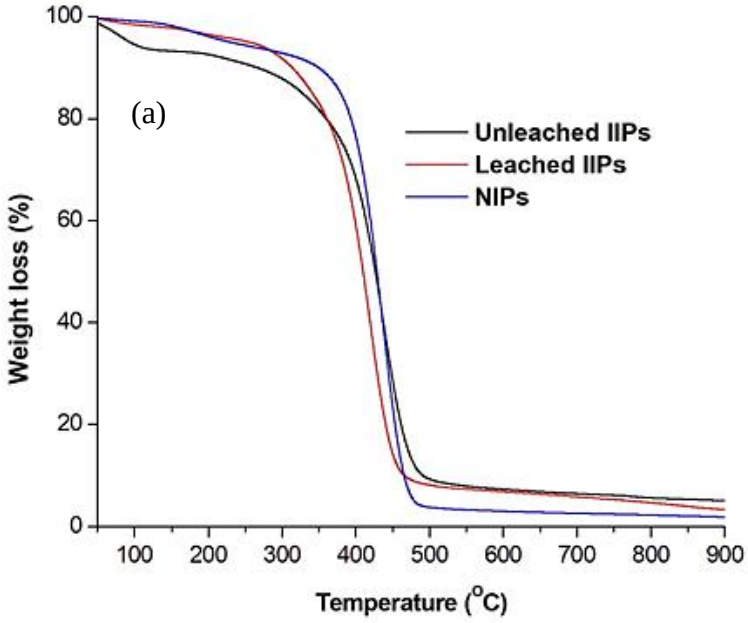

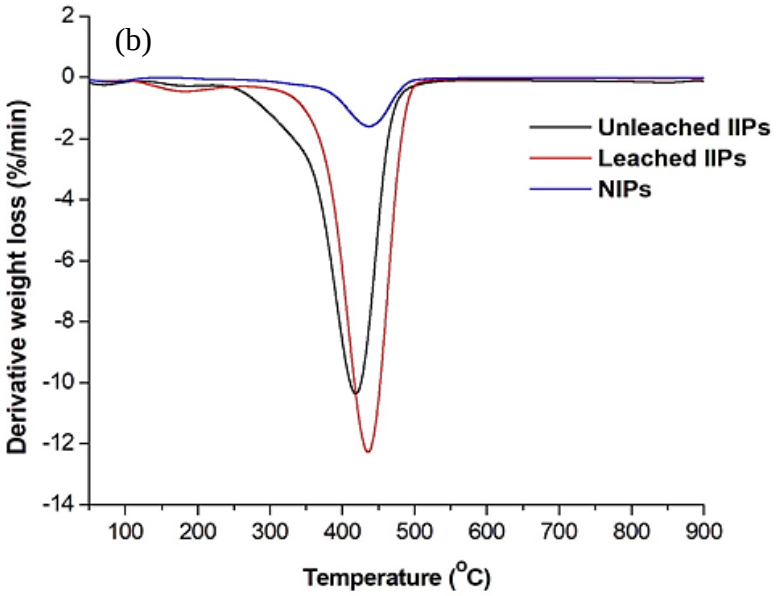

Figure 5.28: TGA (a) and DTA (b) thermograms of polymeric materials.

5.3.1.4. Scanning electron microscopy

The morphological characteristics of the IIP and NIP were examined using SEM analysis. Figure 5.29 shows that all materials had some degree of porosity.

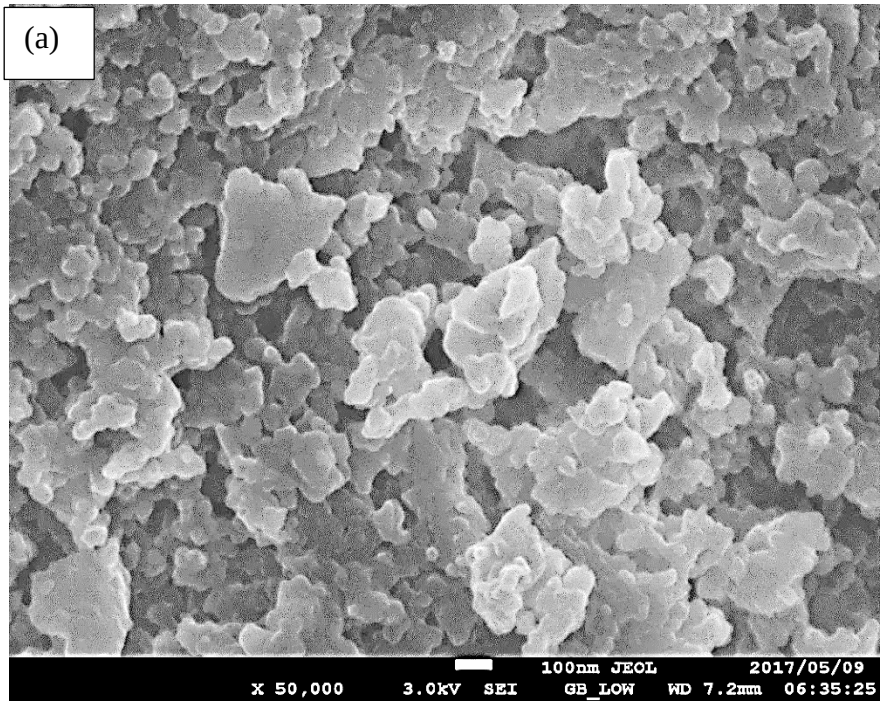

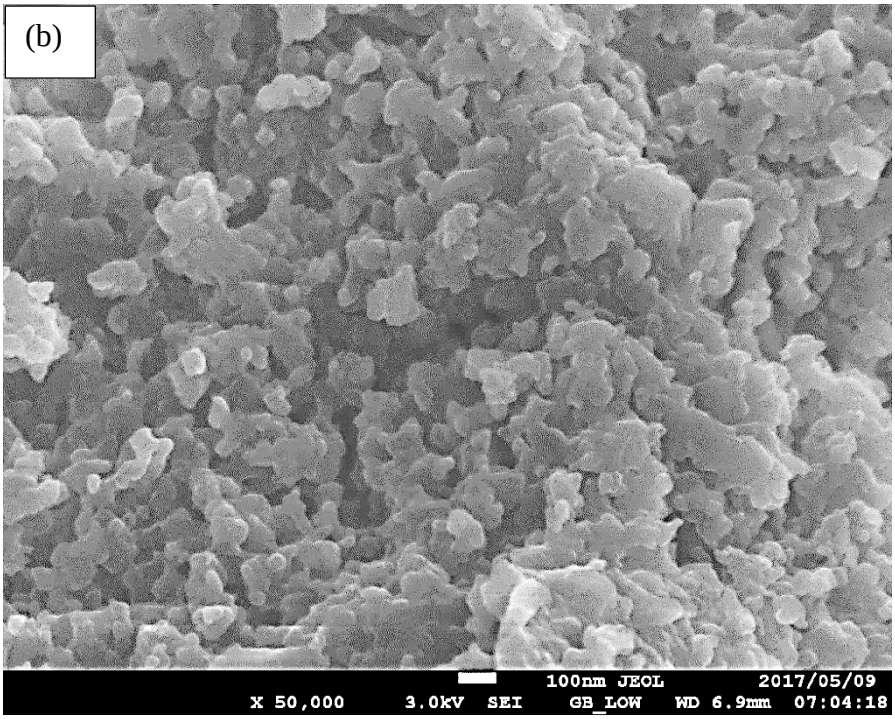

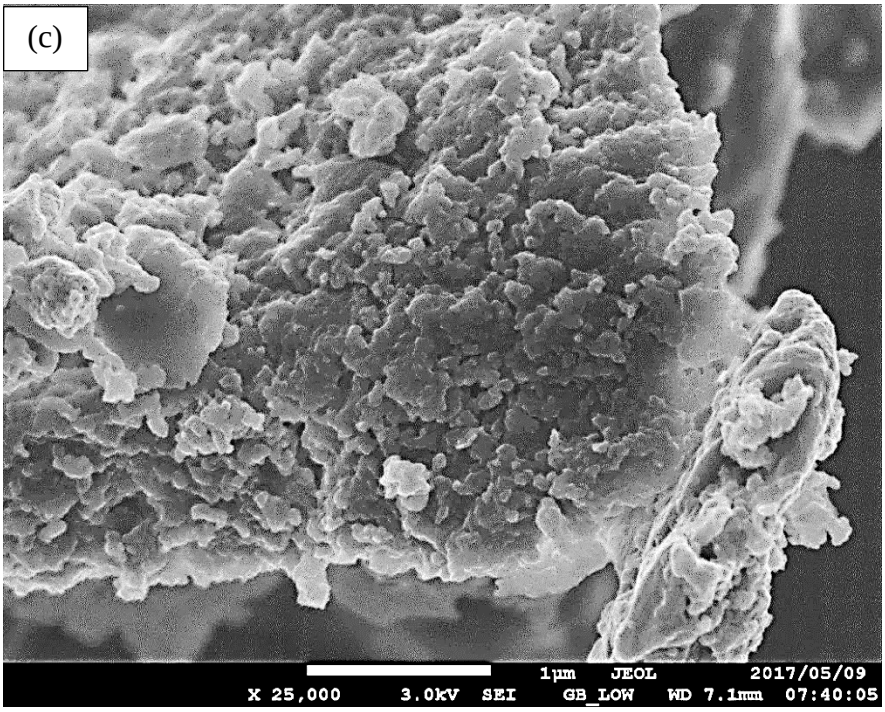

Figure 5.29: SEM micrographs of unleached Cr(III)-IIPs (a), leached IIPs (b) and the NIPs (c).

Figure 5.29a shows a much rough surface texture with some lumps on the surface compared to Figure 5.29(b). This roughness was attributed to the presence of

Cr(III) ions on the unleached IIP. Figure 5.29c showed a bit of scaling with lesser pores. The difference observed on the materials were a result of imprinting effect

5.3.2. Adsorption studies

5.3.2.1. Effect of solution pH on Cr(III) adsorption

Figure 5.30 shows the effect of solution pH on the removal of Cr^{3+} ions by Cr(III)-IIP and NIP over the pH range of 1-9. The removal of Cr(III) increased from pH 2 to pH 4 attaining 68 and 59% removal for IIP and NIP, respectively. As the pH was increased beyond pH 4 to pH 9, the %removal decreased in both materials. Therefore, pH 4 gave the maximum adsorption efficiency. In this case, the Cr(III) species assumed to be prevalent as per Figure 5.15 were a mixture of Cr(III) and $Cr(OH)^{2+}$. Increased efficiencies at highly alkaline media were associated with the precipitation to $Cr(OH)_3$ complexes as suggested in the literature (Kumar et al., 2009). Therefore, adsorption could not be carried beyond pH 8.

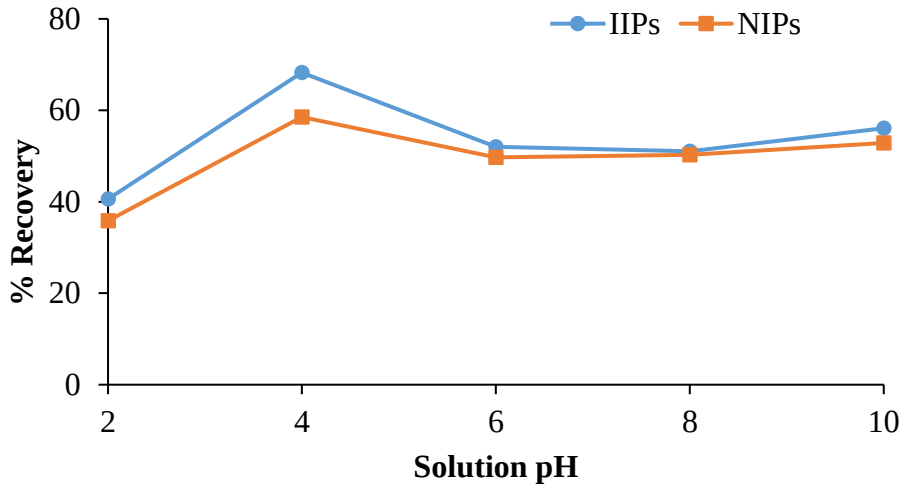

Figure 5.30: Effect of solution pH on the % recovery of Cr(III) by IIPs and NIPs.

5.3.2.2. Selectivity studies

The presence of other cations is known to create a competitive environment for the re-binding of the target analyte by IIPs. Cr(III) uptake was assessed in the existence

of other metal ions. The binary mixture constituted of Cr^{3+}/Cr^{6+}, Cr^{3+}/Ni^{2+}, Cr^{3+}/Cd^{2+} and Cr^{3+}/Cu^{2+}. The distribution coefficient (K_d), the selectivity coefficient (K) and the relative selectivity coefficient (K`) values of the competing ions with respect to the target Cr^{3+} ions are profiled in Table 5.13. It was deduced that Ni^{2+} possessed a higher K_d value than its competing counterparts. This may signify that Ni^{2+} ions were able to permeate and populate considerable fragments of the imprinting cavities.

Primarily, metal ionic radius and charge influence the ability of the polymer to recognize the specific template ion. It was noted that the competing ions under study retained comparable ionic radii (Cr^{3+}:62 pm, Cr^{6+}:52 pm, Ni^{2+}:70 pm, Cu^{2+}:73 pm and Cd^{2+}:95 pm). In view of this factor, all cationic competitors possess similar K_d values. This may be associated with partial polymerization as a result of the rapid formation of polymer monolith (observation during polymer synthesis). Therefore this may have resulted in disorderly arranged complementary imprinting sites. In spite of this aspect, the extraction ability (K_d) of the ion imprinted polymer per unit mass of a specific ion was superior to that of the corresponding NIP. On this basis, it could be inferred that the degree of corresponding order of metal sorption by IIPs followed the sequence: $Ni^{2+} > Cr^{6+} > Cu^{2+} > Cd^{2+}$.

Table 5.13: Imprinting factor, selectivity and separation ratios of IIPs.

Cationic competitor	K_d (L/g)		K		K'
	IIP	NIP	IIP	NIP	
Cr^{3+}	0.161	0.157	-	-	-
Cr^{6+}	0.153	0.127	1.27	1.03	1.24
Ni^{2+}	0.158	0.151	1.02	1.00	1.05
Cd^{2+}	0.118	0.121	1.05	1.29	1.05
Cu^{2+}	0.143	0.157	1.36	0.99	1.03

No further batch adsorption experiments were undertaken with Cr(III)-IIP/NIP because the material has already been studied by Leśniewska et al. (2012). However, we needed the IIP for our applications hence we have to synthesize it ourselves as we cannot get it from the mentioned authors. Thus, the aim of synthesizing Cr(III)-IIP was to use it together with MACN and $MACN_{20}$-IIP adsorbents for the simultaneous sequestration of Cr(VI) and Cr(III) ions from aqueous media. It was established in the recent study and other studies from our group that during the adsorption of Cr(VI) by MAC, some of the Cr(VI) were transformed into Cr(III) through reduction mechanism induced by the presence of electron donating groups on the surface of MAC (Pakade et al., 2017). In the next section, an attempt was made to remove both Cr(VI) and Cr(III) from aqueous solution using $MACN_{20}$/$MACN_{20}$-IIP and $MACN_{20}$/Cr(III)-IIP combinations.

5.4. Simultaneous removal of Cr(VI) and Cr(III)

As mentioned from the previous Chapters (2 and 4), the principal objective of the research was to simultaneously remediate the two predominant forms of chromium,

Cr(VI) and Cr(III). Two approached were adopted, first Cr(VI) was contacted with $MACN_{20}$ and $MACN_{20}$-IIP simultaneously. A typical experimental method was as follows:

A mixture of 0.2 g $MACN_{20}$ and 0.2 g $MACN_{20}$-IIP was stirred with 100 mg/L of Cr(VI) solution at pH 2. The contents of Cr(VI) and Cr(III) were determined using UV-vis spectroscopy and FAAS, respectively. In the second approach, the same combination of adsorbents was used separately, that is first the Cr(VI) solution was contacted with $MACN_{20}$, and after a lapse of reaction time the adsorbent was separated from the solution by centrifugation. Further adsorption was carried out on the same solution but using $MACN_{20}$-IIP instead. Cr(VI) and Cr(III) were measured in both solutions as detailed above. Simultaneous removal of Cr(VI) and Cr(III) was also examined by employing a combination of MAC_{20} and IIPs.

Figure 5.31 depicts the concentration of the total chromium, Cr(VI) and Cr(III) vis-à-vis the blend of adsorbents used. The studied adsorbent blends displayed a comparable performance on metal sorption.

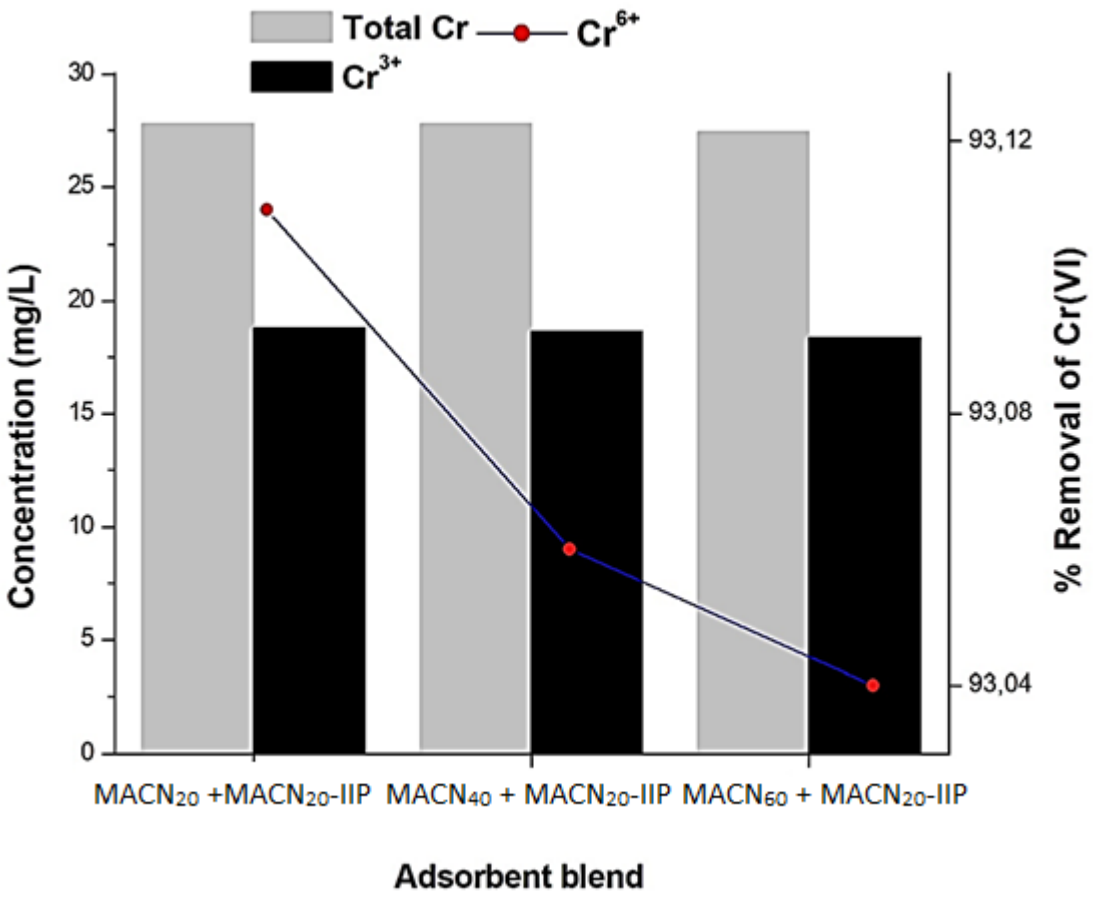

Figure 5.31: Showing % removal of Cr(VI), equilibrium total chromium Cr(III) concentration after adsorption by MACN/$MACN_{20}$-IIP adsorbent blends.

The magnitude of the percentage removal of Cr(VI), total chromium and Cr(III) concentration attained after adsorption ranged around 93%, 28 mg/L, and 19 mg/L, respectively on all adsorbent combinations. The application of these sorbent combinations revealed their efficiency regarding mitigating Cr(VI) from solutions as 93% was removed from the initial concentration of 100 mg/L. Meaning that there was only about 7 mg/L of Cr(VI) left in solution. However, the total chromium analysis by FAAS revealed that in fact there was 28 mg/L of Cr in solution asserting that a reduction to Cr(III) took place and that Cr(III) was not reabsorbed but let in solution. This could pose serious environmental and health issues if such water were to be discharged into wastewater streams because Cr(III)

can be reoxidized into the toxic Cr(VI) certain conditions causing recurrence of the problem.

The rationale behind these studies was that, during adsorption of Cr(VI) by MAC adsorbents, adsorption and reduction of Cr(VI) to Cr(III) took place and there was also an increase in solution pH after adsorption due to exhaustion of protons. It was then envisaged that there would be the simultaneous uptake of the formed Cr(III) by $MACN_{20}$-IIP due to favourable pH (pH 3-5) for Cr(III) adsorption leading to total sequestration of both Cr(VI) and Cr(III) in solution by the sorbent blend combinations. In the past approach where a mixture of adsorbents was utilized simultaneously only minimum synergy was observed. In the next sections, the adsorbents were employed in succession that is, using approach two.

Table 5.14 summarizes the final chromium contents after adsorption following the application of adsorbents in succession for the uptake of both Cr(VI) and Cr(III) from an initial concentration of 100 mg/L. It was evident from the outlined results that MACN materials removed a significant amount of Cr(VI) producing 28.95 mg/L, 27.89 mg/L and 26.23 mg/L of Cr(III) for MAC_{20}, $MACN_{40}$, and $MACN_{60}$, respectively. Maximum uptake of Cr(VI) was primarily achieved with $MACN_{20}$. The material facilitated 98.23% removal.

The overall quantity of the remaining total chromium concentration was examined to be 30.72 mg/L ($MACN_{20}$), 31.60 mg/L ($MACN_{40}$) and 31.09 mg/L ($MACN_{60}$). Subsequently, the addition of $MACN_{20}$-IIP into the reaction vessel resulted in a notable decrease in chromium concentration. The total chromium concentration decreased significantly from 30.72 mg/L to 9.20 mg/L, and the remaining Cr(III) also decreased while there was a slight decrease from 1.77 mg/L to 1.66 mg/L in

Cr(VI) concentration. A succession combination of MAC_{40} and MAC_{60} with $MACN_{20}$-IIP also yielded similar results but not with the efficiency observed for the $MACN_{20}$/$MACN_{20}$-IIP combination. Notably, there was 55% (from 3.71 mg/L to 1.68 mg/L) and 45% (from 4.86 mg/L to 2.62 mg/L) decrease in equilibrium Cr(VI) concentration after the application of $MACN_{20}$-IIP, demonstrating its efficiency in Cr(VI) removal. Comparing the approach two (succession) and approach one (mixture), it can be said that approach two worked better if taking into account the total chromium left in solution 9.20-24.51 mg/L versus 28 mg/L.

Table 5.14: Total chromium, Cr(VI) and Cr(III) concentration by different MACN/$MACN_{20}$-IIP adsorbent blends.

Adsorbent blend						
MACN				$MACN_{20}$-IIP		
Carbon material	Chromium concentration (mg/L) remaining after adsorption					
	Cr^{6+}	Total Cr	Cr^{3+}	Cr^{6+}	Total Cr	Cr^{3+}
$MACN_{20}$	1.77	30.72	28.95	1.66	9.20	7.54
$MACN_{40}$	3.71	31.60	27.89	1.68	19.42	17.75
$MACN_{60}$	4.86	31.09	26.23	2.62	24.51	21.89

To further explore the feasibility of chromium removal a blend of MACN/IIP were investigated. The total chromium concentration, Cr(VI) and Cr(III) concentrations were monitored, and the results are tabulated below. Notably, the outlined findings revealed MACN adsorbents promoted Cr(VI) adsorption by subsequent reduction to Cr(III). The total chromium concentrations remaining in solution were 15.19 mg/L, 22.21 mg/L and 24.49 mg/L for $MACN_{20}$/IIP, $MACN_{40}$/IIP, and $MACN_{60}$/IIP, respectively. The corresponding Cr(III) concentrations were 13.76

mg/L, 18.23 mg/L and 21.63 mg/L for $MACN_{20}$/IIP, $MACN_{40}$/IIP, and $MACN_{60}$/IIP, respectively.

Minimal quantity of chromium content was achieved with $MACN_{20}$/IIP with 15.19 mg/L total chromium of which 1.43 mg/L was Cr(VI), and 13.76 mg/L was Cr(III). Xie et al. (2017), established one-step removal of Cr(VI) by reduction to Cr(III) followed by in-situ Cr(III) precipitation. Although spontaneous precipitation of Cr(III) was expected, < 10% chromium removal was achieved 60 min after addition of precipitant.

Though there was slight variation in chromium concentration with the respective adsorbent combination used, the adsorbents still displayed great potential of removing both Cr(VI) and Cr(III) in aqueous solutions.

Table 5.15: Total chromium, Cr(VI) and Cr(III) concentration by different MACN/ IIP adsorbent blends.

Adsorbent blend						
MACN			IIP			
Carbon material	Chromium concentration (mg/L) after adsorption					
	Cr^{6+}	Total Cr	Cr^{3+}	Cr^{6+}	Total Cr	Cr^{3+}
$MACN_{20}$	1.52	35.29	33.77	1.43	15.19	13.76
MAC_{40}	4.23	34.63	30.40	3.98	22.21	18.23
$MACN_{60}$	3.56	34.52	30.96	2.86	24.49	21.63

Based on the reported findings in this section, $MACN_{20}$ showed great potential for Cr(VI) adsorption and reduction. However, *Macadamia* activated carbon blends ($MACN_{20}$/$MACN_{20}$-IIP) worked better than $MACN_{20}$/IIP. This was based on the total chromium content remaining in solution after adsorption.

Additionally, this study demonstrated feasible systematic chromium adsorption coupled reduction. It is confirmed that Cr(VI) can be efficiently transformed to Cr(III) and subsequently re-adsorbed by specific ion-imprinted polymers. In summary, the adsorbents have shown the great potential of removing both Cr(VI) and Cr(III) in aqueous solutions.

CHAPTER 6

Conclusions and Recommendations

6.1. Conclusions

Macadamia nutshell-based activated carbons were chemically oxidized using different concentrations of nitric acid. Elemental analysis, BET, FTIR, TGA, and SEM were all used to evaluate the structural and chemical changes of the prepared adsorbents.

Elemental analysis revealed that treatment of MAC with HNO_3 reduced the %C from 78.09 to 73.40% as HNO_3 concentration was increased from 20 to 60%. The incorporation of nitrogen as a result of nitric acid treatment was evidenced by the %N contents of 1.46%, 1.70%, and 1.69%, corresponding to $MACN_{40}$ > $MACN_{60}$ > $MACN_{20}$, respectively. Subsequently increase in oxygen content was also observed. The %O sharply increased from 9.27% (pristine MAC) to 23.40% ($MACN_{60}$). This avowed that treatment of MAC with inorganic acid oxidized its surface to produce oxygenated functional groups.

FTIR spectra of acid treated materials showed attenuation of the hydroxyl band at 3400 cm^{-1} and appearance of a new band at around 986 cm^{-1} attributed to C-O-C. The spectra displayed the presence of oxygenated moieties like COOH and C=O at 1690 cm^{-1}, respectively. FTIR spectroscopy further displayed the in-plane vibration of N-H at 1000 cm^{-1} was enhanced by acid treatment which could imply the introduction of amine groups by acid treatment.

A suggestion was made that, HNO_3 modification introduced hydroxyl groups and carboxylic acid groups which could have formed ester linkages during heating of

virgin activated carbon under acidic conditions. The postulation was echoed by the presence of new peaks at 1416, 1404, and 1412 cm^{-1} attributable to ester linkages.

Thermogravimetric studies displayed the disintegration of water associating functional groups. This was accredited to the loss of less moisture content and greater thermal stability. All the carbon materials exhibited residue content above 75%.

SEM revealed different surface morphological properties showing distinct pore structures resulting from the various concentration and acid effects. $MACN_{20}$ had a rougher surface with relatively smaller pores than $MACN_{40}$. However, the structural character of $MACN_{60}$ displayed the more widened pores. This affirmed that increased strength of activating agent (high HNO_3 concentration) led to rupture and disruption of pore walls. Therefore, modification necessitates optimum concentration of the modifying agent.

BET analysis indicated a notable increase in surface area from 545 m^2/g to 583 m^2/g for virgin MAC and $MACN_{60}$, respectively. Moreover, all the adsorbents exhibited mesopores. This was attributable of an increase in the pore size and volume deducing that modification of MAC with HNO_3 facilitated pore formation on the adsorbent surface.

The optimum adsorption conditions for MACN were pH 1, 10.67 g/L, 100 mg/L and 480 min. Generally, nitric acid modified carbons had superior removal performances with adsorption capacities ranging from 38.53 mg/g to 40.99 mg/g. All adsorbents ($MACN_{20}$, $MACN_{40}$, and $MACN_{60}$) obeyed the PFO rate model, same as they all fitted into Langmuir isotherm. Intra-particle diffusion was not the sole rate controlling step as multi-linear plots were obtained.

The uptake of the resultant Cr(III) as a result of Cr(VI) reduction was made possible by incorporating Cr(III)-imprinted *Macadamia* activated carbons for effective total Cr in waste water. SEM, TGA, BET analysis and FTIR spectroscopy were used to examine the microscopic morphological characteristics, thermal stability, surface porosity and surface functionalities of the prepared adsorbents.

The ultimate analysis revealed a significant increase in nitrogen content. Prior imprinting, the found %N was 1.46% ($MACN_{20}$), upon imprinting with an amine ligand, the %N increased to 13.3%. This signified that the ligand was fixed on the surface of the activated carbon.

BET results indicated a greater surface area for leached $MACN_{20}$-IIP (64.20 m^2/g) than the non-imprinted counterpart, $MACN_{20}$-NIP (49.92 m^2/g) was attributable to the exposure of internal surface area resulting from formed cavities in leached $MACN_{20}$-IIP.

Notably, SEM analysis of the leached $MACN_{20}$-IIP displayed a rougher surface compared to the unleached adsorbent. This morphology was essential particularly for the specific adsorption of the imprint ion. However, the non-imprinted adsorbent had a lower degree of microporosity compared to the imprinted sorbents.

Maximum conditions were achieved at pH 5, 50 mg/L Cr(III) initial concentration and 33.33 g/L of adsorbent dosage. The maximum Langmuir adsorption capacity of $MACN_{20}$-IIP (69.61 mg/g) was considerably larger than that of $MACN_{20}$-NIP (68.37 mg/g). The selectivity coefficient of the imprinted MAC for Cr(III)/Cr(VI), Cr(III)/Ni(II), Cr(III)/Cu(II) and Cr(III)/Cd(II) were 5.12, 6.41, 16.49 and 2.98.

Moreover, the imprinted material showed higher selectivity than the corresponding non-imprinted counterpart. The prepared sorbents proved applicability in the extraction of Cr(III) ions from complex samples, AMD simulated sample. These prepared adsorbents (MACN and MAC-IIP) were successfully applied for the selective extraction of respective analytes through simultaneous adsorption approaches for complete total chromium recovery in solutions.

The prepared adsorbents (MACN, MAC_{20}, and Cr^{3+}-IIP) showed great potential in the simultaneous removal of Cr(VI) and Cr(III) in aqueous solutions. Initially, MACN could recover about 93% of Cr(VI) with 32.49 mg/L remaining in solution in the form of both Cr(VI) and Cr(III). Remarkably, the application of adsorbent combinations for simultaneous sequestration of chromium ions reduced the Cr(VI) and total chromium concentration from 1.77 mg/L to 1.66 mg/L and 15.19 mg/L to 1.43 mg/L, respectively.

6.2. Recommendations

Due to simplicity and cost-effectiveness, the method described herein can be extended to prepare similar activated carbon imprinted sorbents for the application in remediation of other heavy metals from wastewater samples, particularly where oxidation state transformation is a big challenge for total removal of a pollutant.

REFERENCES

ABDEL SALAM, O. E., REIAD, N. A. & ELSHAFEI, M. M. 2011. A study of the removal characteristics of heavy metals from wastewater by low-cost adsorbents. *Journal of Advanced Research,* 2**,** 297-303.

ACHARYA, J., SAHU, J. N., SAHOO, B. K., MOHANTY, C. R. & MEIKAP, B. C. 2009. Removal of chromium(VI) from wastewater by activated carbon

developed from Tamarind wood activated with zinc chloride. *Chemical Engineering Journal,* 150**,** 25-39.

AHAMED, M. E. H., MBIANDA, X. Y., MULABA-BAFUBIANDI, A. F. & MARJANOVIC, L. 2013. Ion imprinted polymers for the selective extraction of silver(I) ions in aqueous media: Kinetic modeling and isotherm studies. *Reactive and Functional Polymers,* 73**,** 474-483.

AHMARUZZAMAN, M. 2011. Industrial wastes as low-cost potential adsorbents for the treatment of wastewater laden with heavy metals. *Advances in Colloid and Interface Science,* 166**,** 36-59.

ALIZADEH, T., GANJALI, M. R. & ZARE, M. 2011. Application of an Hg(II) selective imprinted polymer as a new modifying agent for the preparation of a novel highly selective and sensitive electrochemical sensor for the determination of ultratrace mercury ions. *Analytica Chimica Acta,* 689**,** 52-59.

AL-OTHMAN, Z. A., ALI, R. & NAUSHAD, M. 2012. Hexavalent chromium removal from aqueous medium by activated carbon prepared from peanut shell: Adsorption kinetics, equilibrium and thermodynamic studies. *Chemical Engineering Journal,* 184**,** 238-247.

AMOR, H. B. & ISMAIL, M. 2013. Adsorption of chromium (VI) on Activated Carbon prepared by acid activation of Date Stones. *International Journal of Science and Research,* 4**,** 309-314.

ANIRUDHAN, T. S. & SUCHITHRA, P. S. 2010. Synthesis and characterization of iron(III)-coordinated amine-modified poly(glycidylmethacrylate)- grafted densified cellulose and its applicability in defluoridation from industry effluents. *Industrial and Engineering Chemistry Research,* 49**,** 12254-12262.

ASHOURI, N., MOHAMMADI, A., HAJIAGHAEE, R., SHEKARCHI, M. & KHOSHAYAND, M. R. 2015. Preparation of a new nanoparticle Cd(II)-imprinted polymer and its application for selective separation of cadmium(II) ions from aqueous solutions and determination via inductively coupled plasma optical emission spectrometry. *Desalination and Water Treatment,* 57**,** 14280-14289.

ASHRAF, S., CLULEY, A., MERCADO, C. & MUELLER, A. 2011. Imprinted polymers for the removal of heavy metal ions from water. *Water Science and Technology,* 64, 1325-1332.

AZWA, Z. N. & YOUSIF, B. F. 2013. Thermal degradation study of kenaf fibre/epoxy composites using thermo gravimetric analysis. In: NOOR, M.M., ISMAIL, M. R. J., (ed.) *3rd Malaysian postgraduate conference (MPC2013)* Sydney, New South Wales, Australia, 4, 309-314.

BABEL, S. & KURNIAWAN, T. A. 2004. Cr(VI) removal from synthetic wastewater using coconut shell charcoal and commercial activated carbon modified with oxidizing agents and/or chitosan. *Chemosphere,* 54**,** 951-967.

BEHBAHANI, M., SALARIAN, M., BAGHERI, A., TABANI, H., OMIDI, F. & FAKHARI, A. 2014. Synthesis, characterization and analytical application of Zn(II)-imprinted polymer as an efficient solid-phase extraction technique for trace determination of zinc ions in food samples. *Journal of Food Composition and Analysis,* 34**,** 81-89.

BELLO, G., CID, R., GARCıIA, R. & ARRIAGADA, R. 1999. Retention of Cr(VI) and Hg(II) in Eucalyptus globulus- and peach stone-activated carbons. *Journal of Chemical Technology and Biotechnology,* 74**,** 904-910.

BERGMANN, N. M. & PEPPAS, N. A. 2008. Molecularly imprinted polymers with specific recognition for macromolecules and proteins. *Progress in Polymer Science,* 33**,** 271-288.

BERNARDO, G. R., RENE, R. M. & MA CATALINA, A. D. 2009. Chromium (III) uptake by agro-waste biosorbents: chemical characterization, sorption-desorption studies, and mechanism. *Journal of Hazardous Materials,* 170**,** 845-854.

BEUKES, J., PIENAAR, J. & LANCHMANN, G. 2000. The reduction of hexavalent chromium by slphite in wastewater - An explanation of the observed reactiity partern. *Water SA,* 3**,** 393-395.

BOCHENEK, R., SITARZ, R. & ANTOS, D. 2011. Design of continuous ion exchange process for the wastewater treatment. *Chemical Engineering Science,* 66**,** 6209-6219.

BRANGER, C., MEOUCHE, W. & MARGAILLAN, A. 2013. Recent advances on ion-imprinted polymers. *Reactive and Functional Polymers,* 73**,** 859-875.

CECHINEL, M. A. P., ULSON DE SOUZA, S. M. A. G. & ULSON DE SOUZA, A. A. 2014. Study of lead (II) adsorption onto activated carbon originating from cow bone. *Journal of Cleaner Production,* 65**,** 342-349.

CHEN, C. Y., YANG, C. Y. & CHEN, A. H. 2011. Biosorption of Cu(II), Zn(II), Ni(II) and Pb(II) ions by cross-linked metal-imprinted chitosans with epichlorohydrin. *Journal of Environmental Management,* 92**,** 796-802.

CHEN, T., ZHOU, Z., XU, S., WANG, H. & LU, W. 2015. Adsorption behavior comparison of trivalent and hexavalent chromium on biochar derived from municipal sludge. *Bioresource Technology,* 190**,** 388-394.

CHEUNG, W. H., SZETO, Y. S. & MCKAY, G. 2007. Intraparticle diffusion processes during acid dye adsorption onto chitosan. *Bioresource Technology,* 98**,** 2897-2904.

CHOI, H. D., PARK, S. W., RYU, B. G., CHO, J. M., KIM, K. J. & BAEK, K. 2009. Adsorption characteristics of As(V) onto cationic surfactant-modified activated carbon. *Environmental Engineering Research,* 9**,** 153-157.

COOK, W. G. & OLIVE, R. P. 2012. Pourbaix diagrams for chromium, aluminum and titanium extended to high-subcritical and low-supercritical conditions. *Corrosion Science,* 58**,** 291-298.

CORMACK, P. A. & ELORZA, A. Z. 2004. Molecularly imprinted polymers: synthesis and characterisation. *Journal of chromatography. B, Analytical Technologies in the Biomedical and Life Sciences,* 804**,** 173-182.

CUI, Y., LIU, X. Y., CHUNG, T. S., WEBER, M., STAUDT, C. & MALETZKO, C. 2016. Removal of organic micro-pollutants (phenol, aniline and nitrobenzene) via forward osmosis (FO) process: Evaluation of FO as an alternative method to reverse osmosis (RO). *Water Research,* 91**,** 104-114.

CUNLIFFE, D., KIRBY, A. & ALEXANDER, C. 2005. Molecularly imprinted drug delivery systems. *Advanced Drug Delivery Reviews,* 57**,** 1836-1853.

DA COSTA LOPES, A. S., DE CARVALHO, S. M. L., DO SOCORRO BARROS BRASIL, D., DE ALCÂNTARA MENDES, R. & LIMA, M. O. 2015. Surface modification of commercial activated carbon (CAG) for the adsorption of benzene and toluene. *American Journal of Analytical Chemistry,* 06**,** 528-538.

DANIEL, S., PRABHAKARA RAO, P. & PRASADA RAO, T. 2005. Investigation of different polymerization methods on the analytical performance of

palladium(II) ion imprinted polymer materials. *Analytica Chimica Acta*, 536**,** 197-206.

DEHDASHTI, A., KHAVANIN, A., REZAEE, A., ASSILIAN, H. & MOTALEBI, M. 2011. Application of microwave irradiation for the Treatment of adsorbed volatile organic compounds on granular activated carbon. *Iran Journal of Environvironmental Health Sciences and Engineering,* 8, 85-94.

DEJANG, N., SOMPRASIT, O. & CHINDARUKSA, S. 2015. A preparation of activated carbon from *Macadamia* shell by microwave irradiation activation. *Energy Procedia,* 79**,** 727-732.

FERRERA-LORENZO, N., FUENTE, E., SUÁREZ-RUIZ, I. & RUIZ, B. 2014. KOH activated carbon from conventional and microwave heating system of a macroalgae waste from the Agar–Agar industry. *Fuel Processing Technology,* 121**,** 25-31.

FOO, K. Y. & HAMEED, B. H. 2012. Preparation, characterization and evaluation of adsorptive properties of orange peel based activated carbon via microwave induced K_2CO_3 activation. *Bioresource Technology*, 104**,** 679-686.

FU, F. & WANG, Q. 2011. Removal of heavy metal ions from wastewaters: a review. *Journal of Environmental Management*, 92, 407-418.

GAD, S. C. 2014. Chromium speciation in aquous media. *Journal of Hazardous Materials,* 1**,** 952-954.

GHOSH, P. K. 2009. Hexavalent chromium [Cr(VI)] removal by acid modified waste activated carbons. *Journal of Hazardous Materials*, 171, 116-122.

GROEN, J. C., PEFFER, L. A. A. & PÉREZ-RAMíREZ, J. 2003. Pore size determination in modified micro- and mesoporous materials. Pitfalls and

limitations in gas adsorption data analysis. *Microporous and Mesoporous Materials,* 60**,** 1-17.

HOSEINZADEH HESAS, R., ARAMI-NIYA, A., WAN DAUD, W. M. A. & SAHU, J. N. 2013a. Comparison of oil palm shell-based activated carbons produced by microwave and conventional heating methods using zinc chloride activation. Journal of Analytical and Applied Pyrolysis, 104, 176-184.

HOSEINZADEH HESAS, R., WAN DAUD, W. M. A., SAHU, J. N. & ARAMI-NIYA, A. 2013b. The effects of a microwave heating method on the production of activated carbon from agricultural waste: A review. *Journal of Analytical and Applied Pyrolysis*, 100, 1-11.

HUANG, R., MA, X., LI, X., GUO, L., XIE, X., ZHANG, M. & LI, J. 2017. A novel ion-imprinted polymer based on graphene oxide-mesoporous silica nanosheet for fast and efficient removal of chromium (VI) from aqueous solution. *Journal of Colloid and Interface Science,* 514**,** 544-553.

HUANG, G., SHI, J. X. & LANGRISH, T. A. G. 2009. Removal of Cr(VI) from aqueous solution using activated carbon modified with nitric acid. Chemical Engineering Journal, 152, 434-439.

IBRAHIM, W. M., HASSAN, A. F. & AZAB, Y. A. 2016. Biosorption of toxic heavy metals from aqueous solution by *Ulva lactuca* activated carbon. *Egyptian Journal of Basic and Applied Sciences,* 3**,** 241-249.

ISLAM, M. A., BENHOURIA, A., ASIF, M. & HAMEED, B. H. 2015. Methylene blue adsorption on factory-rejected tea activated carbon prepared by conjunction of hydrothermal carbonization and sodium hydroxide activation processes. *Journal of the Taiwan Institute of Chemical Engineers,* 52**,** 57-64.

JUNG, C., HEO, J., HAN, J., HER, N., LEE, S.-J., OH, J., RYU, J. & YOON, Y. 2013. Hexavalent chromium removal by various adsorbents: Powdered activated carbon, chitosan, and single/multi-walled carbon nanotubes. *Separation and Purification Technology,* 106**,** 63-71.

KABANOV, V. A., EFENDIEV, A. A. & ORUJEV, D. D. 1979. Complex-forming polymeric sorbents with macromolecular arrangement favourable for ion sorption. *Journal of Applied Polymer Science,* 29**,** 259-267.

KARNIB, M., KABBANI, A., HOLAIL, H. & OLAMA, Z. 2014. Heavy metals removal using activated carbon, silica and silica activated carbon composite. *Energy Procedia,* 50**,** 113-120.

KIRTI , S., SREEMOYEE, C. & BHUMIKA, J. 2015. Chromium toxicity and its health hazards. *International Journal of Advanced Research,* 3**,** 167-172.

KOŁODYŃSKA, D., KRUKOWSKA-BĄK, J., KAZMIERCZAK-RAZNA, J. & PIETRZAK, R. 2017. Uptake of heavy metal ions from aqueous solutions by sorbents obtained from the spent ion exchange resins. *Microporous and Mesoporous Materials,* 244**,** 127-136.

KONG, D., ZHANG, F., WANG, K., REN, Z. & ZHANG, W. 2014. Fast removal of Cr(VI) from aqueous solution using Cr(VI)-imprinted polymer particles. *Industrial & Engineering Chemistry Research,* 53**,** 4434-4441.

KONGSRICHAROEM, N. & POLPRASERT, C. 1996. Chromium removal by bipolar electro-chemical precipitation. *Water Science and Technology,,* 34**,** 109-116.

KOPAC, T., KIRCA, Y. & TOPRAK, A. 2016. Synthesis and characterization of KOH/boron modified activated carbons from coal and their hydrogen sorption characteristics. *International Journal of Hydrogen Energy,* 1,1-11.

KORAK, J. A., HUGGINS, R. & ARIAS-PAIC, M. 2017. Regeneration of pilot-scale ion exchange columns for hexavalent chromium removal. *Water Research,* 118**,** 141-151.

KÖSEOĢLU, E. & AKMIL-BAŞAR, C. 2015. Preparation, structural evaluation and adsorptive properties of activated carbon from agricultural waste biomass. *Advanced Powder Technology,* 26**,** 811-818.

KUMAR, A. & JENA, H. M. 2017. Adsorption of Cr(VI) from aqueous phase by high surface area activated carbon prepared by chemical activation with $ZnCl_2$. *Process Safety and Environmental Protection,* 109**,** 63-71.

KUMAR, P. A., RAY, M. & CHAKRABORTY, S. 2009. Adsorption behaviour of trivalent chromium on amine-based polymer aniline formaldehyde condensate. *Chemical Engineering Journal,* 149**,** 340-347.

KWIATKOWSKI, M. & BRONIEK, E. 2017. An analysis of the porous structure of activated carbons obtained from hazelnut shells by various physical and chemical methods of activation. *Colloids and Surfaces A: Physicochemical and Engineering Aspects,* 529**,** 443-453.

LANGMUIR, I. 1918. The adsorption of gases on plane surfaces of glass, mica and platinum. *Journal of the American Chemical Society,* 40**,** 1361-1403.

LANSDOWN, A. B. G. 2014. *The carcinogenicity of metals: Human risk through occupational and environmental exposure*, RSCP Publishing, Cambridge, Occupational Medicine, 65, 768–769.

LEŚNIEWSKA, B., GODLEWSKA-ŻYŁKIEWICZ, B. & WILCZEWSKA, A. Z. 2012. Separation and preconcentration of trace amounts of Cr(III) ions on ion imprinted polymer for atomic absorption determinations in surface water and sewage samples. *Microchemical Journal,* 105**,** 88-93.

LI, M., FENG, C., LI, M., ZENG, Q., GAN, Q. & YANG, H. 2015. Synthesis and characterization of a surface-grafted Cd(II) ion-imprinted polymer for selective separation of Cd(II) ion from aqueous solution. *Applied Surface Science,* 332**,** 463-472.

LI, W., ZHANG, L.-B., PENG, J.-H., LI, N. & ZHU, X.-Y. 2008. Preparation of high surface area activated carbons from tobacco stems with K_2CO_3 activation using microwave radiation. *Industrial Crops and Products,* 27**,** 341-347.

LI, Z., LI, J., WANG, Y. & WEI, Y. 2014. Synthesis and application of surface-imprinted activated carbon sorbent for solid-phase extraction and determination of copper (II). *Spectrochimica Acta Part A: Molecular and Biomolecular Spectroscopy,* 117**,** 422-427.

LIANG, S.-T., ZHANG, H.-L., LUO, M.-T., LUO, K.-J., LI, P., XU, H.-B. & ZHANG, Y. 2014. Colour performance investigation of a Cr_2O_3 green pigment prepared via the thermal decomposition of CrOOH. *Ceramics International,* 40**,** 4367-4373.

LIN, C. X., LIU, M. H. & ZHAN, H. Y. 2011. Pb(II)-Imprinted polymer prepared by graft copolymerization of acrylic acid onto cellulose. *Manufacturing Science and Technology, Pts 1-3,* 295-297**,** 2045-2048.

LIN, C., WANG, H., WANG, Y. & CHENG, Z. 2010. Selective solid-phase extraction of trace thorium(IV) using surface-grafted Th(IV)-imprinted polymers with pyrazole derivative. *Talanta,* 81**,** 30-36.

LIN, L., XU, X., PAPELIS, C., CATH, T. Y. & XU, P. 2014. Sorption of metals and metalloids from reverse osmosis concentrate on drinking water treatment solids. *Separation and Purification Technology,* 134**,** 37-45.

LIU, W., ZHANG, J., ZHANG, C., WANG, Y. & LI, Y. 2010. Adsorptive removal of Cr (VI) by Fe-modified activated carbon prepared from Trapa natans husk. *Chemical Engineering Journal,* 162**,** 677-684.

LIU, X., ZHANG, W. & ZHANG, Z. 2014. Preparation and characteristics of activated carbon from waste fiberboard and its use for adsorption of Cu(II). *Materials Letters,* 116**,** 304-306.

LU, J., WANG, Z.-R., LIU, Y.-L. & TANG, Q. 2016. Removal of Cr ions from aqueous solution using batch electrocoagulation: Cr removal mechanism and utilization rate of in situ generated metal ions. *Process Safety and Environmental Protection,* 104**,** 436-443.

MANEECHAKR, P. & KARNJANAKOM, S. 2017. Adsorption behaviour of Fe(II) and Cr(VI) on activated carbon: Surface chemistry, isotherm, kinetic and thermodynamic studies. *Journal of Chemical Thermodynamics,* 106**,** 104-112.

MARTIN, R. B. 2000. *Are There Proteins Containing Chromium? In Handbook of Metalloproteins,* New York Marcel Dekker.

MELLA, B., GLANERT, A. C. & GUTTERRES, M. 2015. Removal of chromium from tanning wastewater and its reuse. *Process Safety and Environmental Protection,* 95**,** 195-201.

MENENDEZ, J. A., MENENDEZ, E. M., IGLESIAS, M. J., GARCIA, A. & PIS, J. J. 1999. Modification of the surface chemistry of active carbons by means of microwave-induced treatments. *Carbon,* 37**,** 1115-1121.

MISHRA, P. C. & PATEL, R. K. 2009. Removal of lead and zinc ions from water by low cost adsorbents. *Journal of Hazardzadous Materials,* 168**,** 319-325.

MISHRA, S. & VERMA, N. 2017. Surface ion imprinting-mediated carbon nanofiber-grafted highly porous polymeric beads: Synthesis and application

towards selective removal of aqueous Pb(II). *Chemical Engineering Journal,* 313**,** 1142-1151.

MITREVA, M., DAKOVA, I. & KARADJOVA, I. 2017. Iron(II) ion imprinted polymer for Fe(II)/Fe(III) speciation in wine. *Microchemical Journal,* 132**,** 238-244.

MOHAMMADI, S. Z., KARIMI, M. A., AFZALI, D. & MANSOURI, F. 2010. Removal of Pb(II) from aqueous solutions using activated carbon from Sea-buckthorn stones by chemical activation. *Desalination,* 262**,** 86-93.

MOHAN, D. & PITTMAN, C. U., JR. 2006. Activated carbons and low cost adsorbents for remediation of tri- and hexavalent chromium from water. *Journal of Hazardous Materials,* 137**,** 762-811.

MOHAN, D., SINGH, K. P. & SINGH, V. K. 2005. Removal of hexavalent chromium from aqueous solution using low-cost activated carbons derived from agricultural waste materials and activated carbon fabric cloth. *Industrial & Engineering Chemistry Research,* 44**,** 1027-1042.

MOHANTY, K., JHA, M., MEIKAP, B. C. & BISWAS, M. N. 2005. Removal of chromium (VI) from dilute aqueous solutions by activated carbon developed from Terminalia arjuna nuts activated with zinc chloride. *Chemical Engineering Science,* 60**,** 3049-3059.

MOMČILOVIĆ, M., PURENOVIĆ, M., BOJIĆ, A., ZARUBICA, A. & RANĐELOVIĆ, M. 2011. Removal of lead(II) ions from aqueous solutions by adsorption onto pine cone activated carbon. *Desalination,* 276**,** 53-59.

MOSHA, D. M. S. & MKAYULA, L. L. 2005. Metal ion sequestration: an exciting dimension for molecularly imprinted polymer technology. *Tanzania Journal of Science,* 31**,** 91-98.

MOURA, R. C. A., BERTUOL, D. A., FERREIRA, C. A. & AMADO, F. D. R. 2012. Study of chromium removal by the electrodialysis of tannery and metal-finishing effluents. *International Journal of Chemical Engineering,* 2012**,** 1-7.

NAYAK, A., BHUSHAN, B., GUPTA, V. & SHARMA, P. 2017. Chemically activated carbon from lignocellulosic wastes for heavy metal wastewater remediation: Effect of activation conditions. *Journal of Colloid and Interface Scince,* 493**,** 228-240.

NGUYEN, T. A., NGO, H. H., GUO, W. S., ZHANG, J., LIANG, S., YUE, Q. Y., LI, Q. & NGUYEN, T. V. 2013. Applicability of agricultural waste and by-products for adsorptive removal of heavy metals from wastewater. *Bioresource Technology,* 148**,** 574-585.

NISHIDE, H., DEGUCHI, J. & TSUCHIDA, E. 1976. Selective adsorption of metalions on cross-linked poly(vinylpyridine) resin prepared with a metal ion as a template. *Chemistry Letters,* 5**,** 169-174.

OHGAMI, N., YAMANOSHITA, O., THANG, N. D., YAJIMA, I., NAKANO, C., WENTING, W., OHNUMA, S. & KATO, M. 2015. Carcinogenic risk of chromium, copper and arsenic in CCA-treated wood. *Environmental Pollution,* 206**,** 456-460.

OTERO-ROMANI, J., MOREDA-PINEIRO, A., BERMEJO-BARRERA, P. & MARTIN-ESTEBAN, A. 2008. Synthesis, characterization and evaluation of ionic-imprinted polymers for solid-phase extraction of nickel from seawater. *Analytica Chimica Acta,* 630**,** 1-9.

ÖZKARA, S., ANDAÇ, M., KARAKOÇ, V., SAY, R. & DENIZLI, A. 2011. Ion-imprinted PHEMA based monolith for the removal of Fe^{3+} ions from aqueous solutions. *Journal of Applied Polymer Science,* 120**,** 1829-1836.

PAKADE, V. E., NCHOE, O. B., HLUNGWANE, L. & TAVENGWA, N. T. 2017. Sequestration of hexavalent chromium from aqueous solutions by activated carbon derived from *Macadamia* nutshells. *Water Science and Technology,* 75**,** 196-206.

PAKADE, V. E., NTULI, T. D. & OFOMAJA, A. E. 2017. Biosorption of hexavalent chromium from aqueous solutions by *Macadamia* nutshell powder. *Applied Water Science,* 1, 1-16.

PAKADE, V., LINDAHL, S., CHIMUKA, L. & TURNER, C. 2012. Molecularly imprinted polymers targeting quercetin in high-temperature aqueous solutions. *Journal of Chromatography A,* 1230**,** 15-23.

PENG, W., XIE, Z., CHENG, G., SHI, L. & ZHANG, Y. 2015. Amino-functionalized adsorbent prepared by means of Cu(II) imprinted method and its selective removal of copper from aqueous solutions. *Journal of Hazardous Materials,* 294**,** 9-16.

PEZOTI JUNIOR, O., CAZETTA, A. L., GOMES, R. C., BARIZÃO, É. O., SOUZA, I. P. A. F., MARTINS, A. C., ASEFA, T. & ALMEIDA, V. C. 2014. Synthesis of $ZnCl_2$-activated carbon from *Macadamia* nut endocarp (*Macadamia* integrifolia) by microwave-assisted pyrolysis: Optimization using RSM and methylene blue adsorption. *Journal of Analytical and Applied Pyrolysis,* 105**,** 166-176.

POLYAKOVA, I., BOROVIKOVA, L., OSIPENKO, A., VLASOVA, E., VOLCHEK, B. & PISAREV, O. 2016. Surface molecularly imprinted organic-inorganic polymers having affinity sites for cholesterol. *Reactive and Functional Polymers,* 109**,** 88-98.

POOTS, V. J. P., MCKAY, G. & HEALY, J. J. 1976. The removal of acid dye from effluent, using natural adsorbents: I. Peat. *Water Research,* 10**,** 1061-1066.

PUIGDOMENECH, I. & BEVERSKOG, B. 1997. Revised pourbaix diagrams for chromium at 25-300°C. *Corrosion Science,* 39, 43-57.

QU, G., JI, H., XIAO, R. & LIANG, D. 2012. Effect of modification with nitric acid and hydrogen peroxide on chromium (VI) adsorption by activated carbon fiber. *Advanced Materials Research,* 518-523**,** 2099-2103.

RAD, S., MIRBAGHERI, S. & MAHAMMADI, T. 2009. Using reverse osmosis membrane for chromium removal from aqueous solution. *Journal of Engineering and Technology,* 3**,** 348-352.

RAI, D., EARY, L. E. & ZACHARA, J. M. 1989. Environmental chemistry of chromium. *Science of the Total Environment,* 86**,** 15-23.

RAI, M. K., SHAHI, G., MEENA, V., MEENA, R., CHAKRABORTY, S., SINGH, R. S. & RAI, B. N. 2016. Removal of hexavalent chromium Cr (VI) using activated carbon prepared from mango kernel activated with H_3PO_4. *Resource-Efficient Technologies,* 2**,** S63-S70.

RAJESH, N., MISHRA, B. G. & PAREEK, P. K. 2008. Solid phase extraction of chromium(VI) from aqueous solutions by adsorption of its diphenylcarbazide complex on a mixed bed adsorbent (acid activated montmorillonite-silica gel) column. *Spectrochimica Acta Part A: Molecular and Biomolecular Spectroscopy,* 69**,** 612-618.

RAMMIKA, M., DARKO, G. & TORTO, N. 2011. Incorporation of Ni(II)-dimethylglyoxime ion-imprinted polymer into electrospun polysulphone nanofibre for the determination of Ni(II) ions from aqueous samples. *Water SA,* 37**,** 539-546.

RAMNANI, S. P. & SABHARWAL, S. 2006. Adsorption behavior of Cr(VI) onto radiation crosslinked chitosan and its possible application for the treatment of wastewater containing Cr(VI). *Reactive and Functional Polymers,* 66**,** 902-909.

RANGABHASHIYAM, S. & SELVARAJU, N. 2015. Evaluation of the biosorption potential of a novel Caryota urens inflorescence waste biomass for the removal of hexavalent chromium from aqueous solutions. *Journal of the Taiwan Institute of Chemical Engineers,* 47**,** 59-70.

RAO, C. R. M., SAHUQUILLO, A. & LOPEZ SANCHEZ, J. F. 2008. A review of the different methods applied in environmental geochemistry for single and sequential extraction of trace elements in soils and related materials. *Water, Air, and Soil Pollution,* 189**,** 291-333.

RAO, T. P., KALA, R. & DANIEL, S. 2006. Metal ion-imprinted polymers--novel materials for selective recognition of inorganics. *Analytica Chimica Acta,* 578**,** 105-116.

RAZZAZ, A., GHORBAN, S., HOSAYNI, L., IRANI, M. & ALIABADI, M. 2016. Chitosan nanofibers functionalized by TiO_2 nanoparticles for the removal of heavy metal ions. *Journal of the Taiwan Institute of Chemical Engineers,* 58**,** 333-343.

REGARAJ, S., YEON, K. & MOON, S. 2001. Removal of chromium (VI) from water and waste water by ion exchange reisns. *Journal of hazardous materials,* 87**,** 273-287.

RENU, M. A., SINGH, K., UPADHYAYA, S. & DOHARE, R. K. 2017. Removal of heavy metals from wastewater using modified agricultural adsorbents. *Materials Today: Proceedings,* 4**,** 10534-10538.

RUSEN, E., DIACON, A., MOCANU, A., RIZEA, F., BUCUR, B., BUCUR, M. P., RADU, G.-L., BACALUM, E., CHEREGI, M. & DAVID, V. 2017. Synthesis and retention properties of molecularly imprinted polymers for antibiotics containing a 5-nitrofuran ring. *RSC Advances,* 7**,** 50844-50852.

SAHA, P. 2010. Assessment on the removal of methylene blue dye using *Tamarind* fruit shell as biosorbent. *Water, Air, and Soil Pollution,* 213**,** 287-299.

SANCHES, D., RAMOS, A. M., COELHO, J. F. J., COSTA, C. S. M. F., VILARIGUES, M. & MELO, M. J. 2017. Correlating thermophysical properties with the molecular composition of 19th century chrome yellow oil paints. *Polymer Degradation and Stability,* 138**,** 201-211.

SANCIOLO, P., OSTARCEVIC, E., ATHERTON, P., LESLIE, G., FANE, T., COHEN, Y., PAYNE, M. & GRAY, S. 2012. Enhancement of reverse osmosis water recovery using interstage calcium precipitation. *Desalination,* 295**,** 43-52.

SAPUTRO, S., YOSHIMURA, K., MATSUOKA, S., TAKEHARA, K., NARSITO, AIZAWA, J. & TENNICHI, Y. 2014. Speciation of dissolved chromium and the mechanisms controlling its concentration in natural water. *Chemical Geology,* 364**,** 33-41.

SARWAR, M., AHMAD, S., AHMAD, S., ALI, S. & AWAN, S. A. 2006. Copper(II) complexes of pyrrolidine dithiocarbamate. *Transition Metal Chemistry,* 32**,** 199-203.

SELOMULYA, C., MEEYOO, V. & AMAL, R. 1999. Mechanisms of Cr(VI) removal from water by various types of activated carbons. *Journal of Chemical Technology and Biotechnoly,* 74**,** 111-122.

SHAHID, M., SHAMSHAD, S., RAFIQ, M., KHALID, S., BIBI, I., NIAZI, N. K., DUMAT, C. & RASHID, M. I. 2017. Chromium speciation, bioavailability,

uptake, toxicity and detoxification in soil-plant system: A review. *Chemosphere,* 178**,** 513-533.

SHAKERIAN, F., KIM, K.-H., KWON, E., SZULEJKO, J. E., KUMAR, P., DADFARNIA, S. & HAJI SHABANI, A. M. 2016. Advanced polymeric materials: Synthesis and analytical application of ion imprinted polymers as selective sorbents for solid phase extraction of metal ions. *Trac Trends in Analytical Chemistry,* 83**,** 55-69.

SHAMSIPUR, M. & BESHARATI-SEIDANI, A. 2011. Synthesis of a novel nanostructured ion-imprinted polymer for very fast and highly selective recognition of copper(II) ions in aqueous media. *Reactive and Functional Polymers,* 71**,** 131-139.

SHAMSIPUR, M., FASIHI, J. & ASHTARI, K. 2007. Grafting of ion-imprinted polymers on the surface of silica gel particles through covalently surface-bound initiators: A selective sorbent for uranyl ion. *Analytical Chemistry,* 79**,** 7116-7123.

SHI, J., ZHAO, Z., CUI, F., LIANG, Z., SUN, T. & NIE, Y. 2016. Enhancement of heavy metals adsorption on activated carbon fibers by chemically modification. *Harbin Gongye Daxue Xuebao/Journal of Harbin Institute of Technology,* 48**,** 102-107.

SIBRIAN-VAZQUEZ, M. & SPIVAK, D. A. 2004. Characterization of molecularly imprinted polymers employing crosslinkers with nonsymmetric polymerizable groups. *Journal of Polymer Science Part A: Polymer Chemistry,* 42**,** 3668-3675.

SILGADO, K., MARRUGO, G. & PUELLO, J. 2014. Adsorption of chromium(VI) by activated carbon produced from oil palm endocarp. *Chemical Engineering Transactions,* 87**,** 721-726.

SILVA, B., FIGUEIREDO, H., NEVES, I. C. & TAVARES, T. 2008. The role of pH on Cr(VI) reduction and removal by *Arthrobacter Viscosus*. *International Journal of Chemical, Molecular, Nuclear, Materials and Metallurgical Engineering,* 2**,** 70-73.

SINGH, D. K. & MISHRA, S. 2009. Synthesis, characterization and removal of Cd(II) using Cd(II)-ion imprinted polymer. *Journal of Hazardous Materials,* 164**,** 1547-1551.

SINGH, K., CHANDRA, B. & GAUTAM, M. 2016. Development of inexpensive adsorbent from agro-waste for phenol adsorption. *Journal of Scientific and Industrial Research,* 75**,** 444-451.

SINGHA, S., SARKAR, U. & LUHARUKA, P. 2013. Functionalized granular activated carbon and surface complexation with chromates and bi-chromates in wastewater. *Science of the Total Environment,* 447**,** 472-487.

STUMM, W., SIGG, L. & SULZBERGER, B. 1992. Chemistry of the solid–water interface: processes at the mineral-water and particle-water interface in natural systems, Wiley, 57, 205-226.

SUGANTHI, N. 2013. Removal of chromium(VI) from wastewater using phosphoric acid treated activated carbon. *Carbon Materials,* 128**,** 128-134.

SUWALSKY, M., CASTRO, R., VILLENA, F. & SOTOMAYOR, C. P. 2008. Cr(III) exerts stronger structural effects than Cr(VI) on the human erythrocyte membrane and molecular models. *Journal of Inorganic Biochemistry,* 102**,** 842-849.

TAJODINI, N. & MOGHIMI, A. 2010. Preconcentration and determination of ultra-trace cobalt (II) in water samples using Co(II)-imprinted diazoaminobenzene-vinylpyridine copolymers. *Asian Journal of Chemistry,* 22**,** 335-344.

TAN, I. A. W., CHAN, J. C., HAMEED, B. H. & LIM, L. L. P. 2016. Adsorption behavior of cadmium ions onto phosphoric acid-impregnated microwave-induced mesoporous activated carbon. *Journal of Water Process Engineering,* 14**,** 60-70.

TONG, Y., GUAN, H., WANG, S., XU, J. & HE, C. 2011. Syntheses of chitin-based imprinting polymers and their binding properties for cholesterol. *Carbohydrate Research,* 346**,** 495-500.

TOR, A., BÜYÜKERKEK, T., ÇENGELOLU, Y. & ERSÖZ, M. 2005. Simultaneous recovery of Cr(III) and Cr(VI) from the aqueous phase with ion-exchange membranes. *Desalination,* 171**,** 233-241.

TSENG, R. L. & TSENG, S. K. 2005. Pore structure and adsorption performance of the KOH-activated carbons prepared from corncob. *Journal of Colloid and Interface Science,* 287**,** 428-437.

TSOI, Y. K., HO, Y. M. & LEUNG, K. S. 2012. Selective recognition of arsenic by tailoring ion-imprinted polymer for ICP-MS quantification. *Talanta,* 89**,** 162-168.

USEPA & OAR, 2012. *Chromium compounds| Technology Transfer Networks Air Toxicswebsite|USEPA.*[Online]Availableat:http:/www3.epa.gov/airtoxics/hlthet/chromium.html [Accessed 17 March 2017].

VAN DER VOORT, P., BENJELLOUN, M. & VANSANT, E. F. 2002. Rationalization of the Synthesis of SBA-16: Controlling the Micro- and Mesoporosity. *The Journal of Physical Chemistry B,* 106**,** 9027-9032.

VELASCO-PEREZ, M. & HISCOCK, K. M. 2013. Optimisation of sugar cane activated carbon for arsenic(V) and arsenic(III) removal from water. *Water Science and Technology: Water Supply,* 13, 319-327.

WANG, D., HE, S., SHAN, C., YE, Y., MA, H., ZHANG, X., ZHANG, W. & PAN, B. 2016. Chromium speciation in tannery effluent after alkaline precipitation: Isolation and characterization. *Journal of Hazardzous Materials,* 316**,** 169-77.

WEBER, T. W. & CHAKRAVORTI, R. K. 1974. Pore and solid diffusion models for fixed-bed adsorbers. *AIChE Journal,* 20**,** 228-238.

WENTEN, I. G. & KHOIRUDDIN 2016. Reverse osmosis applications: Prospect and challenges. *Desalination,* 391**,** 112-125.

WHO 2003. Guidelines for drinking-water quality [electronic resource] 3rd ed. Geneva.

WILLIAMS, R. J. P. 1999. What is wrong with aluminium? The J. D. Birchall memorial lecture. *Journal of Inorganic Biochemistry,* 76**,** 81-88.

XIE, B., SHAN, C., XU, Z., LI, X., ZHANG, X., CHEN, J. & PAN, B. 2017. One-step removal of Cr(VI) at alkaline pH by UV/sulfite process: Reduction to Cr(III) and in situ Cr(III) precipitation. *Chemical Engineering Journal,* 308**,** 791-797.

XU, Z., SONG, C., HU, Y. & LI, G. 2011. Molecularly imprinted stir bar sorptive extraction coupled with high performance liquid chromatography for trace analysis of sulfa drugs in complex samples. *Talanta,* 85**,** 97-103.

YAHYA, M. A., AL-QODAH, Z. & NGAH, C. W. Z. 2015. Agricultural bio-waste materials as potential sustainable precursors used for activated carbon production: A review. *Renewable and Sustainable Energy Reviews,* 46**,** 218-235.

YAN, H. & HO ROW, K. 2008. Characteristic and synthetic approach of molecularly imprinted polymer. *International Journal of Molecular Sciences,* 7**,** 155-178.

YANG, B., ZHANG, T., TAN, W., LIU, P., DING, Z. & CAO, Q. 2013. Determination of rhodium by resonance light-scattering technique coupled with solid phase extraction using Rh(III) ion-imprinted polymers as sorbent. *Talanta,* 105**,** 124-130.

YANG, Y., LONG, Y., CAO, Q., LI, K. & LIU, F. 2008. Molecularly imprinted polymer using beta-cyclodextrin as functional monomer for the efficient recognition of bilirubin. *Analytica Chimica Acta,* 606**,** 92-97.

YAO, S., ZHANG, J., SHEN, D., XIAO, R., GU, S., ZHAO, M. & LIANG, J. 2016. Removal of Pb(II) from water by the activated carbon modified by nitric acid under microwave heating. *Journal of Colloid and Interface Science,* 463**,** 118-127.

YORGUN, S. & YıLDıZ, D. 2015. Preparation and characterization of activated carbons from Paulownia wood by chemical activation with H_3PO_4. *Journal of the Taiwan Institute of Chemical Engineers,* 53**,** 122-131.

YUE, Z., BENDER, S. E., WANG, J. & ECONOMY, J. 2009. Removal of chromium Cr(VI) by low-cost chemically activated carbon materials from water. *Journal of Hazardous Materials,* 166**,** 74-78.

YUEN, F. K. & HAMEED, B. H. 2009. Recent developments in the preparation and regeneration of activated carbons by microwaves. *Advances in Colloid and Interface Science,* 149**,** 19-27.

ZEWAIL, T. M. & YOUSEF, N. S. 2014. Chromium ions (Cr^{6+} & $Cr^{3+)}$ removal from synthetic wastewater by electrocoagulation using vertical expanded Fe anode. *Journal of Electroanalytical Chemistry,* 735**,** 123-128.

ZHANG, G., SUN, Y., ZHAO, P., XU, Y., SU, A. & QU, J. 2017a. Characteristics of activated carbon modified with alkaline $KMnO_4$ and its performance in catalytic reforming of greenhouse gases CO_2 /CH_4. *Journal of CO_2 Utilization,* 20**,** 129-140.

ZHANG, J., FU, H., LV, X., TANG, J. & XU, X. 2011. Removal of Cu(II) from aqueous solution using the rice husk carbons prepared by the physical activation process. *Biomass and Bioenergy,* 35**,** 464-472.

ZHANG, T., YUE, X., ZHANG, K., ZHAO, F., WANG, Y. & ZHANG, K. 2017. Synthesis of Cu(II) ion-imprinted polymers as solid phase adsorbents for deep removal of copper from concentrated zinc sulfate solution. *Hydrometallurgy,* 169**,** 599-606.

ZHANG, Y., SONG, D., LANNI, L. M. & SHIMIZU, K. D. 2010. Importance of functional monomer dimerization in the molecular imprinting process. *Macromolecules,* 43**,** 6284-6294.

ZHANG, Y.J., OU, J.L., DUAN, Z.K., XING, Z.J. & WANG, Y. 2015. Adsorption of Cr(VI) on bamboo bark-based activated carbon in the absence and presence of humic acid. *Colloids and Surfaces A: Physicochemical and Engineering Aspects,* 481**,** 108-116.

ZHU, L., ZHU, Z., ZHANG, R., HONG, J. & QIU, Y. 2011. Synthesis and adsorption performance of lead ion-imprinted micro-beads with combination of two functional monomers. *Journal of Environmental Sciences,* 23**,** 1955-1961.

ZUBRIK, A., MATIK, M., HREDZÁK, S., LOVÁS, M., DANKOVÁ, Z., KOVÁČOVÁ, M. & BRIANČIN, J. 2017. Preparation of chemically activated carbon from waste biomass by single-stage and two-stage pyrolysis. *Journal of Cleaner Production,* 143**,** 643-653.

APPENDIX

Example calculation of the adsorption capacity, q_e and percentage removal (% R).

The table below shows the results obtained during the **effect of concentration experiment on Cr(VI) removal by $MACN_{20}$**

Working conditions: Solution pH: 1

Time: 12hrs

Adsorbent dosage: 3.33 g/L

Solution volume: 30 mL

Varying concentration: 30, 50,100,150, 200 & 300 mg/L

TABLE A: Data obtained during batch adsorption

C_o(mg/L)	C_e (mg/L)	% R	q_e
30	0,043724	99,85425	8,986883
50	0,77574	98,44852	14,76728
100	2,671016	97,32898	29,1987
150	39,97708	73,34861	33,00688
200	72,99365	63,50317	38,1019
300	138,1171	53,96098	48,56488

Given: C_o = 30 mg/L

The capacity is given as:

$$qe = \frac{(C_0 - C_e) \times V}{M} \qquad (4.4)$$

$$= \frac{(30.00\, mg/L - \ 0{,}04372\ \text{mg/L}) \ \times 0.03\ L}{0.1\ g} = 8.986\, mg/g$$

The percentage removal is given as:

$$\% R = \frac{(C_o - C_e)}{C_o} \times 100 \quad (4.5)$$

$$= \frac{(30.00\, mg/L - \ 0{,}04372\, mg/L)}{30.00\, mg/L} \times 100 = 99.85\%$$

Example on the **selectivity studies of pseudo-MACN$_{20}$-IIP and the non-imprinted counterpart on Cr(III) removal**.

The distribution ratios, the selectivity coefficients and the relative selectivity coefficients were deduced as follows:

Metal ion	K_d (L/g)		K		K'
	MACN$_{20}$-IIP	MACN$_{20}$-NIP	MACN$_{20}$-IIP	MACN$_{20}$-NIP	
Cr(III)	18.01	11.34	-	-	-
Cr(VI)	3.52	2.72	5.12	4.17	1.23
Cd(II)	6.05	5.81	2.98	1.95	1.53
Cu(II)	1.09	1.16	16.49	9.77	1.69
Ni(II)	2.81	3.03	6.41	3.74	1.72

Equation 4.7 below was used to calculate the **selectivity coefficient of Cr^{3+}** ions in the presence of the aforementioned competing cations.

Given: $K_d\,(Cr^{3+}) = 18.01$

: $K_d\,(Cr^{6+}) = 3.52$

MACN$_{20}$-IIP

$$K = \frac{K_d\,(Cr^{3+})}{K_d\,(B)} \quad (4.7)$$

$$= \frac{18.01\ L/g}{3.52\ L/g} = 5.12$$

$MACN_{20}$-NIP

$$K = \frac{K_d\,(Cr^{3+})}{K_d\,(B)}$$

$$= \frac{11.34\ L/g}{2.72\ L/g} = 4.17$$

The **enhanced imprinting selectivity** effect and affinity of the template ion by the polymers is indicated by K'. This is calculated as follows:

Given: $K_{MACN20\text{-}IIP}\,(Cr^{6+}) = 5.12$

: $K_{MACN20\text{-}NIP}\,(Cr^{6+}) = 4.17$

$$K' = \frac{K_{IIP}}{K_{NIP}} \qquad (4.8)$$

$$= \frac{5.12}{4.17} = 1.23$$